UNIVERSITÀ DI PISA

FACOLTA' DI SCIENZE MATEMATICHE, FISICHE E NATURALI

CORSO DI LAUREA MAGISTRALE IN FISICA
ANNO ACCADEMICO 2012/2013

TESI DI LAUREA MAGISTRALE

TRAP EFFECTS IN THE HUBBARD MODEL

IL CANDIDATO

Adriano Angelone

IL RELATORE

Prof. Ettore Vicari

Contents

Introduction

The Hubbard Model

The Hubbard Model is the most basic model describing a lattice system of interacting fermions, simply containing a term representing hopping between different sites and an on–site repulsion. In the second quantization formalism, the Hubbard Model Hamiltonian is

$$\widehat{H} = -w \sum_{\{i,j\}} \sum_{\sigma=\uparrow,\downarrow} \left(\widehat{C}^{\dagger}_{i\sigma} \widehat{C}_{j\sigma} + \widehat{C}^{\dagger}_{j\sigma} \widehat{C}_{i\sigma} \right) + U \sum_{i} \widehat{N}_{i\uparrow} \widehat{N}_{i\downarrow} \tag{1}$$

In terms of the fermionic operators $\widehat{C}_j$, and with $\sum_{\{i,j\}}$ denoting a sum over nearest–neighbour sites. This model has a bosonic counterpart (called **Bose–Hubbard Model**) for bosons with on–site interaction, and also a continuous counterpart, called **Gaudin–Yang Model**: this describes a continuous system of fermions with a contact interaction (correspondent to the on–site Hubbard interaction) and its Hamiltonian in the first quantization formalism, for a system of N fermions, is

$$\widehat{H} = \sum_{i=1}^{N} \left(-\frac{\hbar^2}{2m} \nabla_i^2 \right) + g \sum_{i<j} \delta \left(\boldsymbol{x}_i - \boldsymbol{x}_j \right) \tag{2}$$

Despite being the simplest possible model to keep into account fermionic interactions, no general consistent treatment for the Hubbard Model has been found: exact solutions have been found only for the one–dimensional case ($d = 1$) and $d = +\infty$. In the former (our case of interest) the solution has been found using the **Bethe *Ansatz*** formalism.

The fundamental idea behind this method is to reduce the complex scattering processes happening in the system to unions of two–body elastic scatterings, where particle momenta are exchanged but not changed. A wavefunction form is proposed to keep into account this identification, and model–specific conditions are applied to it to determine the charachteristic of the model (for instance, the particle density). This method has been successfully applied to many systems besides the 1D Hubbard Model: for instance, the 1D Heisenberg Spin Chain, the XXZ model, and continuous models like the Gaudin–Yang model itself.

The Hubbard Model has many applications in solid state physics, both in one dimension and in higher–dimensional systems.

- Graphene is composed by 2D monolayers of carbon atoms arranged in a hexagonal lattice: the Hubbard Model can be used to describe Graphene Sheets and Graphene Nanostructures like Nanoribbons (as, for instance, in [1, 2, 3, 4]).
- Some materials (for instance, transition metal oxides with a partially–filled d electron band,

like V_2O_3), classified as conductors by band theory, prove to be poor conductors or even insulants.

These insulating properties, rather than being due to the double filling of the conduction band, are caused by interelectronic interactions: at low temperatures, these hinder electronic motion even for smaller fillings. This kind of insulating phase is called **Mott Insulator**, and the Hubbard Hamiltonian and enhanced models derived from it can be used to describe these materials and their behaviour ([5]).

- The Hubbard Model, and models derived from it or based on extensions of its Hamiltonian, are used to describe the main features of high–T_C superconductors (see, for instance, [6, 7, 8]).

Besides these applications, the Hubbard Model is applied to describe the behaviour of cold fermionic atoms in optical lattices: we will now discuss the approximations in which these systems provide an experimental realization to the model.

Cold Atomic Systems in Optical Lattices

Over the past few decades, experimental progress has allowed the study of the behaviour of cold atoms in optical lattices (for reviews on the subject, see for instance [13, 14, 15]). In these systems the particles are placed in a potential generated by superimposing propagating LASER waves: as the equilibrium positions in this potential are in quantized and equispaced positions, the system allows a lattice description. Experimental setups have been realized with both bosonic (for instance, [18]) and fermionic (for instance, [16, 17]) atoms.

As these systems are built at very low temperatures, they are very useful to study many phenomena difficult to observe in other conditions. For instance, the low temperature allows these systems to experience **Quantum Many–Body (QMB) Effects**, physical phenomena in which the system shows both quantum and statistical phenomena. As temperatures grow higher, the effects of the former vanish in most systems, while statistical properties revert to the classical ones: cold atoms in optical lattices are therefore instrumental experimental setups in investigating QMB effects.

In general, interactions between the atoms in such system cannot be modelled exactly: however, several approximations can be made in order to find a lattice model to describe these systems.

- Atomic interactions can be kept in account using scattering theory, and the first commonly made approximation is to neglect all scattering processes happening with angular momentum $L > 0$, since the centrifugal potential in the Schrodinger Equation introduces, for higher L, a potential barrier which deters the particles from approaching enough to interact (the very low system temperature does not allow the atoms to significantly overcome this barrier).
- At low energy an interaction is fully charachterized by its scattering length. We can therefore introduce an effective model, tuned to have the same scattering length as the physical interaction, to simplify the system analysis: in particular, the system interaction is usually modelled with a contact interaction.
- We can suppose that only one band is relevant in describing the system physics (for a fermionic system, only one band must be close enough to the Fermi level to be relevant) and that interband interactions are weak. This approximation is good for strong lattice potentials and low temperatures ([15]): anyway, the presence of multiple bands can be kept in account using band–charachteristic interactions and hopping coefficients, or with a single–band Hamiltonian with effective coefficients.
- We can also apply the tight–binding approximation, assuming isotropy of the hopping coefficients between nearest–neighbouring sites and neglecting the possibility of further hopping.

The hypotheses we just made shape a single–band, lattice Hamiltonian with constant nearest–neighbour hopping coupling and on–site (contact) interactions, which is nothing but the Hubbard Hamiltonian (1) for Fermionic atoms or its bosonic counterpart for Bosonic atoms. This implies that cold atomic systems in optical lattices, and the physical phenomena they allow to observe, can be described by lattice models for interacting particles, like the Hubbard Model or the Bose–Hubbard Model. The Hubbard Model has indeed been used to modelize such systems (see, for instance, [9, 10, 11, 12, 19]).

Optical Lattices are useful to experimentally realize Hubbard–like models, since the hopping and the interaction coupling in these models are determined by the lattice structure, which in turn depends on experimental parameters like the lattice potential intensity and the magnetic field: varying these, the Hubbard (or Bose–Hubbard) system can be studied for different values of the Hamiltonian parameters, allowing to explore a wide range of physical phenomena.

A key feature in these systems is the presence of a confining potential (usually harmonic) in order to prevent the particles from escaping the optical lattice: this can be provided by the optical lattices beam themselves, or by an additional optical or magnetic trap. The use of trapping potentials allows to manipulate the geometry of the system: for instance, a quasi–1D system is created adding to the system a very strong confining potential in two directions (therefore hindering the atoms from changing sites along those directions) and leaving the confining potential much weaker in the other direction, effectively restricting the system to one spatial dimension.

Our previous approximations for the system behaviour still hold, and therefore the Hubbard model (in the effective number of spatial dimensions) can still be used to describe this kind of systems (in particular, an effective 1D scattering length a_{1D} can be defined from the original 3D one). However, the presence of the confining potential forces to employ an *inhomogeneous* Hubbard Model, due to the spatial inhomogeneity induced by the particle trap: this changes the physics of the model, along with the possible solution methods.

The most basic approach to study the behaviour of a confined system is the **Local Density Approximation** (LDA), which describes a system confined in a potential $V(x)$ as a nonconfined one with a position–dependent chemical potential, $\mu_{\text{eff}}(x) = \mu - V(x)$: some of the system properties, like the now position–dependent density, can be computed as $n(x) = n_h(\mu_{\text{eff}}(x))$ from the unconfined solution $n_h(\mu)$. This approach can be applied to describe confined systems of cold fermions (as in [19, 20]).

Critical Behaviour in Confined Systems

One of the interesting subjects to study using cold atoms in optical lattices are **Quantum Critical Behaviours**: in particular, **Quantum Phase Transitions** can be observed. These phase transitions are not driven by thermal fluctuations, as their Classical counterparts, but are rather induced by Quantum Fluctuations generated by non–commuting terms in a Quantum Hamiltonian. Quantum Critical Behaviour is observed only at temperatures low enough to allow quantum fluctuations to become dominant (an example of it is the Superfluid–Mott Insulator Transition, experimentally observed for bosonic systems in optical lattices, as described in [18]).

Quantum Critical Phenomena are strongly dependent on the system dimensionality: this feature increases the usefulness of optical lattices as means to study them, as the dimensionality of an atomic gas in an optical lattice can be modified, in order to observe quasi–2D or quasi–1D systems and to study their behaviour.

However, while the critical behaviour of the unconfined models is well understood, the presence of the confining potential induces changes in the critical properties, whose effect is determined by the **Trap Size** l (the charachteristic scale of the potential, usually defined as $V(x) = (x/l)^p$ for a power–law potential). For instance, the presence of the trapping interaction allows (at $T = 0$) the coexistence in different portions of the same lattice of different quantum phases (e. g. the

coexistence of quantum phases in a confined Hubbard System in [10, 19]).

The original critical behaviour can be observed around the middle of the trap only if the correlation length ξ is much smaller than the trap size l, but large enough to show the universal scaling behaviour. If the latter condition is verified while the former is not (this is usually the interesting regime) the trap will change the features of the observed critical behaviour, though some of the original ones may remain.

While the LDA could be used to approximate the system behaviour, it is a local approximation, and therefore it fails when correlations become important: namely, when nonlocal quantities need to be computed, or close to phase transitions (when the correlation range diverges): simulation data shows in these conditions significant differences from the LDA results. In order to describe the trap effects in these conditions, the trap can be added to the critical theory of the model as a relevant perturbation term, whose effects can be computed with the aid of the RG methods. This approach is called **Trap Size Scaling** (TSS) and has been used to describe the corrections to the LDA behaviour: for instance, for the trapped Hardcore (infinitely repulsive) Bose–Hubbard model in [21].

Objectives and Organization

The present work aims to study the corrections to the LDA approach in a one–dimensional system described by the Repulsive, unpolarized Hubbard Model in the presence of an external, harmonic confining potential.

After introducing all the required physical instruments, the homogeneous Hubbard Model will be solved using the Bethe *Ansatz* method: in particular, this approach will lead to the solution of integral numerical equations for the fermionic density in the model.

The system will be analyzed in the limit of large trap size l, in order to understand the scaling behaviour induced by l in quantities like the density and the density correlation functions. This analysis will be done using numerical simulation data, generated by M. Campostrini, and will focus on two different ways of realizing the large–l limit:

- At first, the system will be studied in the **Dilute Limit** ($l \to +\infty$ at fixed N). In the limit of large l quantities like the density function or the density–density correlation show a TSS dependence on the trap size l at constant rescaled interaction strength U_r. The TSS *ansatz* is confirmed by numerical simulation data.
- The system will then be studied in the **Trapped Thermodynamic Limit** (fixed N/l for $l \to +\infty$). The LDA results at fixed N/l will be obtained from the solution of the homogeneous model, and will predict the coexistence, in different zones of the confined system, of the quantum phases described by the homogeneous model.

  The LDA data will then be compared with the simulation data, showing evidence of two different trap–size dependences: one around the trap center, with $O(l^{-1})$ corrections to the LDA results, and one in proximity of the low–density region of the lattice, with a different scaling behaviour implying larger corrections.

In order to calculate the LDA behaviour and study the corrections, many physical concepts need to be introduced: these have been organized in the following fashion.

1. In **Chapter 1** the Hubbard Model and several lattice models connected to it are described.
   - The Hubbard Model is obtained by adding the interaction term to a noninteracting tight–binding model, which shapes many of its properties: an analysis of the physics of this

lattice model will prove very useful for further developments, and is carried out in **Section 1.1**. The Bosonization method, fundamental to the analysis of the critical properties of the Hubbard Model, is also introduced and applied to this simpler model.

- The Bose–Hubbard Model, the bosonic equivalent of the Hubbard Model, shares many similarities with it: we study it in **Section 1.2**, focusing on its behaviour in the **Hard-core Limit** (the limit of impenetrable particles, equivalent to infinite on–site repulsion).
- In **Section 1.3** the Hubbard Model is introduced, the phases it describes are charachterized, and the bosonization method is employed to understand its critical behaviour.

2. **Chapter 2** contains an outline of the Bethe *Ansatz* solution method for the Hubbard Model.

   - In **Section 2.1**, after a description of some of the most relevant symmetries of the model, the Bethe *Ansatz* wavefunctions and results are presented in the form of relations, called **Lieb–Wu Equations**, for the fermionic parameters. These equations are then solved, and the completeness issues for these solutions are briefly discussed.
   - In **Section 2.2** the solutions of the Lieb–Wu Equations are used to derive relations for the thermodynamic quantities of the Hubbard Model. These quantities are obtainable solving numerically a system of integral equations: the results allow to describe some aspects of the $T = 0$ Phase Diagram of the Repulsive Hubbard Model in absence of magnetic field, and to calculate the homogeneous $n(\mu)$ function, instrumental for the LDA method.
   - In **Section 2.3** the solution algorithm to the model integral equations is outlined, and the results of the controls on the accuracy of the algorithm (based on both numerical and analytical conditions) are shown.

3. In **Chapter 3** the LDA method and the TSS formalism, the two methods we will employ to analyze the physics of confined systems, are described from a general point of view and applied to the noninteracting, spinless tight–binding model.

4. **Chapter 4** contains the results obtained from the numerical solution of the model integral equations, both for the homogeneous system and (applied in the LDA approximation and compared with simulation data) for the confined system.

   - In **Section 4.1** the results of the numerical solution are employed to describe the $T = 0$ Phase Diagram of the Repulsive Hubbard Model in absence of magnetic field from a quantitative point of view, and to calculate the nonuniversal (interaction–dependent) behaviour of the correlation functions in the conducting phase.
   - In **Section 4.2** the TSS is used to predict the behaviour of the confined system in the **Dilute Limit** (increasing trap size l at fixed number of particles N) and the TSS accuracy is verified checking the actual convergence to the TSS behaviour of numerical simulation data.
   - In **Section 4.3** the solutions of the Model Integral Equations (in particular, the $n(\mu)$ function) are used to derive the spatial density of the confined system using the LDA method, and we study the structure of the corrections with respect to the LDA behaviour, quantified using simulation data.

Chapter 1

Lattice Models

1.1 The Tight–Binding Fermionic Model

1.1.1 Introduction

We study the tight–binding noninteracting model, following the analysis in [25], in order to determine its basic properties (Fermi Level and Level Occupation) and to determine its $T = 0$ phase diagram in absence of magnetic field: this will show a conducting phase delimited by two conductor–insulator transitions.

In the following, $\widehat{H}$ will always identify "Canonical" Hamiltonians, while $\widehat{K}$ will identify "Grand Canonical" ones (with the subtraction of $\mu\widehat{N}$). We will work on a one–dimensional lattice with L sites and unitary spacing (L is then the system length as well). The following Hamiltonian describes a $(1/2)$–spin fermionic tight–binding gas on this lattice, with a magnetic field in the z direction.

$$\widehat{K} = -w\sum_{j=1}^{L}\sum_{\sigma}\left(\widehat{C}^{\dagger}_{j\sigma}\widehat{C}_{(j+1)\sigma} + \widehat{C}^{\dagger}_{(j+1)\sigma}\widehat{C}_{j\sigma}\right) - \mu\sum_{j=1}^{L}\sum_{\sigma}\widehat{C}^{\dagger}_{j\sigma}\widehat{C}_{j\sigma} - 2B\sum_{j=1}^{L}\left(\frac{1}{2}\left(\widehat{C}^{\dagger}_{j\uparrow}\widehat{C}_{j\uparrow} - \widehat{C}^{\dagger}_{j\downarrow}\widehat{C}_{j\downarrow}\right)\right) \tag{1.1}$$

$$\equiv -\sum_{\sigma}\left[w\sum_{j=1}^{L}\left(\widehat{C}^{\dagger}_{j\sigma}\widehat{C}_{(j+1)\sigma} + \widehat{C}^{\dagger}_{(j+1)\sigma}\widehat{C}_{j\sigma}\right) + \mu_{\sigma}\sum_{j=1}^{L}\widehat{C}^{\dagger}_{j\sigma}\widehat{C}_{j\sigma}\right] \tag{1.2}$$

Defining $\mu_{\uparrow} \equiv \mu + B$ and $\mu_{\downarrow} \equiv \mu - B$. The w term allows fermionic "hopping" to nearest–neighbouring sites; the chemical potential and the magnetic field term, instead, introduce an energy offset, multiplied by the site occupation. Spin components are indipendent, and therefore the system behaves as the union of two spinless fermionic gases in the tight–binding approximation, with different chemical potentials.

Imposing periodic boundary conditions on the fermionic wavefunctions results in quantized momenta $k_j = (2\pi/L)n_j$, with n_j taking L integer values between $-(L/2)$ and $(L/2)$ (one of these endpoints must be dropped for even L). We can define creation and destruction operators in the momentum space, satisfying the identities

$$\widetilde{C}_{k_l\sigma} \equiv \frac{1}{\sqrt{L}} \sum_{j=1}^{L} e^{-ijk_l} \widehat{C}_{j\sigma} \qquad\qquad \widehat{C}_{j\sigma} \equiv \frac{1}{\sqrt{L}} \sum_{l=1}^{L} e^{ijk_l} \widetilde{C}_{k_l\sigma} \tag{1.3}$$

In terms of the operators in (1.3) the Hamiltonian (1.2) becomes

$$\widehat{K} = -\sum_{\sigma} \left[w \sum_{l=1}^{L} \left(\widetilde{C}^{\dagger}_{k_l\sigma} e^{ik_l} \widetilde{C}_{k_l\sigma} + \widetilde{C}^{\dagger}_{k_l\sigma} e^{-ik_l} \widetilde{C}_{k_l\sigma} \right) + \mu_\sigma \sum_{l=1}^{L} \widetilde{C}^{\dagger}_{k_l\sigma} \widetilde{C}_{k_l\sigma} \right] \equiv \sum_{\sigma} \sum_{l=1}^{L} \left(-2w \cos k_l - \mu_\sigma \right) \widetilde{N}_\sigma(k_l) \tag{1.4}$$

In the thermodynamic limit ($N, L \to \infty$ at fixed ratio N/L) this Hamiltonian becomes

$$\widehat{K} = \sum_{\sigma} \frac{L}{2\pi} \int_{-\pi}^{+\pi} \left(-2w \cos k - \mu_\sigma \right) \widetilde{N}_\sigma(k)\, dk \equiv \sum_{\sigma} \frac{L}{2\pi} \int_{-\pi}^{+\pi} \epsilon^0_\sigma(k) \widetilde{N}_\sigma(k)\, dk \tag{1.5}$$

$\epsilon^0_\sigma(k)$ is a single–particle energy contribution. Working at constant chemical potential, levels are filled until their occupation is not thermodynamically favourite: for $B = 0$, the Fermi Momentum can be found as the minimum of the momenta with $\epsilon^0_\sigma(k) \geq 0$. This implies

$$|k_{F\sigma}| = \begin{cases} 0 & \mu_\sigma \leq -2w \\ \arccos\left(-\dfrac{\mu_\sigma}{2w} \right) & -2w \leq \mu_\sigma \leq 2w \\ \pi & \mu_\sigma \geq 2w \end{cases} \tag{1.6}$$

The overall spatial density $n_c \equiv (n_\uparrow + n_\downarrow)$ is uniform due to the system spatial homogeneity, and may be found as the ratio between the number of particles and the system size: the former is not a conserved quantity in the Grand Canonical ensemble, and may be found since the N particles have their momenta, spaced of $2\pi/L$, in the interval $[-k_F, k_F]$, and each of these momenta is assigned to two particles (due to the spin degree of freedom).

$$n_c(\mu) = \frac{N}{L} = \frac{1}{L} \left(2 \cdot \frac{2k_F}{(2\pi/L)} \right) = \frac{2k_{F\sigma}}{\pi} \equiv 2n_\sigma(\mu) \qquad n_\sigma(\mu_\sigma) = \begin{cases} 0 & \mu_\sigma \leq -2w \\ \dfrac{1}{\pi} \arccos\left(-\dfrac{\mu_\sigma}{2w} \right) & |\mu_\sigma| \leq 2w \\ 1 & \mu_\sigma \geq 2w \end{cases} \tag{1.7}$$

Each spin polarization gives an occupation contribution n_σ; this function may be plotted, obtaining the graph in **Figure 1.1**. The system becomes an insulator, in absence of magnetic field, at $\mu = (\pm 2w)$ (the negative case corresponds to the empty lattice), when the Fermi Level reaches the limit of the cosine–shaped band described by $\epsilon^0_\sigma(k)$. At the $\mu = 2w$ transition both the polarized fermionic components have density $n_\sigma(2w) = 1$, and therefore the system becomes insulant when its band is twice–filled, as predicted by band theory.

It will also be useful to find the **Isothermal Compressibility** κ_T of the system as a function of the chemical potential. Thermodynamical relations can be used to link it to μ and the total density n_c:

$$\kappa_T = \left(-\frac{1}{v} \frac{\partial v}{\partial P} \right) = \frac{1}{n_c^2} \frac{\partial n_c}{\partial \mu} \equiv \frac{1}{n_c^2} \cdot \chi_n(\mu) \tag{1.8}$$

χ_n is also called **Charge Susceptivity**, and its counterpart for the magnetic field χ_m (with m replacing n and B replacing μ) is the Magnetic Susceptivity. The tight–binding fermionic gas is

then incompressible in the insulating region, while (1.7) yields, in the conducting region $(-2w) \leq \mu_\sigma \leq 2w$,

$$\chi_n(\mu) = \left[\frac{2}{\pi w}\left(\frac{1}{\sqrt{4-(\mu/w)^2}}\right)\right] \qquad \kappa_T = \frac{\pi^2}{4\left(\arccos\left(-\frac{\mu}{2w}\right)\right)^2}\cdot\chi_n(\mu) \tag{1.9}$$

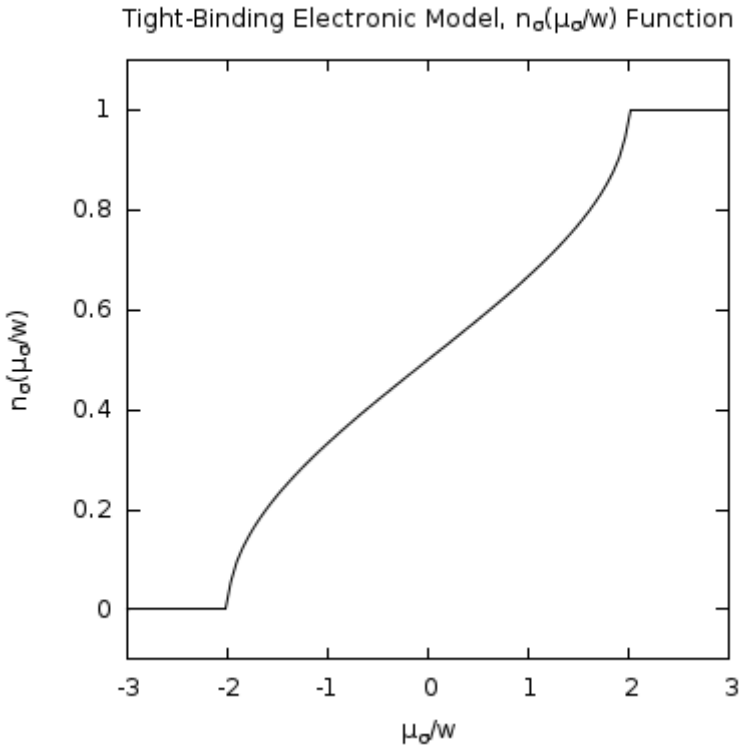

Figure 1.1: $n_\sigma(\mu_\sigma/w)$ *function for the Tight–Binding Fermionic Model.*

1.1.2 Critical Behaviour

In this section we study the noninteracting tight–binding model using the Path Integral formalism, described in [27]: the application of this method, following the arguments in [28], allows to charachterize the two quantum phase transitions at the borders of the conducting phase of the model.

The behaviour of the system in the conducting phase is analyzed using the Bosonization Method, following the arguments in [26]: we find this phase is equivalent to a collection of critical points, one for each value of μ between the two transition points, with correlation functions showing a power–law decay behaviour.

Finally, we study the effect of magnetic fields on the model, and extend the phase diagram to keep into account its presence, following the arguments in [25].

We will apply the Path Integral formalism to the $(1/2)$–Spin Tight Binding Model. As we are working in the Second Quantization Formalism, it turns out to be convenient to adapt the Path Integral Formalism in order to use eigenstates of the destruction operators: these vectors are called **Coherent States**, and their properties are described in [27].

Their use greatly simplifies the final relations, which will allow to write the Grand Partition Function in terms of classical fields (the eigenvalues of destruction operators over coherent states) instead of the operators themselves. The eigenvalues, though, need to anticommute as the operators, and this prohibits them from being standard complex numbers (as for bosonic operators). Eigenvalues belong to **Grassmann Algebras**, sets of anticommuting objects whose properties are described in [27].

Taking $B = 0$ for the sake of simplicity, the Path Integral Formalism allows to write the $T = 0$ Grand Partition Function for the "Canonical" Hamiltonian $\widehat{H}\left(\widehat{C}^{\dagger}_{i\sigma}, \widehat{C}_{i\sigma}\right)$ in terms of the fermionic, anticommuting, classical fields $\Psi_{i\sigma}$ as

$$Z = \int D\Psi^* \; D\Psi \; e^{-S} \qquad \begin{cases} S = \displaystyle\int_0^{+\infty} \left[\left(\sum_{i,\sigma} \Psi^*_{i\sigma}(\tau) \left(\frac{\partial}{\partial \tau} - \mu \right) \Psi_{i\sigma}(\tau) \right) + H\left(\Psi^*_{i\sigma}(\tau), \Psi_{i\sigma}(\tau)\right) \right] d\tau \\ \displaystyle\int D\Psi^* \; D\Psi \equiv \lim_{N\to\infty} \int \prod_{\sigma} \prod_{l=1}^{N} \prod_{i} d\Psi^*_{il\sigma} \; d\Psi_{il\sigma} \end{cases} \tag{1.10}$$

N is the number of slicings of the imaginary time interval $[0, \beta] = [0, +\infty)$. Fermionic eigenvalues $(\Psi_{i\sigma}, \Psi^*_{i\sigma})$ replace, in $\widehat{H}$, their operators $\left(\widehat{C}_{i\sigma}, \widehat{C}^{\dagger}_{i\sigma}\right)$.

This formalism can be applied both in the coordinate and in the momentum space: to simplify calculations, we will work in the momentum domain (where i runs on the reciprocal lattice and identifies fields $\Psi_{k_i\sigma} \equiv \Psi_{i\sigma}$). In this case the Spinless, Tight–Binding "Grand Canonical" Hamiltonian (1.5) and the corresponding action $S\left(\Psi^*_{i\sigma}, \Psi_{i\sigma}\right)$ in (1.10) are

$$\widehat{K} = \sum_{i,\sigma} \left(-2w \cos k_i - \mu\right) \Psi^*_{i\sigma} \Psi_{i\sigma} \equiv \sum_{i,\sigma} \epsilon^0(k_i) \Psi^*_{i\sigma} \Psi_{i\sigma} \qquad S = \int_0^{+\infty} \sum_{i,\sigma} \left(\Psi^*_{i\sigma} \frac{\partial \Psi_{i\sigma}}{\partial \tau} + \epsilon^0(k) \Psi^*_{i\sigma} \Psi_{i\sigma} \right) d\tau \tag{1.11}$$

In the Thermodynamic Limit, the theory becomes (omitting the τ dependence of the fields to enlighten the notation)

$$Z = \int D\Psi^* \; D\Psi \; \exp\left(- \int_0^{+\infty} \int_{-\pi}^{+\pi} \mathcal{L}(\Psi_\sigma^*, \Psi_\sigma) \; \frac{dk}{2\pi} \; d\tau \right) \tag{1.12}$$

$$\mathcal{L}(\Psi_\sigma^*, \Psi_\sigma) = \sum_\sigma \left\{ \Psi_\sigma^*(k) \frac{\partial \Psi_\sigma(k)}{\partial \tau} + (-2w \cos k - \mu) \, \Psi_\sigma^*(k) \Psi_\sigma(k) \right\} \equiv \sum_\sigma \mathcal{L}_\sigma(\Psi_\sigma^*, \Psi_\sigma) \tag{1.13}$$

Isolated Critical Points. The critical behaviour of the model can be investigated by looking for invariance under scaling transforms (these imply the existence of a fixed point, which must be linked to a critical surface). The single–particle energy contribution can be expanded in power series to identify them.

The first critical point is at $T = 0$, $\mu' \equiv \mu + 2w = 0$ (corresponding, according to (1.6), to $k_F = 0$). This can be shown expanding $\epsilon^0(k)$ in proximity of $k = 0$ (implying single–particle excitations with long wavelength modes are dominant) up to the second order in (1.13) to find the effective low–energy Lagrangian Density

$$\mathcal{L}_0(\Psi_\sigma^*(k), \Psi_\sigma(k)) \equiv \sum_\sigma \left\{ \Psi_\sigma^*(k) \frac{\partial \Psi_\sigma(k)}{\partial \tau} + \frac{k^2}{2m} \Psi_\sigma^*(k) \Psi_\sigma(k) - \mu' \Psi_\sigma^*(k) \Psi_\sigma(k) \right\} \tag{1.14}$$

Defining $m \equiv (2w)^{-1}$. Every spin component acts indipendently from the other, and therefore in this limit the system behaves as the union of two spinless non–relativistic fermionic gases. The theory is invariant under a scaling transform of rescaling factor b if this yields the scale factor b^{z-1} the Lagrangian needs to keep the action scale–invariant: this happens if the transform for $\mu' = 0$ is defined as

$$k \to k' \equiv k b^{+1} \qquad \tau \to \tau' \equiv \tau b^{-z} \qquad \Psi_\sigma(k) \to \Psi'_\sigma(k) \equiv \Psi_\sigma(k) b^{-1/2} \qquad m \to m' \equiv m \qquad z = 2 \tag{1.15}$$

In order to keep invariant the theory, a nonzero chemical potential μ' must satisfy the identities

$$\mu' \to \mu'' \equiv \mu' \cdot b^2 \qquad y^0_{\mu'} \equiv \dim \mu' = 2 \qquad \nu_0 = \left(y^0_{\mu'} \right)^{-1} = \frac{1}{2} \tag{1.16}$$

The last equality holds since μ' is the main relevant perturbation in proximity of the critical point. More perturbations may be defined and added to the theory, provided they do not vanish: for instance, a simple contact interaction in the coordinate domain, regardless of the involved spin components (a, b), does,

$$\mathcal{L}' = \left(\Psi_a^*(x) \Psi_b(x) \right)^2 = \Psi_a^*(x) \Psi_b(x) \Psi_a^*(x) \Psi_b(x) = -\Psi_a^*(x) \Psi_b^2(x) \Psi_a^*(x) = 0 \tag{1.17}$$

The fields are anticommuting but classical: it would be nonzero if written in terms of fermionic quantum operators, for $a \neq b$. Momenta (gradients in the spatial domain) may be employed to avoid this: however, the more gradients are added, the more irrelevant the coupling becomes (its dimension must decrease in order to keep the overall dimension of the term fixed to 1). This means this kind of perturbations will not modify the core properties around the $(T = 0, \mu' = 0)$ critical point (they may only introduce some corrections to scaling behaviour, but their importance decreases as the critical point becomes closer). This kind of terms are also what arises from considering further neighbour interactions, making them irrelevant as well ([28]).

The critical properties at $T = 0, \mu' = 0$ (in terms of the fermionic fields around the Fermi Level) can be extended to the point $\mu = 2w$ (corresponding to $k_F = \pi$) by noting that the system is invariant under particle–hole inversion: for $k_F = \pi$ the dominant fluctuations are fermionic holes whose effective theory is equivalent to (1.14) in terms of the hole fields (at $\mu = 2w$ their Fermi Level is $k_F^{(h)} = 0$). We have therefore another critical point at $T = 0, \mu = 2w$ with $z = 2$ and $\nu = 1/2$.

Conducting Phase. For $T = 0$ and $(-2w) < \mu < (2w)$ (that is, $0 < k_F < \pi$) the system can be modelized as a conductor in its ground state, with all levels occupied up to the Fermi Momentum, and no particles with higher momentum. In our description momenta are continuous, and therefore excitations can happen at arbitrarily low energies if they involve fermions in proximity of the Fermi Momentum: this kind of fluctuations will therefore be dominant.

The expansion of $\epsilon^0(k)$ around the Fermi Momentum, this time, shows a nonzero, dominant linear term: excitations may happen for $k \cong k_F$ (we will call these "right–movers", identified in the coordinate domain by a continuous *quantum* field $\psi_{R\sigma}(x)$) and for $k \cong -k_F$ (these will be named "left–movers", $\psi_{L\sigma}(x)$).

Instead of describing the system with single–particle, fermionic fields, it is more useful to linearize the original Quantum Hamiltonian (1.5) and to rephrase it in terms of new effective fields: these will represent density fluctuations, corresponding in this case to particle–hole excitations.

As density operators contain two fermionic operators, they satisfy bosonic commutation rules, and therefore the nature of these excitations is bosonic: bosonic quantum fields may therefore be used to create the effective theory of the model. This formalism will be especially useful in the case of interacting systems.

For spinful systems, these fluctuations can be divided in pure–charge, spinless excitations (**Charge Density Waves**, CDW, described by a bosonic field $\phi_\rho(x)$ and its canonically conjugate field $\Pi_\rho(x)$) and as pure–spin excitations (**Spin Density Waves**, SDW, described by the fields $\phi_\sigma(x)$ and $\Pi_\sigma(x)$). Their fields can be appropriately defined in terms of fermionic operators, and applying the mapping described in [26] we find the effective Hamiltonian

$$\widehat{K} = \frac{1}{2\pi} \sum_{\nu=\rho,\sigma} \int v_F \left[(\pi \Pi_\nu(x))^2 + (\nabla \phi_\nu(x))^2 \right] dx \qquad v_F \equiv \left(\frac{\partial \epsilon^0(k)}{\partial k} \right)_{k=k_F} = 2w \sin k_F(\mu) \quad (1.18)$$

This is a noninteracting bosonic field theory, with dynamical critical exponent $z = 1$. It allows several kinds of fluctuations: the most common are the previously introduced CDW and SDW, **Singlet Pairs** (two–particle fluctuations, with the components in an overall $S = 0$ state) and **Triplet Pairs**. In terms of the continuum fermionic fields $\psi_{(R,L)\sigma}(x)$, these are described by the operators (for $a = x, y, z$)

$$\begin{aligned} O_{CDW}(x) &\equiv \sum_{\sigma,\sigma'} \psi^\dagger_{R\sigma} \delta_{\sigma\sigma'} \psi_{L\sigma'}(x) & O^a_{SDW}(x) &\equiv \sum_{\sigma,\sigma'} \psi^\dagger_{R\sigma} \widehat{\sigma}^a_{\sigma\sigma'} \psi_{L\sigma'}(x) \\ O_{SP}(x) &\equiv \sum_{\sigma,\sigma'} \psi^\dagger_{R\sigma} \delta_{\sigma\sigma'} \psi^\dagger_{L,-\sigma'}(x) & O_{TP}(x) &\equiv \sum_{\sigma,\sigma'} \psi^\dagger_{R\sigma} \widehat{\sigma}^a_{\sigma\sigma'} \psi^\dagger_{L,-\sigma'}(x) \end{aligned} \quad (1.19)$$

For the noninteracting lattice model, the correlation functions G of all these fluctuations show a universal power–law behaviour $G \sim x^{-2}$. The conducting phase for $(-2w) < \mu < 2w$ can therefore be interpreted as a collection of critical points, each one defined by a different value of μ, as pointed out by the charachteristic power–law, critical behaviour of the correlation functions.

Magnetic Field Effects

We can now study the effects of a magnetic field $B > 0$ on the noninteracting tight–binding model. In the thermodynamical limit overall density and magnetization can be found (exploiting (1.7)) as

$$n_c = \sum_{\sigma=\uparrow,\downarrow} \int_{-k_{F\sigma}}^{k_{F\sigma}} n_\sigma(k)\, dk = \frac{1}{\pi} \sum_\sigma k_{F\sigma} \qquad m = \frac{1}{2}\left[\int_{-k_{F\uparrow}}^{k_{F\uparrow}} n_\uparrow(k)\, dk - \int_{-k_{F\downarrow}}^{k_{F\downarrow}} n_\downarrow(k)\, dk \right] = \frac{(k_{F\uparrow} - k_{F\downarrow})}{2\pi} \tag{1.20}$$

Considering the case $\mu < 0$ (which corresponds to a less–than–half filled band) the phase diagram for the tight–binding model can be drawn as in **Figure 1.2**. If we describe the ground state in terms of two bands (one for each spin polarization) we can identify the following phases:

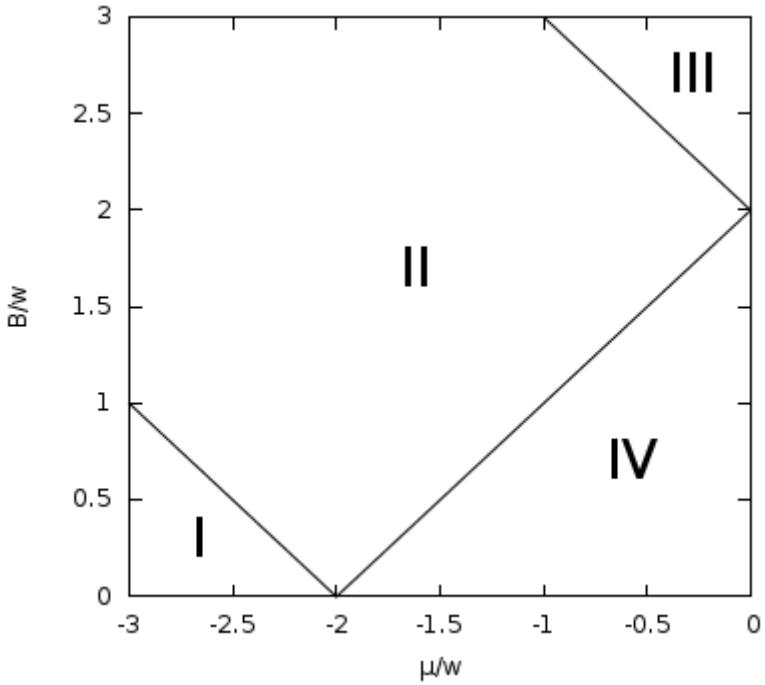

Figure 1.2: $T = 0$ *Phase Diagram of the Fermi Gas.*

- **Phase I,** $k_{F\uparrow} = k_{F\downarrow} = 0$**: Empty Lattice.** Here both bands are empty, and the ground state is an empty lattice (every increase in site occupation increases the system energy). Both density and magnetization are 0; the chemical potential must be negative enough ($\max(\mu_\uparrow, \mu_\downarrow) = (\mu + B)/w \leq (-2)$, and then $\mu \leq (-2w - B)$) to allow this to happen.
- **Phase II,** $k_{F\downarrow} = 0$ **and** $0 \leq k_{F\uparrow} \leq \pi$**: Partially Filled, Spin–Polarized Band.** Here the spin–down band is empty while the spin–up one is partially filled by fermions in the conducting phase seen in the previous section. The magnetization is equal to half the density, which varies between 0 and 1. Using (1.7) we find

$$n_c = 2m = \frac{k_{F\uparrow}}{\pi} = \frac{1}{\pi} \arccos\left(-\frac{\mu + B}{2w}\right) \qquad \chi_n(\mu, B) = \frac{\partial n_c}{\partial \mu} = \frac{1}{\pi w \sqrt{4 - [(\mu + B)/w]^2}} \tag{1.21}$$

  χ_n diverges for $B \to \pm 2w - \mu$, as the boundaries with, respectively, Phases III (+) and I (-) are approached.

- **Phase III, $k_{F\downarrow} = 0$ and $k_{F\uparrow} = \pi$: Half Filled, Spin–Polarized Band.** The spin–down band is empty and the spin–up one is completely filled by conducting fermions. In this phase $n_c = 1$ and $m = \frac{1}{2}$.
- **Phase IV, $0 \leq k_{F\uparrow}, k_{F\downarrow} \leq \pi$: Partially Filled, Magnetized Band.** Both bands are partially filled by conducting fermions, density varies between 0 and 1 and magnetization between 0 and $\frac{1}{2}$. In this phase

$$n_c = \frac{1}{\pi}\left[\arccos\left(-\frac{\mu+B}{2w}\right) + \arccos\left(-\frac{\mu-B}{2w}\right)\right] \tag{1.22}$$

$$m = \frac{1}{2\pi}\left[\arccos\left(-\frac{\mu+B}{2w}\right) - \arccos\left(-\frac{\mu-B}{2w}\right)\right] \tag{1.23}$$

$$\chi_n(\mu, B) = \frac{\partial n_c}{\partial \mu} = 2\frac{\partial m}{\partial B} = 2\chi_m(\mu, B) = \frac{1}{\pi w}\left[\frac{1}{\sqrt{4 - [(\mu+B)/w]^2}} + \frac{1}{\sqrt{4 - [(\mu-B)/w]^2}}\right] \tag{1.24}$$

  Susceptivities diverge for $B \to (\mu + 2w)$, as the boundary with Phase II approaches.

Susceptivities diverge at the boundaries between Phases II–I, II–III and II–IV, suggesting Quantum Phase Transitions: in all of them, the Susceptivity Critical Exponent is $\frac{1}{2}$, as its singular part becomes $\chi^* \sim A + B|g|^{-1/2}$, where g is the critical parameter ($g = (2w \pm (\mu + B))$ for, respectively, the II–I and II-III transitions, while $g = (2w + (\mu - B))$ for the II-IV).

1.2 The Bose–Hubbard Model

We introduce the Bose–Hubbard Model, the bosonic equivalent of the Hubbard Model, deriving its Hamiltonian by discretizing a continuous bosonic model with a contact interaction, similarly to what done in [29]. Subsequently, we prove the equivalence in $d = 1$ between the model in its Hardcore Limit (the limit of infinitely strong interactions) and a spinless, tight–binding fermionic gas, following the arguments in [28].

The Bose–Hubbard Model, the bosonic counterpart of the Hubbard Model, can be used to modelize a system of interacting bosons on a 1D lattice. Its Hamiltonian can be derived by the discretization of a continuous model for interacting bosons: using the approximations outlined in the introduction, bosonic interactions can be approximated with a contact interaction, and the resulting continuous model is

$$\widehat{H} = \int \phi^\dagger(x) \left(-\frac{\hbar^2}{2m} \frac{\partial^2}{\partial x^2} \right) \phi(x)\, dx + g_{1D} \iint \phi^\dagger(x)\phi^\dagger(y)\delta\left(x-y\right)\phi(x)\phi(y)\, dx\, dy \tag{1.25}$$

In terms of the bosonic fields $\phi(x)$, and with g_{1D} appropriately defined in terms of the effective 1D Scattering Length. Bosonic fields can be expanded over a complete function set: to keep into account lattice effects, we will choose a set of localized functions centered on lattice sites x_i (**Wannier Functions**, denoted by $W(x - x_i)$). The field can then be expanded as

$$\phi(\boldsymbol{x}) = \sum_{i=1}^{L} W(\boldsymbol{x} - \boldsymbol{x}_i)\widehat{b}_i \tag{1.26}$$

Replacing the field definitions in terms of the Wannier functions in (1.25) and exploiting the set orthogonality yields

$$\widehat{H} = \sum_{i,j=1}^{L} \widehat{b}_j^\dagger \widehat{b}_i \left(\int W^*(x - x_j) \left(-\frac{\hbar^2}{2m} \frac{\partial^2}{\partial x^2} \right) W(x - x_i)\, dx \right) + g_{1D} \sum_{i=1}^{L} \widehat{b}_i^\dagger \widehat{b}_i^\dagger \widehat{b}_i \widehat{b}_i \left(\int |W(x - x_i)|^4\, dx \right) \tag{1.27}$$

The integrals may be collected into conveniently defined coefficients, and bosonic operators may be rearranged using their commutation rules. Finally, the **Tight–Binding** hypothesis may be applied: this consists in supposing hopping contribution are nonzero only between nearest neighbours, and in this case all contributions have the same value w. This approximation is good as long as Wannier functions are strongly localized on their sites. The resulting "Canonical" and "Grand Canonical" Hamiltonians are

$$\widehat{H} = -w \sum_{\{i,j\}} \widehat{b}_i^\dagger \widehat{b}_j + \frac{U}{2} \sum_{i=1}^{L} \widehat{b}_i^\dagger \widehat{b}_i \left(\widehat{b}_i^\dagger \widehat{b}_i - 1 \right) \qquad \widehat{K} \equiv \widehat{H} - \mu \sum_{i=1}^{L} \widehat{b}_i^\dagger \widehat{b}_i \tag{1.28}$$

This Hamiltonian describes the **Bose–Hubbard Model**, and is used to approximate quantitatively the behaviour of bosonic optical lattices ([29], [30], [31]).

Henceforth we will restrict to the analysis of the repulsive Bose–Hubbard Model ($U > 0$): similarly to the fermionic model in (1.2), the BH Hamiltonian $\widehat{K}$ contains a hopping term and an offset term, while the last term depends on U and pictures the simplest repulsive interaction between bosons, depending on the number of pairs on the same site (in this model only bosons on the same site interact).

The Hardcore Limit

It is instructive to understand what happens to the Bose–Hubbard Model in the **Hardcore Limit** (the limit of infinite repulsion strength, $w/U \to 0$). Physically, in order to avoid large increases in the system energy, the ground state site occupation numbers $\widehat{n}_i$ can only assume the values 0 and 1, making the interaction term vanish and leaving a bosonic tight–binding Hamiltonian, with an effective "Pauli Restraint" applied (due only to interactions, since the particles are bosonic). This model is very similar to a spinless fermionic tight–binding model.

For $N < L$ (or depending on external conditions determining the particle number, in the hypothesis μ is the indipendent variable) bosons may hop to empty sites, while their positions are locked for $N = L$, and it becomes impossible to add more bosons by changing μ. These two cases describe respectively a conducting and an insulating ground state: the insulating properties of the latter are caused entirely by the interaction, and this kind of phase is called **Mott Insulator** (as we will see, such phases can appear in fermionic systems as well).

Similarities between the hardcore Bose–Hubbard gas and the fermionic spinless tight–binding one can be proven more rigorously in $d = 1$: the first step is mapping the model to a set of $(1/2)$–spin fermions with nearest–neighbour exchange interaction, defining $\mid n_i = 0 \rangle \to \mid \uparrow_i \rangle$, $\mid n_i = 1 \rangle \to \mid \downarrow_i \rangle$ and

$$\widehat{\sigma}_j^x \equiv \widehat{b}_j^\dagger + \widehat{b}_j \qquad \widehat{\sigma}_j^y \equiv i\left(\widehat{b}_j^\dagger - \widehat{b}_j\right) \qquad \widehat{\sigma}_j^z \equiv 1 - 2\widehat{b}_j^\dagger \widehat{b}_j \tag{1.29}$$

The commutation rules for bosonic operators, paired with the condition $\left(\widehat{b}_i^\dagger\right)^2 = 0$ on the hardcore states, ensures these transformations satisfy the commutation rules $\left[\widehat{\sigma}_i^a, \widehat{\sigma}_j^b\right] = 2i\delta_{ij}\epsilon^{abc}\widehat{\sigma}_j^c$. Applying the transformation, and exploiting commutation of the Pauli Matrices over different sites, the Hamiltonian (1.28) becomes (not taking into account an additive constant)

$$\widehat{K}_{XX} \equiv -\frac{w}{2}\sum_{\{i,j\}}\left(\widehat{\sigma}_i^x\widehat{\sigma}_j^x + \widehat{\sigma}_i^y\widehat{\sigma}_j^y\right) + \frac{\mu}{2}\sum_{i=1}^{L}\widehat{\sigma}_i^z \tag{1.30}$$

This Hamiltonian is identical to the **XX Hamiltonian**, which describes $(1/2)$–spin fermions on lattice sites with a nearest–neighbour ferromagnetic exchange interaction and a transverse magnetic field. If $d = 1$ the model can be remapped further using the **Jordan–Wigner Transformation**: this mapping transforms commuting (on different sites) spin operators in anticommuting spinless fermionic operators, and is defined (in terms of spinless fermionic operators $\widehat{c}$) as

$$\widehat{\sigma}_i^+ = \frac{\widehat{\sigma}_i^x + i\widehat{\sigma}_i^y}{2} \equiv \prod_{j<i}\left(1 - 2\widehat{c}_j^\dagger\widehat{c}_j\right)\widehat{c}_i \qquad \widehat{\sigma}_i^- = \frac{\widehat{\sigma}_i^x - i\widehat{\sigma}_i^y}{2} \equiv \prod_{j<i}\left(1 - 2\widehat{c}_j^\dagger\widehat{c}_j\right)\widehat{c}_i^\dagger \tag{1.31}$$

Using this mapping in (1.30) yields

$$\widehat{K} = -\sum_{i=1}^{L}\left(w\left(\widehat{c}_{i+1}^\dagger\widehat{c}_i + \widehat{c}_i^\dagger\widehat{c}_{i+1}\right) + \mu\cdot\widehat{c}_i^\dagger\widehat{c}_i\right) \tag{1.32}$$

This Hamiltonian pictures a spinless tight–binding fermionic system, and all results found for similar systems in previous sections can be applied: for instance, the bosonic lattice will be empty for $\mu \leq (-2w)$ (this is the Mott Insulator configuration with $n_0 = 0$). If, instead, $\mu \geq 2w$, density is fixed to $n = 1$, and indipendent on the chemical potential (picturing the Mott Insulator with $n_0 = 1$): if $|\mu| < 2w$, finally, the system is in a conducting state (in which bosons behave as spinless fermions).

1.3 The Hubbard Model

1.3.1 Introduction

Following the arguments in [25], we introduce the Hubbard Model and analyze its behaviour in the two limits of vanishing and infinite repulsive interaction, in order to understand the two phases favoured by the Hamiltonian terms. These arguments suggest a Quantum Phase Transition between a Conducting and an Insulating ground state at Half–Filling.

The **Hubbard Model** is the simplest model for a lattice system of interacting fermions. In the hypotheses outlined in the introduction, its Hamiltonian can be derived, as done for the Bose–Hubbard one, discretizing a continuous, single–band fermionic model with a contact interaction, called **Gaudin–Yang Model**:

$$H = \sum_{a=\uparrow,\downarrow} \int \psi_a^\dagger(x) \left(-\frac{\hbar^2}{2m} \frac{\partial^2}{\partial x^2} \right) \psi_a(x)\, dx + g_{1D} \iint \psi_\downarrow^\dagger(x) \psi_\uparrow^\dagger(y) \cdot \delta(x-y) \cdot \psi_\uparrow(y) \psi_\downarrow(x)\, dx\, dy \quad (1.33)$$

The process leading to (1.28) (through the expansion of the fields in Wannier functions, integrations and definition of couplings) can be repeated in this case as well. The resulting Hamiltonian is

$$\widehat{H} = -w \sum_{j=1}^{L} \sum_{a=\uparrow,\downarrow} \left(\widehat{C}_{ja}^\dagger \widehat{C}_{(j+1)a} + \widehat{C}_{(j+1)a}^\dagger \widehat{C}_{ja} \right) + U \sum_{j=1}^{L} \widehat{N}_{j\uparrow} \widehat{N}_{j\downarrow} \quad (1.34)$$

This Hamiltonian describes the Hubbard Model: we will complement it with periodic boundary conditions, $\widehat{C}_{(L+1)a} = \widehat{C}_{1a}$, giving the system invariance under cyclical permutations of the sites (or, equivalently, invariance under translations on a ring of L sites). We can also note the system is spatially homogeneous, and therefore all sites will share the same occupation number.

In order to understand the physical phenomena undergoing in the model, we may describe its behaviour in the limits $w/U \to +\infty$ and $w/U \to 0$, where the model is easily diagonalized by two different sets of states. In all our work, we will restrict to the *Repulsive* Hubbard Model ($U > 0$), and we will define **Half–Filling** the situation with site occupation number $n = 1$ (i.e. half the allowed lattice filling).

- For $w/U \to +\infty$ the Hubbard Model reduces to a $(1/2)$–Spin Tight–Binding Model. In the system eigenstates, fermions have definite spin polarization and momentum. These will be called **Momentum States**, and their overall number is finite (it is 4^L, since every site may hold from none to two $(1/2)$–Spin fermions).
- For $w/U \to 0$ the interaction term $\widehat{H}_A$, called **Atomic Hamiltonian**, is dominant. In its eigenstates fermions have definite coordinates and spin polarization: these states will be called **Localized States**. The atomic term modelizes on–site interaction, and its contribution grows as the number of doubly–occupied sites increases since $U > 0$.

  The physics of the model in the limit $U \to +\infty$ can be described noting that in this limit the number of doubly–occupied sites must be small to avoid large increases in the system energy. This allows to restrict the system analysis to states containing only singly–occupied sites, through the action of the projector on these states $\widehat{P}$.

  In this approximation, second–order perturbation theory in the parameter U^{-1} can be applied to the Hubbard Hamiltonian, and we might neglect three–site, $O(U^{-1})$ terms in the outcoming result (this approximation is equivalent to supposing the system is close to half–filling). The resulting Hamiltonian, called $t - J$ **Hamiltonian**, is

$$\widehat{H}_{tJ} = \widehat{P}\left[-w\sum_{j=1}^{L}\left(\widehat{C}^{\dagger}_{ja}\widehat{C}_{(j+1)a} + \widehat{C}^{\dagger}_{(j+1)a}\widehat{C}_{ja}\right)\right]\widehat{P} + \widehat{P}\left[\frac{4w^2}{U}\sum_{j=1}^{L}\left(S^{\alpha}_{j}S^{\alpha}_{(j+1)} - \frac{\widehat{N}_j\widehat{N}_{(j+1)}}{4}\right)\right]\widehat{P} \tag{1.35}$$

$$\equiv \widehat{P}\widehat{H}_w\widehat{P} + \widehat{P}\widehat{H}_h\widehat{P} \tag{1.36}$$

For $\alpha = x, y, z$. At Half–Filling this Hamiltonian becomes the Hamiltonian of an antiferromagnetic Heisenberg Chain (periodic boundary conditions for the spins are imposed). The excitations of the Hubbard Model at half–filling for $U \to +\infty$ are then described by those of the Heisenberg Antiferromagnetic Chain, and in particular the system is an insulator in these conditions (the hopping term vanishes). The insulating properties are caused by fermionic interactions, rather than by the Pauli Principle (the band is half–filled) and therefore the system is in a Mott Insulating Phase.

The tight–binding term and the atomic term do not commute, and therefore neither of these two sets of states solves the Hamiltonian with both terms present (eigenstates for a nonzero but finite value of U will be constructed in the next sections). At half–filling, in particular, the ground states in the two limits differ dramatically (the system conduces for $U = 0$ and is insulating for $U \to +\infty$), suggesting the existence of a Quantum Phase Transition at half–filling, driven by fermionic interactions, between a Mott–Insulating Ground State and a Conducting Ground State.

In the following all couplings will be measured in units of w, and we will use the coefficient $u \equiv U/4w$: the Hubbard Hamiltonian (1.34) becomes

$$\widehat{H} = -\sum_{j=1}^{L}\sum_{a=\uparrow,\downarrow}\left(\widehat{C}^{\dagger}_{ja}\widehat{C}_{(j+1)a} + \widehat{C}^{\dagger}_{(j+1)a}\widehat{C}_{ja}\right) + 4u\sum_{j=1}^{L}\widehat{N}_{j\uparrow}\widehat{N}_{j\downarrow} \tag{1.37}$$

The Hamiltonian can be translated in its "Grand Canonical" version, and a magnetic field B in the z direction can be kept in account: the resulting Hamiltonian is

$$\widehat{K} \equiv \widehat{H} - \mu\sum_{j=1}^{L}\left(\widehat{N}_{j\uparrow} + \widehat{N}_{j\downarrow}\right) - B\sum_{j=1}^{L}\left(\widehat{N}_{j\uparrow} - \widehat{N}_{j\downarrow}\right) \equiv \widehat{H} - \mu\left(\widehat{N}_{\uparrow} + \widehat{N}_{\downarrow}\right) - B\left(\widehat{N}_{\uparrow} - \widehat{N}_{\downarrow}\right) \equiv \widehat{H} - \mu\widehat{N} - 2B\widehat{S}_z \tag{1.38}$$

Since $\left[\widehat{S}_z, \widehat{H}\right] = \left[\widehat{N}, \widehat{H}\right] = 0$, $\widehat{K}$ and $\widehat{H}$ have the same eigenfunctions. These two separate commutations imply the number of both "up" and "down" spins are separately conserved: in the following $N = N_{\uparrow} + N_{\downarrow}$ will denote the total conserved number of fermions and $M = N_{\downarrow}$ will denote the number of "down"–spin fermions (and therefore the z component of the total spin will be $S_z = N/2 - M$).

Another form of the Hamiltonian (1.37), useful due to its symmetry properties for even L, may be obtained summing to it the operator $-2u\widehat{N} + uL$: this term does not change the previously shown symmetries since it commutes with both $\widehat{N}$ and $\widehat{N}_{\downarrow}$, and the Hamiltonian becomes

$$\widehat{H} = -\sum_{j=1}^{L}\sum_{a=\uparrow,\downarrow}\left(\widehat{C}^{\dagger}_{ja}\widehat{C}_{(j+1)a} + \widehat{C}^{\dagger}_{(j+1)a}\widehat{C}_{ja}\right) - 2u\left[\sum_{j=1}^{L}\left(\widehat{N}_{j\uparrow} + \widehat{N}_{j\downarrow} - 2\widehat{N}_{j\uparrow}\widehat{N}_{j\downarrow} - \frac{1}{2}\right)\right]$$

$$= -\sum_{j=1}^{L}\sum_{a=\uparrow,\downarrow}\left(\widehat{C}^{\dagger}_{ja}\widehat{C}_{(j+1)a} + \widehat{C}^{\dagger}_{(j+1)a}\widehat{C}_{ja}\right) + u\sum_{j=1}^{L}\left(1 - 2\widehat{N}_{j\uparrow}\right)\left(1 - 2\widehat{N}_{j\downarrow}\right) \tag{1.39}$$

1.3.2 Critical Properties

We employ the Path Integral and the Bosonization Method to understand the Critical Behaviour of the Hubbard Model: depending on the site occupation, the model is described by different effective theories.

The resulting critical behaviour shows a transition driven by the chemical potential to the empty lattice, a conducting phase showing power–law–decaying correlation functions (whose properties are described following the arguments in [26]) and two Conductor–Insulator transitions at half–filled band: one of them is driven by the chemical potential, while the other is driven by fermionic interactions and belongs to the Kosterlitz–Thouless Universality Class (as shown in [26]).

The critical behaviour of the Hubbard Hamiltonian for $B = 0$ can be studied using different effective theories, depending on the value of the overall site occupation $n_c \equiv n_\uparrow + n_\downarrow$ (shared by all sites due to the model homogeneity).

Dilute Limit. For $n_c \cong 0$, the system excitations can be represented by single–particle modes. In this limit, the Hamiltonian (1.34) generates, applying the Path Integral formalism as in (1.10), the action

$$S = \int_0^{+\infty} \int_{-\pi}^{+\pi} \left\{ \sum_\sigma \Psi_\sigma^*(k) \left[\frac{\partial}{\partial \tau} + \left(\frac{k^2}{2m} - \mu' \right) \right] \Psi_\sigma(k) + U \int_{-\pi}^{+\pi} \Psi_\downarrow^*(q) \Psi_\uparrow^*(k) \Psi_\uparrow(p) \Psi_\downarrow(k-p+q) \, \frac{dp \, dq}{(2\pi)^2} \right\} \frac{dk}{2\pi} \, d\tau \tag{1.40}$$

The parameters m, μ' are defined as for the theory (1.14): this theory shows invariance under the transformations (1.15) at the fixed point $u = 0$, $\mu' = 0$, $T = 0$. At this fixed point, compatibility of scaling dimensions implies $\dim(\mu') = 2$ (as in the free theory) and $\dim(U) = 1$ (the interaction is therefore a relevant perturbation).

Intermediate Filling. For $0 < n_c < 1$ it is convenient to modelize the system using the Bosonization method to describe the resulting collective excitations. In the limit of weak interactions, fluctuations in proximity of the noninteracting Fermi Momentum remain dominant: the kinetic spectrum linearization and the Bosonization mapping that led to (1.18) can be applied to (1.39), yielding

$$\widehat{K} = \frac{1}{2\pi} \sum_{\nu=\rho,\sigma} \int \left[u_\nu K_\nu \left(\pi \Pi_\nu(x) \right)^2 + \frac{u_\nu}{K_\nu} \left(\nabla \phi_\nu(x) \right)^2 \right] \, dx + \frac{2U}{(2\pi\alpha)^2} \int \cos\left(\sqrt{8} \phi_\sigma \right) \, dx \tag{1.41}$$

As will be proven when describing the model symmetries, the phases we describe are those of the $\mu \leq 0$ region, and the phases in this region will be the same of the $\mu \geq 0$ one, only with particles replaced by holes. The first effect of interactions is to introduce anisotropies between the spin and the charge part, giving these two excitations two different "velocities", (u_ρ, u_σ): the parameters (K_ρ, K_σ) are called **Luttinger Parameters**, and α is a short–distance cutoff. Furthermore, a new non–kinetic term for the spin field appears. The Luttinger parameters in (1.41) are

$$u_\rho = v_F \sqrt{1 + \frac{U}{\pi v_F}} \qquad u_\sigma = v_F \sqrt{1 - \frac{U}{\pi v_F}} \qquad K_\rho = \left(1 + \frac{U}{\pi v_F} \right)^{-1/2} \qquad K_\sigma = \left(1 - \frac{U}{\pi v_F} \right)^{-1/2} \tag{1.42}$$

Where v_F is the Fermi Velocity of the noninteracting system in (1.18). The terms in (1.41) must be complemented, for higher U, by higher gradients of the fields and cosine terms of higher harmonics:

although irrelevant by scaling transforms, these terms give nontrivial corrections to the excitation velocities and to the Luttinger Parameters, which deviate from the weak–interaction behaviour in (1.42). The behaviour of the Luttinger parameters and of the excitations velocities will have to be computed using the Bethe *Ansatz* solution data.

The spin part of the Hamiltonian in (1.41) is a **Sine–Gordon Hamiltonian**, whose renormalization flow is such that for $K_\sigma > 1$ the cosine term is irrelevant and flows to $K_\sigma^* = 1$: in the weak coupling limit, this happens for $U > 0$, our case of interest.

Although the extension would be incorrect in general, we can anticipate the critical behaviour remains the same for strong coupling, since we will find no sign of singular behaviour for $0 < n_c < 1$ induced by U in the Bethe *Ansatz* solutions: the effective theory for $0 < n_c < 1$ remains the same even beyond the weak coupling limit (although the functional forms of the Luttinger Parameters in terms of U and μ change: methods to find them from the Bethe *Ansatz* solutions will be described later).

Both the charge part and the spin part describe massless, bosonic, relativistic systems: the correlation functions of the excitations in (1.19) can be calculated, and their dominant scaling behaviour is

$$\begin{cases} \left\langle O^\dagger_{CDW}(x) O_{CDW}(0) \right\rangle \sim \left\langle (O^z)^\dagger_{SDW}(x) O^z_{SDW}(0) \right\rangle \sim \dfrac{e^{2ik_F x}}{2(\pi\alpha)^2} \left(\dfrac{\alpha}{x}\right)^{K_\rho + K_\sigma} \\ \left\langle (O^x)^\dagger_{SDW}(x) O^x_{SDW}(0) \right\rangle \sim \left\langle (O^y)^\dagger_{SDW}(x) O^y_{SDW}(0) \right\rangle \sim \dfrac{e^{2ik_F x}}{2(\pi\alpha)^2} \left(\dfrac{\alpha}{x}\right)^{K_\rho + 1/K_\sigma} \\ \left\langle O^\dagger_{SS}(x) O_{SS}(0) \right\rangle \sim \left\langle (O^z)^\dagger_{TS}(x) O^z_{TS}(0) \right\rangle \sim \dfrac{1}{2(\pi\alpha)^2} \left(\dfrac{\alpha}{x}\right)^{1/K_\rho + K_\sigma} \\ \left\langle (O^x)^\dagger_{TS}(x) O^x_{TS}(0) \right\rangle \sim \left\langle (O^y)^\dagger_{TS}(x) O^y_{TS}(0) \right\rangle \sim \dfrac{1}{2(\pi\alpha)^2} \left(\dfrac{\alpha}{x}\right)^{1/K_\rho + 1/K_\sigma} \end{cases} \tag{1.43}$$

k_F is the Fermi Momentum of the noninteracting tight–binding model calculated using the single–species density $n_c/2$ of the Hubbard model and (1.7). Similarly, the density–density and spin–spin correlation functions (completed with logarithmic corrections due to the irrelevant cosine term) can be computed, yielding

$$\langle \delta n_c(x) \delta n_c(0) \rangle = -\frac{4K_\rho}{\pi^2 x^2} + \frac{4k_F^2}{\pi^2} A_2 \cos(2k_F x) \left(\frac{\alpha}{x}\right)^{K_\rho + 1} \ln^{-3/2}\left(\frac{\alpha}{x}\right) + \frac{4k_F^2}{\pi^2} A_4 \cos(4k_F x) \left(\frac{\alpha}{x}\right)^{4K_\rho} + \dots \tag{1.44}$$

$$\langle \boldsymbol{S}(x) \cdot \boldsymbol{S}(0) \rangle = -\frac{K_\rho}{4\pi^2 x^2} + B_2 \cos(2k_F x) \left(\frac{\alpha}{x}\right)^{K_\rho + 1} \ln^{1/2}\left(\frac{\alpha}{x}\right) + \dots \tag{1.45}$$

Where $\delta n_c(x) \equiv \left(n_c(x) - n_c^0\right)$, with the last quantity being the density of the tight–binding model computed in (1.7). The first, universal term is a $q = 0$ contribution, which has been neglected in the fluctuations definitions (1.19) (those contained only the contributions coming from fermions close to the Fermi Momentum).

The actual correlation functions for $U > 0$ must be calculated at the fixed point $K_\sigma^* = 1$, and since (anticipating again the results of the Bethe *Ansatz* solutions) $K_\rho < 1$, the superconducting fluctuations decay faster than the SDW and CDW (whose correlation functions share the same exponent): the latter are then the dominant excitations in the conducting phase (although they do not manage to order the system).

Half–Filling. For $n_c = 1$ a previously rapidly–oscillating term for the charge field loses its oscillating factor, and must be kept in account: the Hamiltonian becomes

$$\widehat{H} = \sum_{\nu=\rho,\sigma} \int \left[\frac{u_\nu K_\nu}{2\pi} \left(\pi \Pi_\nu(x)\right)^2 + \frac{u_\nu}{2\pi K_\nu} \left(\nabla \phi_\nu(x)\right)^2 + \frac{2U}{(2\pi\alpha)^2} \cos\left(\sqrt{8}\phi_\nu\right) \right] dx \tag{1.46}$$

The Hamiltonian of the charge sector acquires a potential term, becoming a Sine–Gordon Hamiltonian. Since $K_\rho < 1$ for $n_c = 1$ the coupling of the cosine term becomes relevant, with U flowing to the critical point $U = +\infty$. In order to minimize the energy contribution, the field ϕ_ρ will set in one of the minima of the cosine, around whom quadratic fluctuations appear: these can be viewed as a mass term, and therefore the charge field theory becomes relativistic but massive, with a gap (the spin theory remains massless). The appearance of this gap transforms the $n_c = 1$ phase in an insulator (particularly, in a Mott Insulator, since $n_c = 1$) as the charge spectrum does not allow anymore arbitrarily low–energy excitations.

The Mott Insulating Phase can be approached undergoing two different phase transitions.

- The former is induced by the interaction coupling U at fixed $n_c = 1$. This Phase Transition belongs to the **Kosterlitz–Thouless Universality Class**, and takes place at the critical point $K_\rho^* = 1$, where the model switches between having a massless and a massive charge field. The transition point is at $U = 0$, and the Insulating Phase appears for any $U > 0$: the dynamical critical exponent of this transition is $z = 1$.
- Another kind of transition may be induced by changing the chemical potential μ (and therefore the density n_c) at fixed U. If the theory (1.46) is analyzed in the Path Integral formalism, the presence of the chemical potential in the critical theory induces a space–time anisotropy in the Hamiltonian, changing the physical properties of the transition: in particular, this transition has a dynamical critical exponent $z = 2$ and a correlation length exponent $\nu = 1/2$.

Chapter 2

The Bethe *Ansatz* Solution of the Hubbard Model

2.1 The Bethe *Ansatz*

The Bethe Ansatz *method is instrumental to solve the 1D Hubbard Model: as previously stated, this method assumes the scattering processes happening in the system can be decomposed as the union of many 2–Particle Elastic scatterings, and therefore proposes a wavefunction in which particle momenta are exchanged but not modified.*

Imposing this function to satisfy the system conditions (fixed–N Schrodinger Equations, symmetry conditions) results in equations for the parameters of the solutions and the system degrees of freedom, called **Lieb–Wu Equations***. Albeit the solutions to these are difficult to find in general, the most important solutions to determine the thermodynamic properties (called* **Regular Solution***) have properties which allow to exploit them to describe the system in the thermodynamic limit.*

2.1.1 Model Symmetries

Following the arguments in [25], we introduce some of the most important symmetries of the model, whose role in the Bethe Ansatz *solution or in the following thermodynamical analysis is instrumental. We will see the system is symmetric under* **Site Permutation***,* **Fermionic Shift***,* **Global Spin Flip***, and under more complex symmetries like the* **Shiba Symmetry***. Furthermore, we will see the model is invariant under an $SO(4)$ symmetry, extending the $SU(2)$ rotational spin invariance due to another symmetry.*

The Hubbard Hamiltonian satisfies several symmetry conditions: those we will list here will prove useful in finding its solutions. Unless differently specified, both "Canonical" Hamiltonians (1.37) and (1.39) satisfy the symmetries, for any L.

Permutations. The model is symmetric under spinwise permutations of site indices, implemented by the operators $\widehat{P}_{ia,jb}$ for $i,j = 1,\dots,L$ and $a,b = \uparrow,\downarrow$ as

$$\widehat{P}_{ia,jb}\widehat{C}_{jb} = \widehat{C}_{ia}\widehat{P}_{ia,jb} \qquad \widehat{P}_{ia,jb}\widehat{C}^{\dagger}_{ia} = \widehat{C}^{\dagger}_{jb}\widehat{P}_{ia,jb} \tag{2.1}$$

We may note $\left[\widehat{P}_{ia,ja}, \widehat{C}_{kb}\right] = 0$ for any $(i, j \neq k)$ or $a \neq b$.

Fermionic Shift. The model is symmetric under fermionic shift: this operator is defined for spinless fermions as product of spinless permutations $\widehat{P}_{ij}$.

$$\widehat{U}_L \equiv \widehat{P}_{(L-1),L} \dots \widehat{P}_{2,3}\widehat{P}_{1,2} \qquad \widehat{U}_L \widehat{c}_j = \begin{cases} \widehat{c}_{(j-1)}\widehat{U}_L & j = 2, \dots, L \\ \widehat{c}_L \widehat{U}_L & j = 1 \end{cases} \tag{2.2}$$

For $(1/2)$–Spin fermions the symmetry is implemented by operators U_{La}, for $a = \uparrow, \downarrow$, composed of spinwise permutations. The global operator may then be written as

$$\widehat{U} \equiv \left(\widehat{U}_{L\uparrow}\right)\left(\widehat{U}_{L\downarrow}\right) \equiv \left(\widehat{P}_{(L-1)\uparrow,L\uparrow} \dots \widehat{P}_{2\uparrow,3\uparrow}\widehat{P}_{1\uparrow,2\uparrow}\right)\left(\widehat{P}_{(L-1)\downarrow,L\downarrow} \dots \widehat{P}_{2\downarrow,3\downarrow}\widehat{P}_{1\downarrow,2\downarrow}\right) \tag{2.3}$$

$\widehat{U}$ is well defined since $\left[\widehat{U}_{La}, \widehat{C}_{jb}\right] = 0$ for $a, b = \uparrow, \downarrow$ and $a \neq b$ (due to the commuting properties of spinwise permutations). This operator induces a left shift of one lattice site for all fermions in the system.

Global Spin Flip. The Hubbard Hamiltonian is symmetric under inversion of all spins, enforced by the operator

$$\widehat{J}^{(s)} = \prod_{j=1}^{L} P_{j\uparrow,j\downarrow} \tag{2.4}$$

In our quest for solutions to the model we may therefore restrict ourselves to the case of non–negative $S_z = (N/2 - M)$, since solutions for the negative case can be found applying this operator to those of the positive case.

Shiba Transformation. Only (1.39) satisfies this symmetry. On a lattice with an even number of sites L, the definition and the action on fermionic operators of the **Shiba Transformation** are, for $a = \uparrow, \downarrow$,

$$\widehat{J}_a^{(sh)} \equiv \left(\widehat{C}^\dagger_{La} - \widehat{C}_{La}\right)\left(\widehat{C}^\dagger_{(L-1)a} + \widehat{C}_{(L-1)a}\right) \dots \left(\widehat{C}^\dagger_{2a} - \widehat{C}_{2a}\right)\left(\widehat{C}^\dagger_{1a} + \widehat{C}_{1a}\right) = \prod_{i=L}^{1}\left(\widehat{C}^\dagger_{ia} + (-1)^{i-1}\widehat{C}_{ia}\right) \tag{2.5}$$

$$\left[\widehat{J}_a^{(sh)}, \widehat{C}_{jb}\right] = 0 \quad \text{for} \quad a \neq b \qquad \widehat{J}_a^{(sh)}\widehat{C}_{ja}\left(\widehat{J}_a^{(sh)}\right)^\dagger = (-1)^j \widehat{C}^\dagger_{ja} \tag{2.6}$$

For a lattice with an even number of sites, this operator generates a particle–hole transformation accompanied by a change of sign on every even lattice site: for instance, the empty state is mapped in the half–filled, fully–polarized state, since $\widehat{J}_a^{(sh)} \mid 0 \rangle = \widehat{C}^\dagger_{La} \dots \widehat{C}^\dagger_{1a} \mid 0 \rangle$. If applied to the Hamilton (1.39), a single $\widehat{J}_a^{sh}$ leaves unchanged the tight–binding term while the u term changes sign, mapping $H(u)$ in $H(-u)$.

For odd L the transformation can be redefined, but the tight–binding term in the Hamiltonian is not invariant anymore, since the terms $\widehat{C}^\dagger_1\widehat{C}_L$ and $\widehat{C}^\dagger_L\widehat{C}_1$ ($i = 1$ and $i = L$ are nearest neighbours with periodic boundary conditions) acquire a (-) sign. This can be avoided changing boundary conditions: as we will keep the periodic ones, we will work in the hypothesis of even L.

If both $\widehat{J}_\uparrow^{(sh)}$ and $\widehat{J}_\downarrow^{(sh)}$ are applied the Hamiltonian is not altered, but the empty state is mapped on a state with all sites doubly occupied: in general all eigenstates of the Hamiltonian with N particles are mapped on eigenstates with $2L - N$ particles. In the next sections, then, we may

restrict on finding solutions for $N \leq L$ (applying the symmetry operator on them will provide the others).

The spin–flip transform $\widehat{J}^{(s)}$ and the Shiba Transform act on the particle number and on the z component of the total spin as

$$\begin{cases} \widehat{J}^s \widehat{N} \widehat{J}^s = \widehat{N} \\ \widehat{J}^{(sh)}_{\downarrow} \widehat{N} \left(\widehat{J}^{(sh)}_{\downarrow} \right)^{\dagger} = L + 2\widehat{S}^z \\ \widehat{J}^{(sh)}_{\uparrow} \widehat{N} \left(\widehat{J}^{(sh)}_{\uparrow} \right)^{\dagger} = L - 2\widehat{S}^z \end{cases} \qquad \begin{cases} \widehat{J}^s \widehat{S}^z \widehat{J}^s = -\widehat{S}^z \\ \widehat{J}^{(sh)}_{\downarrow} \widehat{S}^z \left(\widehat{J}^{(sh)}_{\downarrow} \right)^{\dagger} = \frac{1}{2} \left(\widehat{N} - L \right) \\ \widehat{J}^{(sh)}_{\uparrow} \widehat{S}^z \left(\widehat{J}^{(sh)}_{\uparrow} \right)^{\dagger} = \frac{1}{2} \left(L - \widehat{N} \right) \end{cases} \tag{2.7}$$

These effects are felt in the free energy per lattice site f, which conveys all equilibrium thermodynamical properties. Its expression in terms of the thermodynamical variables is

$$f\left(\mu, B, T, u\right) = -\frac{T}{L} \cdot \ln \left\{ \mathrm{tr} \left[\exp \left(-\frac{\widehat{H}(u) - \mu \widehat{N} - 2B\widehat{S}_z}{T} \right) \right] \right\} \tag{2.8}$$

The global spin flip and the Shiba operator change the value of the fields (μ, B) are conjugate to, and switch sign of u itself: the symmetries may be applied to all orders exploiting the mutual commutativity of $\widehat{H}, \widehat{N}, \widehat{S}_z$ and the invariance of the trace of a matrix product under cyclic permutations. The resulting relations (where the argument order in f is fixed) link the free energy values in different regions of the parameter space.

$$f\left(\mu, B, T, u\right) = f\left(\mu, -B, T, u\right) = f\left(B, \mu, T, -u\right) - \mu + B = f\left(-B, -\mu, T, -u\right) - \mu - B \tag{2.9}$$

Combining these equations we also find the identity

$$f(\mu, B, T, u) + \mu = f(-\mu, B, T, u) - \mu \tag{2.10}$$

Spin Symmetries. Both (1.37) and (1.39) conserve $\widehat{N}$ and the component z of the total spin, as well as satisfying further symmetries connected to the spin operators: in the following we will show (1.39) for even L commutes with another $SU(2)$ representation. We may now define the operators linked to the remaining spin components (according to the standard one–body operator definition in the second quantization) and show their commutation properties, for $\alpha, \beta, \gamma = (x, y, z)$:

$$\widehat{S}^{\alpha} \equiv \sum_{i=1}^{L} \left[\sum_{a,b=\uparrow,\downarrow} \left(\frac{1}{2} \sigma^{\alpha} \right)_{ab} \widehat{C}^{\dagger}_{ia} \widehat{C}_{ib} \right] \qquad \left[\widehat{S}^{\alpha}, \widehat{S}^{\beta} \right] = i\epsilon^{\alpha\beta\gamma} \widehat{S}^{\gamma} \qquad \left[\widehat{S}^{\alpha}, \widehat{H} \right] = 0 \tag{2.11}$$

The former commutation relation implies these operators generate a representation of $SU(2)$ (as expected) while the latter implies the system is fully invariant under rotation in the spin space. In order to show another symmetry of the Hamiltonian it is convenient to define the usual spin ladder operators, $\widehat{S}^{\pm} \equiv \widehat{S}^x \pm i\widehat{S}^y$, and to apply the Shiba Operator to these operators to find the generators of a new transformation.

$$\begin{cases} \widehat{J}_{\downarrow}^{sh}\widehat{S}^{+}\left(\widehat{J}_{\downarrow}^{sh}\right)^{\dagger} = \sum_{j=1}^{L}(-1)^{j}\widehat{C}_{j\uparrow}^{\dagger}\widehat{C}_{j\downarrow}^{\dagger} \equiv -\widehat{\eta}^{+} \\ \widehat{J}_{\downarrow}^{sh}\widehat{S}^{-}\left(\widehat{J}_{\downarrow}^{sh}\right)^{\dagger} = \sum_{j=1}^{L}(-1)^{j}\widehat{C}_{j\downarrow}\widehat{C}_{j\uparrow} \equiv -\widehat{\eta}^{-} \\ \widehat{J}_{\downarrow}^{sh}\widehat{S}^{z}\left(\widehat{J}_{\downarrow}^{sh}\right)^{\dagger} = \frac{1}{2}\sum_{j=1}^{L}\left(\widehat{N}_{j\uparrow}+\widehat{N}_{j\downarrow}-1\right) = \frac{1}{2}\left(\widehat{N}-L\right) \equiv \widehat{\eta}^{z} \end{cases} \tag{2.12}$$

The component operators $\widehat{\eta}^{x}, \widehat{\eta}^{y}$ can be defined as in the spin case, and the commutation behaviour of these operators can be derived from the spin commutation rules (2.11) (by expanding the definition or by applying the appropriate Shiba Operators). We find, for $\alpha, \beta, \gamma = x, y, z$,

$$\left[\widehat{\eta}^{z}, \widehat{\eta}^{\pm}\right] = \pm\widehat{\eta}^{\pm} \qquad \left[\widehat{\eta}^{+}, \widehat{\eta}^{-}\right] = 2\widehat{\eta}^{z} \qquad \left[\widehat{\eta}^{\alpha}, \widehat{\eta}^{\beta}\right] = i\epsilon^{\alpha\beta\gamma}\widehat{\eta}^{\gamma} \qquad \left[\widehat{H}, \widehat{\eta}^{\alpha}\right] = 0 \tag{2.13}$$

These operators therefore are another representation of $SU(2)$, and commute with the Hamiltonian (1.39) for even L (the last result is found exploiting the commutation of $H(-u)$ with the spin operators in (2.11) and applying the Shiba Transform). Commuting with all components of $\widehat{S}^{\alpha}$ and $\widehat{\eta}^{\alpha}$, the Hamiltonian can also be proven to commute with $\left(\widehat{S}^{\alpha}\right)^{2}$ and $(\widehat{\eta}^{\alpha})^{2}$. Finally, the commutation relations

$$\left[\widehat{S}^{\alpha}, \widehat{\eta}^{\beta}\right] = 0 \quad \text{for} \quad \alpha, \beta = x, y, z \tag{2.14}$$

can be proven by direct calculation. The symmetry induced by the $\widehat{\eta}$ operators (called $\widehat{\eta}$**–Pairing Symmetry**) holds only for even L, while the spin symmetry is satisfied for any L: for even L, then, the Hamiltonian commutes with the direct sum of two $SU(2)$ representations. From (2.12) we find

$$\widehat{S}^{z} + \widehat{\eta}^{z} = \frac{1}{2}\left(\widehat{N}_{\uparrow} - \widehat{N}_{\downarrow}\right) + \frac{1}{2}\left(\widehat{N} - L\right) = \widehat{N}_{\uparrow} - \frac{L}{2} \tag{2.15}$$

For even L, then, both operators must have integer or half–integer eigenvalues together on simultaneous highest–weight states. In this case, the model symmetry is $SU(2)\times SU(2)/\mathbb{Z}_2 \sim SO(4)$: any magnetic field term $-2BS^{z}$ breaks this symmetry, since then the $\widehat{\eta}$–pairing symmetry is conserved but the spin–rotational one is broken (the opposite happens if a $-\mu\widehat{N}$ term is present).

2.1.2 The Lieb–Wu Equations

Following the arguments in [25], we overview the solution of the Hubbard Model using the Bethe Ansatz Method: this method allows to find solutions for the model at fixed number of particles N using a particular choice of wavefunction. This class of solutions depends on parameters satisfying relations called **Lieb–Wu Equations***: the solutions of these equations fully determine the system solution, and will be shown to be directly connected to the thermodynamical properties of the system.*

In the following section we will introduce the Bethe *Ansatz* formalism to solve the Hubbard Model. Due to their length and mostly mathematical nature, we defer for the detailed calculations to [25], limiting to list the most important results and physical intuitions. The Bethe *Ansatz* solution is composed by a series of steps.

1. The first step is passing in the First Quantization Formalism: this will allow to find solutions for the model at fixed particle number N and number of "down" spins M. This passage involves constructing expressions for the Hamiltonian, the Periodic Boundary Conditions and the Shift operator $\widehat{U}$ in a fixed–N formalism (previously, the particle number was not a fixed quantity).

2. The next step is proposing the actual Bethe *Ansatz* wavefunction. These wavefunctions will be requested to be simultaneous eigenvectors of the fixed–N Hamiltonian (paired with the Periodic Boundary Conditions) and of the Shift Operator: the proposed wavefunctions will have the form

$$\psi(\boldsymbol{x}, \boldsymbol{a}, \boldsymbol{k}) = \sum_{P \in \Theta^N} \operatorname{sign}(PQ) \cdot A(\boldsymbol{k}P, \boldsymbol{a}Q) \cdot e^{i(\boldsymbol{k}P|\,\boldsymbol{x}Q)} \tag{2.16}$$

   Where $(\boldsymbol{x}, \boldsymbol{k}, \boldsymbol{a})$ are the N–sized position, momentum and spin polarization vectors for the system of fermions and P, Q are permutations belonging to the symmetric group of N elements Θ^N. As physically required, this function is antisymmetric under exchange of pairs of momenta or positions.

   As we can see, the function can be interpreted as result of the union of many two–particle scatterings on a lattice of free fermions: the particles exchange their positions and their momenta (but conserve the latter) and all possible states are kept in account, although weighted with the appropriate scattering amplitudes $A(\boldsymbol{k}P, \boldsymbol{x}Q)$.

3. In the third step conditions for the amplitudes of the wavefunctions (2.16) will be derived: these can be extracted from the physical necessity of vanishing wavefunction when two or more fermions have the same position. The wavefunctions and the amplitude conditions are then rephrased in a permutation recursive relation over the symmetric group, instrumental to solve the problem.

   This problem is then completed by adding the periodic boundary conditions, to transform it in a true secular problem, and is finally solved by interpreting it as a problem over spin space. This causes the introduction of an additional degree of freedom charachterizing the system spin behaviour, the **Spin Rapidity** vector $\boldsymbol{\lambda} = \{\lambda_1, \ldots, \lambda_M\}$.

   The translation of the secular problem in spin space produces several eigenvalue conditions, involving the system degrees of freedom: these relations generate the fundamental relations for our goals, called **Lieb–Wu Equations**.

Both the versions of the "Canonical" Hubbard Hamiltonian, (1.37) and (1.39) may be chosen for this approach: all the following results will be related to the problem obtained first–quantizing the latter (its increased symmetry will be useful in discussing the solution completeness). The Lieb–Wu equations, the main results of the procedure, have the form

$$e^{ik_l L} = \prod_{j=1}^{M} \frac{\lambda_j - \sin k_l - iu}{\lambda_j - \sin k_l + iu} \tag{2.17}$$

$$\prod_{l=1}^{N} \frac{\lambda_j - \sin k_l - iu}{\lambda_j - \sin k_l + iu} = \prod_{k=1,\ldots,M}^{k\neq j} \frac{\lambda_j - \lambda_k - 2iu}{\lambda_j - \lambda_k + 2iu} \tag{2.18}$$

Every solution of these equations is defined by the momenta vector $\{k_l : l = 1, \ldots, N\}$ and the Spin Rapidity vector $\{\lambda_j : j = 1, \ldots, M\}$, where these parameters are mutually distinct complex numbers. Their presence requires a generalization of the Bethe *Ansatz* wavefunctions (2.16),

$$\psi(\boldsymbol{x}, \boldsymbol{a}, \boldsymbol{k}, \boldsymbol{\lambda}) = \sum_{P \in \Theta^N} \mathrm{sign}(PQ) \, \langle \boldsymbol{a}Q \mid \boldsymbol{k}P, \boldsymbol{\lambda} \rangle \exp\left[i \left(\boldsymbol{k}P \mid \boldsymbol{x}Q \right) \right] \tag{2.19}$$

This function is an eigenvector for the Fixed–N Hamiltonian derived from (1.39) (and for that derived from (1.37) as well, albeit with a different eigenvalue) and the Momentum Operator: its eigenvalues for the three operators are, respectively,

$$E = -2 \sum_{j=1}^{N} \cos k_j + u \, (L - 2N) \qquad\qquad P = \left(\sum_{i=1}^{N} k_i \right) \mod 2\pi \tag{2.20}$$

As shown in their construction, these eigenfunctions are antisymmetric under simultaneous exchange of position and spin variables and under exchange of momenta (for permutations $R \in \Theta^N$) and they are symmetric under exchange of spin rapidities (for permutations $S \in \Theta^M$).

$$\psi \left(\boldsymbol{x}R, \boldsymbol{a}R, \boldsymbol{k}, \boldsymbol{\lambda} \right) = \psi \left(\boldsymbol{x}, \boldsymbol{a}, \boldsymbol{k}R, \boldsymbol{\lambda} \right) = \mathrm{sign}(R) \cdot \psi \left(\boldsymbol{x}, \boldsymbol{a}, \boldsymbol{k}, \boldsymbol{\lambda} \right) \qquad\qquad \psi \left(\boldsymbol{x}, \boldsymbol{a}, \boldsymbol{k}, \boldsymbol{\lambda}S \right) = \psi \left(\boldsymbol{x}, \boldsymbol{a}, \boldsymbol{k}, \boldsymbol{\lambda} \right) \tag{2.21}$$

It can be proven that the Bethe *Ansatz* states are maximum–weight states for the total spin operator, with weight $(N - 2M)/2$:

$$\widehat{S}^+ \mid \psi(\boldsymbol{x}, \boldsymbol{a}, \boldsymbol{k}, \boldsymbol{\lambda}) \rangle = 0 \qquad\qquad \widehat{S}^z \mid \psi(\boldsymbol{x}, \boldsymbol{a}, \boldsymbol{k}, \boldsymbol{\lambda}) \rangle = \frac{N - 2M}{2} \mid \psi(\boldsymbol{x}, \boldsymbol{a}, \boldsymbol{k}, \boldsymbol{\lambda}) \rangle \tag{2.22}$$

It can also be shown that, for even L, the Bethe *Ansatz* statest are lowest–weight states for the $\widehat{\eta}$ operator, with weight $(N - L)/2$:

$$\eta^- \mid \psi(\boldsymbol{x}, \boldsymbol{a}, \boldsymbol{k}, \boldsymbol{\lambda}) \rangle = 0 \qquad\qquad \eta^z \mid \psi(\boldsymbol{x}, \boldsymbol{a}, \boldsymbol{k}, \boldsymbol{\lambda}) \rangle = \frac{N - L}{2} \mid \psi(\boldsymbol{x}, \boldsymbol{a}, \boldsymbol{k}, \boldsymbol{\lambda}) \rangle \tag{2.23}$$

Each Bethe *Ansatz* wavefunction, therefore, generates a multiplet $\mid \psi_{\alpha\beta} \rangle \equiv (S^-)^\alpha \, (\widehat{\eta}^+)^\beta \mid \psi \rangle$, with $\alpha = 0, \ldots, (N - 2M)$ and $\beta = 0, \ldots, (L - N)$ (in our solutions $N \geq 2M$ and $L > N$, and therefore both these parameters are positive: we have exploited the commutation of the $\widehat{\eta}$ and the $\widehat{S}$ operators, (2.14)). The total number of states in each multiplet is

$$\dim(M, N) = (N - 2M + 1)(L - N + 1) \tag{2.24}$$

The former contribution comes from spin operators, the latter from $\widehat{\eta}^+$–generated states. The role of these multiplets in the Bethe *Ansatz* completeness will be outlined in the next section.

2.1.3 Regular Solutions

While the solution of the Lieb–Wu Equations is generally difficult, a particular class of solutions (the **Regular Solutions***) have, in the limits of infinite L and N, an* a priori *known structure. Following the arguments in [25], we show that supposing all solutions have this structure allows to cast the Lieb–Wu equations in an alternative form, called* **Takahashi Equations***: their solution will be instrumental in describing the thermodynamical behaviour of the model. The concept of regular solutions is also useful in discussing the completeness of the Bethe* Ansatz *solutions.*

Regular Solutions of the Lieb–Wu Equations (2.17), (2.18) are defined as having finite spectral parameters (the roots of the Lieb–Wu equations) and as having a finite number of them, fixed by the conditions $2M \leq N \leq L$. These roots are in general complex numbers, and solving these equations in the complex plane, unless few fermions and therefore few roots are present, is difficult, even numerically.

We will show, however, that for large numbers of solutions (N, M) and large system size L solutions tend to arrange themselves in the complex plane in regular patterns, called **Strings**: making the assumption all solutions behave this way (called **String Hypothesis**) it is possible to find a set of equations involving only the real parts of the roots.

String patterns can be found imposing an appropriate nonzero imaginary part to some of the spectral parameters, and then taking appropriate limits ($L \to \infty$ for the charge momenta, $N \to \infty$ and $M \ll N$ for the spin rapidities) to have divergences in the left hand sides of the Lieb–Wu Equations. Imposing the other hands diverge as well implies their denominators must be close to 0: as they involve other spectral parameters, this generates conditions fixing their values. Different kinds of solutions can be found by this method.

- The first kind of solutions can be found applying this method to the charge momenta k in (2.17), taking the limit $L \to +\infty$. The resulting solution contains both momenta k and spin rapidities (which we will indicate with Λ'): the latter and the sines of the former all share the same real part, aligning as a vertical string in the complex plane (henceforth the name).

  These solutions are called **k–Strings**, and if their length is $2m$ they contain $2m$ momenta k and m spin rapidities Λ', centered around a spin rapidity $(\Lambda')^m$ and with their imaginary parts equispaced. This picture is exact up to corrections $O(e^{-\delta L})$, with δ being a string–charachteristic positive constant (these factors arise in the spin configuration derivation).

- We may also build string solutions involving only spin rapidities, applying to (2.18) the $N \to +\infty$ limit in the hypothesis $M \ll N$. The resulting solutions are called **Λ–Strings** and if their length is m they contain m spin rapidities (which we will name Λ to distinguish them from those involved in the k–Strings). All the Λ share the same real part, while they have equispaced imaginary parts.

  As previously, these are centered around a spin rapidity Λ^m: Λ–Strings may also have $m = 1$ (containing a single spin rapidity), and exponentially depressed corrections are present as in the previous case, depending on a positive, string–charachteristic constant γ as $O(e^{-\gamma N})$.

- Single momenta, not belonging to any k–String, may also solve the Lieb–Wu Equations.

The Lieb–Wu equations are solved by single strings or by union of different strings, with different lengths and real parts as well: to keep this in account, in the following all string parameters (momenta, spin rapidities and (γ, δ) constants) will bear an additional greek index, indentifying which string in the solution they are part of.

Both the k–Strings and the Λ–Strings are derived in the hypothesis of having a divergent left hand side in the Lieb–Wu equations in (2.17), (2.18) for $L \to \infty$ and $N \to \infty$ (as the two parameters are used in different equations it is possible to impose $N/L = [\text{const}]$, therefore implementing the

thermodynamical limit). This implies divergences in the right hand side: in our arguments, this could be only caused by a denominator close to 0, and this allowed to find conditions for the spectral parameters.

Divergences in the right hand side may also happen if roots are not close to poles of the right side, but the number of spin rapidities roots M is size–dependent, having therefore $M \to \infty$ and $M/L = [\text{const}]$ if $L \to \infty$. In this case, the right–hand side terms may remain finite but their sheer number may ensure divergence: although the string hypothesis is not *a priori* valid anymore, the exact results obtained using it turn out to remain valid in this case as well.

The Takahashi Equations

For large lattices ($L \gg 1$) and many fermions ($N \gg 1$) almost all strings are close to ideal (corrections are small) and this means the imaginary part of the spectral parameters composing them are almost equally spaced. An arbitrary solution of the Lieb–Wu equations contains M_n Λ–Strings of length n, M'_n k–Strings of length n and $\mathcal{M}_e$ single momenta k_j. We will call these parameters **Occupation Numbers** of the string configuration under observation, and note they must respect these "sum rules":

$$M = \sum_{n=1}^{+\infty} n \cdot (M_n + M'_n) \qquad\qquad N = \mathcal{M}_e + \sum_{n=1}^{+\infty} 2n \cdot M'_n \tag{2.25}$$

The Lieb–Wu equations (2.17), (2.18) can be rephrased supposing all solutions are arranged in single momenta or in string patterns: the resulting equations involve only single momenta and the centers of the k–Strings and Λ–Strings. The logarithm of these equations can be taken straightforwardly, yielding the **Takahashi Equations**

$$k_l L = 2\pi I_l - \sum_{n=1}^{+\infty}\sum_{\alpha=1}^{M_n} \theta\left(\frac{\sin k_l - \Lambda_\alpha^n}{nu}\right) - \sum_{n=1}^{+\infty}\sum_{\alpha=1}^{M'_n} \theta\left(\frac{\sin k_l - (\Lambda')_\alpha^n}{nu}\right) \tag{2.26}$$

$$\sum_{l=1}^{N-2M'} \theta\left(\frac{\Lambda_\alpha^n - \sin k_l}{nu}\right) = 2\pi J_\alpha^n + \sum_{m=1}^{+\infty}\sum_{\beta=1}^{M_m} \Theta_{nm}\left(\frac{\Lambda_\alpha^n - \Lambda_\beta^m}{u}\right) \tag{2.27}$$

$$2L \cdot \mathrm{Re}\left(\arcsin\left((\Lambda')_\alpha^n - inu\right)\right) = 2\pi (J')_\alpha^n + \sum_{l=1}^{N-2M'} \theta\left(\frac{(\Lambda')_\alpha^n - \sin k_l}{nu}\right) + \sum_{m=1}^{+\infty}\sum_{\beta=1}^{M'_m} \Theta_{nm}\left(\frac{(\Lambda')_\alpha^n - (\Lambda')_\beta^m}{u}\right) \tag{2.28}$$

Even L has been assumed; we have used the definitions $\theta(x) \equiv 2\arctan x$ and

$$\Theta_{nm}(x) \equiv \begin{cases} \theta\left(\frac{x}{|n-m|}\right) + 2\theta\left(\frac{x}{|n-m|+2}\right) + \ldots + 2\theta\left(\frac{x}{n+m-2}\right) + \theta\left(\frac{x}{n+m}\right) & n \neq m \\ 2\theta\left(\frac{x}{2}\right) + 2\theta\left(\frac{x}{4}\right) + \ldots + 2\theta\left(\frac{x}{2n-2}\right) + \theta\left(\frac{x}{2n}\right) & n = m \end{cases} \tag{2.29}$$

The parameters I_j, J_α^n and $(J')_\alpha^n$ are due to the multivaluedness of the logarithm: each of them can be integer or half–odd, depending on the parameters (L, N, M_n, M'_n), and their values are bound by the conditions

$$\begin{cases} -\dfrac{L}{2} \leq I_j \leq \dfrac{L}{2} \\ |J_\alpha^n| \leq \dfrac{1}{2}\left(N - 2M' - \displaystyle\sum_{m=1}^{+\infty} t_{nm} M_m - 1\right) \\ |(J')_\alpha^n| \leq \dfrac{1}{2}\left(L - N + 2M' - \displaystyle\sum_{m=1}^{+\infty} t_{nm} M'_m - 1\right) \end{cases} \tag{2.30}$$

Where $M' \equiv \sum_{n=1}^{+\infty} n M'_n$ is the number of Λs involved in k–Strings and $t_{nm} \equiv 2\min(m,n) - \delta_{mn}$. The Global Energy and Momentum may be obtained from (2.20) as

$$E = -2\sum_{i=1}^{N} \cos k_i + u(L-2N) = -2\sum_{j=1}^{N-2M'} \cos k_j + 4\sum_{n=1}^{+\infty}\sum_{\alpha=1}^{M'_n} \mathrm{Re}\left(\sqrt{1 - \left((\Lambda')_\alpha^n - inu\right)^2}\right) + u(L-2N) \tag{2.31}$$

$$P = \left[\sum_{j=1}^{N-2M'} k_j - \sum_{n=1}^{+\infty}\sum_{\alpha=1}^{M'_n} \left(2 \cdot \mathrm{Re}\left(\arcsin\left((\Lambda')_\alpha^n - inu\right) - (n+1)\pi\right)\right)\right] \mod 2\pi \tag{2.32}$$

The Takahashi Equations will be rephrased in an Integral Form in the next section: they will prove instrumental in studying the thermodynamics of the Hubbard Model. All following considerations will be made on these assumptions:

- Any set of non–repeating integer or half–odd numbers $\{I_j, J_\alpha^n, (J')_\alpha^n\}$ satisfying the conditions (2.30) specifies precisely one regular solution $\{k_j, \Lambda_\alpha^n, (\Lambda')_\alpha^n\}$ of the Takahashi Equations.
- The quantum number sets $\{k_j, \Lambda_\alpha^n, (\Lambda')_\alpha^n\}$ defining the regular solutions of the Takahashi Equation are in one–to–one correspondence to regular solutions of the Lieb–Wu equations.
- For large L and N almost all solutions $\{k_j, \lambda_l\}$ of the Lieb–Wu equations are exponentially close to the corresponding solution $\{k_j, \Lambda_\alpha^n, (\Lambda')_\alpha^n\}$ of the Takahashi Equations, which means the strings the real solutions tend to are well approximated by the ideal strings exactly formed by the regular solution.

Completeness of the Bethe *Ansatz*. As previously shown, the Bethe *Ansatz* generates a fundamental set of solutions (those shown in (2.19)) and the operators $\widehat{S}^-$ and $\widehat{\eta}^+$ generate multiplets when applied to them: it is still in doubt wether these functions are a complete set of eigenstates for the Hubbard Model. In the following we will outline the demonstration of the completeness of the set of multiplets generated by the regular Bethe *Ansatz* solutions.

At first, the overall number of possible regular solutions n_{reg} for a value of (N, M) is calculated, first using (2.30) to determine the number $n(\{M_n\}, \{M'_n\})$ of ways to select the parameters $\{I_j, J_\alpha^n, (J')_\alpha^n\}$ for a given string configuration $\{M_n\}, \{M'_n\}$, and then summing it over the possible values of M_n, M'_n at fixed (N, M).

The total number of states (taking in account the multiplet dimension $\dim(M,N)$, defined in (2.24)) is then found as

$$n_{\mathrm{tot}}(L) = \sum_{M,N} \left[n_{\mathrm{reg}}(M,N) \cdot \dim(M,N)\right] = \sum_{M,N} \left[n_{\mathrm{reg}}(M,N) \cdot (N - 2M + 1)(L - N + 1)\right] \tag{2.33}$$

This calculation yields $n_{\mathrm{tot}}(L) = 4^L$, the total number of indipendent states on an L–sized fermionic lattice, and therefore the states generated by the Bethe *Ansatz*, keeping in account the $SO(4)$ multiplicity, generate a complete eigenset for the Hubbard Model.

2.2 Thermodynamics of the Hubbard Model

The solutions of the Takahashi Equations can be analyzed to find the behaviour of the system in the thermodynamic limit: general equations, called **Thermodynamic Bethe *Ansatz* Equations***, describe the thermodynamics of the Hubbard Model in terms of the* **Dressed Energies** *of the system excitations. These equations dramatically simplify in the $T = 0$ limit for $B = 0$, allowing to ascertain some aspects of the Model Phase Diagram in these conditions.*

2.2.1 Thermodynamic Bethe *Ansatz*

Following the arguments in [25], we apply the Thermodynamical Limit to the Takahashi Equations, and write the Free Energy Density f for the system using quantities related to their solutions: minimizing f will generate a set of equations (called **Thermodynamic Bethe Ansatz (TBA) Equations***) describing the behaviour of the equilibrium state of the system in the Thermodynamic Limit.*

Root Densities. After deriving the Takahashi Equations (2.26) – (2.28), we have assumed a 1–1 relation existed between the quantum numbers corresponding to regular solutions of the LW Equations, $\{k_j, \Lambda_\alpha^n, (\Lambda')_\beta^n\}$ and the integer (or half–odd) Takahashi parameters $\{I_j, J_\alpha^n, (J')_\beta^m\}$. Every allowed set of the latter uniquely determines a set of the former.

This correspondence may be pictured as the relation between the pattern of "particles" and "holes" in the quantum number space (that is, the quantum numbers present in the system and those who are not) and a corresponding pattern in the space of the Takahashi parameters. In both spaces some values may be chosen while some may not, and each configuration in one space fixes a configuration in the other.

We will exploit the fact that, in the thermodynamic limit (sending $L \to \infty$ and keeping $N/L = [\text{const}]$ and $M/L = [\text{const}]$) the roots of the Takahashi Equations become *dense*,

$$k_{j+1} - k_j = O\left(L^{-1}\right) \qquad \Lambda_{\alpha+1}^n - \Lambda_\alpha^n = O\left(L^{-1}\right) \qquad (\Lambda')_{\alpha+1}^n - (\Lambda')_\alpha^n = O\left(L^{-1}\right) \tag{2.34}$$

We can define quantities called **Counting Functions**, $\{y(k), z_n(\Lambda), z'_n(\Lambda')\}$ gathering all terms in the Takahashi Equations (2.26) – (2.28) with the exception of the Takahashi Parameters: if evaluated on a given solution of the Takahashi Equations these functions satisfy the conditions

$$y(k_j) = \frac{2\pi I_j}{L} \qquad z'_n\left((\Lambda')_\alpha^n\right) = \frac{2\pi (J')_a^n}{L} \qquad z_n(\Lambda_a^n) = \frac{2\pi J_\alpha^n}{L} \tag{2.35}$$

These functions can be used to "count" the Bethe *Ansatz* spectral parameters, since

$$\begin{cases} L\left[y(k_j) - y(k_n)\right] = 2\pi\left(I_j - I_n\right) \\ L\left[z_n\left(\Lambda_\beta^n\right) - z_n\left(\Lambda_\alpha^n\right)\right] = 2\pi\left(J_\beta^n - J_\alpha^n\right) \\ L\left[z'_n\left((\Lambda')_\beta^n\right) - z'_n\left((\Lambda')_\alpha^n\right)\right] = 2\pi\left((J')_\beta^n - (J')_\alpha^n\right) \end{cases} \tag{2.36}$$

Taking as example the first counting function, some of the integer (or half–odd) "slots" between I_j and I_n may be occupied (corresponding to an occupied "momentum slot" by a root of the equation, due to the 1–1 correspondence) while others may be empty: $(y(k_j) - y(k_n))$ counts both filled and empty slots.

In the thermodynamic limit (with (2.34) being instrumental in applying it) we may describe this pattern in the quantum number space using a **Particle Density** $\rho^p(k)$ and a **Hole Density** $\rho^h(k)$, so that $L\rho^p(k)\ dk$ is the number of particles (occupied "momentum slots") in $[k, k+dk]$, while $L\rho^h(k)\ dk$ is the corresponding number of holes. Corresponding particle and hole densities may be defined for spin rapidities in Λ–Strings ($\sigma_n^p(\Lambda)$ and $\sigma_n^h(\Lambda)$) and in k–Strings ($(\sigma')_n^p(\Lambda)$ and $(\sigma')_n^h(\Lambda)$).

The number of available "momentum slots" in dk, both occupied and empty, may be written both as $L\left(\rho^p(k)+\rho^h(k)\right)\ dk$ and, by the 1–1 Correspondence, as ΔI (and then as dy, due to (2.36)). Applying similar arguments to all root densities in (2.36) we find

$$\rho^p(k)+\rho^h(k)=\frac{1}{2\pi}\frac{dy(k)}{dk} \qquad \sigma_n^p(\Lambda)+\sigma_n^h(\Lambda)=\frac{1}{2\pi}\frac{dz_n(\Lambda)}{d\Lambda} \qquad (\sigma')_n^p(\Lambda)+(\sigma')_n^h(\Lambda)=\frac{1}{2\pi}\frac{dz'_n(\Lambda)}{d\Lambda} \tag{2.37}$$

Counting Functions contain sums over the spectral parameters, which can be rewritten in the thermodynamic limit as integrals over the (real) string centers (for Λs) and over momenta (for ks). Integrals over Λ and k must respectively contain the particle densities ($L\sigma^p$, $L(\sigma')^p$) and $L\rho^p(k)$, in order to keep into account the original quantization of occupied slots for spectral parameters. As the sum is not carried out on empty slots, hole densities must not appear.

The counting functions can be found from the Takahashi Equations and (2.35): we can differentiate the outcome with respect to their arguments and exploit (2.37) to rewrite the results. The final equations then depend only on particle and hole densities.

$$\begin{cases} \left(\rho^p(k)+\rho^h(k)\right)=\dfrac{1}{2\pi}+(\cos k)\displaystyle\sum_{n=1}^{+\infty}\int_{-\infty}^{+\infty}a_n(\Lambda-\sin k)\left[(\sigma')_n^p(\Lambda)+\sigma_n^p(\Lambda)\right]\ d\Lambda \\ \sigma_n^h(\Lambda)=-\displaystyle\sum_{m=1}^{+\infty}A_{nm}*\sigma_m^p|_\Lambda+\int_{-\pi}^{+\pi}a_n(\sin k-\Lambda)\rho^p(k)\ dk \\ (\sigma')_n^h(\Lambda)=\dfrac{1}{\pi}\mathrm{Re}\dfrac{1}{\sqrt{1-(\Lambda-inu)^2}}-\displaystyle\sum_{m=1}^{+\infty}A_{nm}*(\sigma')_m^p|_\Lambda-\int_{-\pi}^{+\pi}a_n(\sin k-\Lambda)\rho^p(k)\ dk \end{cases} \tag{2.38}$$

We have used the definitions

$$a_n(x)\equiv\frac{1}{2\pi}\cdot\frac{2nu}{(nu)^2+x^2} \qquad A_{nm}*f|_x\equiv\delta_{nm}f(x)+\int_{-\infty}^{+\infty}\frac{d}{dx}\Theta_{nm}\left(\frac{x-y}{u}\right)f(y)\ \frac{dy}{2\pi} \tag{2.39}$$

Free Energy. The free energy density can be calculated only if the entropy density s is known. This may be seen as a function of the root densities, and calculated as the logarithm of available configurations for the particles (this number may be found as the way to assign a fixed amount of particles, and therefore of holes, in a given number of available slots, as a function of the root densities and of the spectral parameters interval).

The free energy per site f may be found in terms of discrete sums, and then rephrased in the thermodynamic limit: applying the thermodynamic limit to (2.31) for the energy contribution, and exploiting the definitions of $n_c=N/L$ (the fermionic density) and $m=\frac{1}{2L}(N-2M)$ (the magnetization) we find

$$e\equiv\frac{E}{L}=-2\int_{-\pi}^{+\pi}\rho^p(k)\cos k\ dk+4\sum_{n=1}^{\infty}\int_{-\infty}^{+\infty}\mathrm{Re}\left(\sqrt{1-(\Lambda-inu)^2}\right)(\sigma')_n^p\ d\Lambda+u-2un_c \tag{2.40}$$

$$n_c = \int_{-\pi}^{+\pi} \rho^p(k)\, dk + \sum_{n=1}^{+\infty} \int_{-\infty}^{+\infty} 2n \cdot (\sigma')_n^p(\Lambda)\, d\Lambda \qquad m = \frac{1}{2}\int_{-\pi}^{+\pi} \rho^p(k)\, dk - \sum_{n=1}^{+\infty} \int_{-\infty}^{+\infty} n \cdot \sigma_n^p(\Lambda)\, d\Lambda \tag{2.41}$$

Density is found collecting contributions from both the single momenta and those belonging to k–Strings; M is found collecting all the Λ, and in the process the contributions of the Λ' vanish. Following the definition, the free energy density can be found as

$$f(\mu, B, T) = e - \mu n_c - 2Bm - Ts \tag{2.42}$$

In terms of the chemical potential μ, of the magnetic field B and of the temperature T. We will consider $B \geq 0$ and $\mu \leq 0$, since (2.9) and (2.10) can be used to extend the result to all other cases: we have $f(\mu, -B, T) = f(\mu, B, T)$ and $f(-\mu, B, T) = f(\mu, B, T) + 2\mu$.

Free Energy Minimization. The final step is imposing the variation of the free energy density f with respect to all root densities is 0. This condition will allow to find a thermal equilibrium state, and must be taken into account with (2.38) as restraint (this equation expresses hole densities in terms of the corresponding particle densities, therefore leaving the latter as the only indipendent variables). The outcome of the minimum condition can be expressed as relations involving the ratios

$$\zeta(k) \equiv \frac{\rho^h(k)}{\rho^p(k)} \qquad \eta_n(\Lambda) \equiv \frac{\sigma_n^h(\Lambda)}{\sigma_n^p(\Lambda)} \qquad \eta_n'(\Lambda) \equiv \frac{(\sigma')_n^h(\Lambda)}{(\sigma')_n^p(\Lambda)} \tag{2.43}$$

These relations are

$$\begin{aligned} \ln \zeta(k) = {} & \frac{-2\cos k - \mu - 2u - B}{T} + \sum_{n=1}^{+\infty} \int_{-\infty}^{+\infty} a_n(\sin k - \Lambda) \ln\left(1 + \frac{1}{\eta_n'(\Lambda)}\right) d\Lambda \\ & - \sum_{n=1}^{+\infty} \int_{-\infty}^{+\infty} a_n(\sin k - \Lambda) \ln\left(1 + \frac{1}{\eta_n(\Lambda)}\right) d\Lambda \end{aligned} \tag{2.44}$$

$$\ln\left(1 + \eta_n(\Lambda)\right) = -\int_{-\pi}^{+\pi} \cos k \cdot a_n(\sin k - \Lambda) \ln\left(1 + \frac{1}{\zeta(k)}\right) dk + \frac{2nB}{T} + \sum_{m=1}^{+\infty} A_{nm} * \ln\left(1 + \frac{1}{\eta_m}\right)\Big|_\Lambda \tag{2.45}$$

$$\begin{aligned} & \ln\left(1 + \eta_n'(\Lambda)\right) + \int_{-\pi}^{+\pi} \cos k \cdot a_n(\sin k - \Lambda) \ln\left(1 + \frac{1}{\zeta(k)}\right) dk \\ & = \frac{4\mathrm{Re}\sqrt{1 - (\Lambda - inu)^2} - 2n\mu - 4nu}{T} + \sum_{m=1}^{+\infty} A_{nm} * \ln\left(1 + \frac{1}{\eta_m'}\right)\Big|_\Lambda \end{aligned} \tag{2.46}$$

These equations are called **Thermodynamic Bethe Ansatz (TBA) Equations**, and together with the restraint conditions (2.38) they can determine the density of particles and holes in the state of thermodynamical equilibrium. It is useful to define **Dressed Energies** as

$$\kappa(k) \equiv T \cdot \ln \zeta(k) \qquad \epsilon_n(\Lambda) = T \cdot \ln \eta_n(\Lambda) \quad n \geq 1 \qquad \epsilon_n'(\Lambda) = T \cdot \ln \eta_n'(\Lambda) \quad n \geq 1 \tag{2.47}$$

These quantities describe the dressed energies of the elementary excitations in the ground state (that is, keep into account the dispersion relation of the model fluctuations).

2.2.2 Zero Temperature Limit in Zero Magnetic Field

Following the arguments in [25], we apply the limit of vanishing temperature to simplify the TBA Equations, reducing them to a system of integral equations for the Takahashi Equations Root Densities and for the Dressed Energies of excitations over the ground state. The additional condition $B = 0$ is imposed to simplify the equations further: the resulting integral equations allow to describe the $T = 0$, $B = 0$ Phase Diagram of the Model, and will be solved numerically in the next sections.

In the limit $T \to 0$ the TBA equations simplify since most of the dressed energies in can be shown to be positive (therefore implying the excitations they parametrize are thermodynamically unfavoured). The remaining relevant dressed energies are $\kappa(k)$ and $\epsilon_1(\Lambda)$, whose behaviour is

$$\begin{cases} \kappa(k) < 0 & |k| < Q \\ \kappa(k) > 0 & |k| > Q \end{cases} \qquad \begin{cases} \epsilon_1(\Lambda) < 0 & |\Lambda| < A \\ \epsilon_1(\Lambda) > 0 & |\Lambda| > A \end{cases} \tag{2.48}$$

With $\kappa(\pm Q) = \epsilon_1(\pm A) = 0$ (due to boundaries in k and Λ spaces, these positive parameters are limited by $Q \leq \pi$, $A \leq +\infty$). The case of positive (negative) dressed energies everywhere is considered choosing $Q = 0$, $A = 0$ ($Q = \pi$, $A = +\infty$). Similar arguments can be applied to the root densities, obtaining

$$\begin{cases} \sigma_n^p(\Lambda) = 0 & n \geq 2 \\ (\sigma')_n^p(\Lambda) = 0 & n \geq 1 \end{cases} \qquad \begin{cases} \sigma_1^p(\Lambda) = 0 & |\Lambda| > A \\ \sigma_1^h(\Lambda) = 0 & |\Lambda| < A \end{cases} \qquad \begin{cases} \rho^p(k) = 0 & |k| > Q \\ \rho^h(k) = 0 & |k| < Q \end{cases} \tag{2.49}$$

In the $B = 0$ hypothesis the system must have no net magnetization: it would spontaneously break the continuous $SU(2)$ spin–rotational symmetry, and therefore violate the Mermin–Wagner Theorem. Imposing $A \to +\infty$ turns out to be a sufficient condition to achieve $m = 0$: the TBA equations, coupled with conditions on the root densities derived from (2.38), become (expliciting the dependence on Q)

$$\begin{cases} \kappa(k) = -2\cos k - \mu - 2u + \displaystyle\int_{-Q}^{+Q} \cos k' \cdot R\left(\sin k' - \sin k\right) \kappa(k')\, dk' \\ \epsilon_1(\Lambda) = \displaystyle\int_{-Q}^{+Q} \frac{\cos k}{4u} \cdot \frac{1}{\cosh \frac{\pi}{2u}\left(\Lambda - \sin k\right)} \kappa(k)\, dk \\ \rho(k) = \dfrac{1}{2\pi} + \displaystyle\int_{-Q}^{+Q} \cos k \cdot R\left(\sin k' - \sin k\right) \rho(k')\, dk' \\ \sigma_1(\Lambda) = \displaystyle\int_{-Q}^{+Q} \frac{1}{4u} \cdot \frac{1}{\cosh \frac{\pi}{2u}\left(\Lambda - \sin k\right)} \rho(k)\, dk \end{cases} \quad \text{for} \quad \begin{cases} \rho(k) \equiv \rho^p(k) + \rho^h(k) \\ \sigma_1(\Lambda) \equiv \sigma_1^p(\Lambda) + \sigma_1^h(\Lambda) \\ R(x) \equiv \displaystyle\int_{-\infty}^{+\infty} \frac{e^{i\omega x}}{1 + e^{2u|\omega|}} \frac{d\omega}{2\pi} \end{cases} \tag{2.50}$$

It is also useful to define **Dressed Momenta**, momenta associated to the possible system excitations. Starting from (2.32), we can derive that in the limit $B = 0$ the excitations generated by adding a momentum k with $|k| > Q$ and by adding a spin rapidity Λ carry respectively dressed momenta $\pm p(k)$ and $\pm p_1(\Lambda)$, with

$$p(k) = 2\pi \int_0^k \rho(k')\, dk' \qquad p_1(\Lambda) = \frac{\pi N}{2L} - 2\int_{-Q}^{+Q} \arctan\left[\exp\left(-\frac{\pi}{2u}\left(\Lambda - \sin k\right)\right)\right] \rho(k)\, dk \tag{2.51}$$

$B = 0$ Ground State Phase Diagram

For $B = 0$ (corresponding to fixed $A = +\infty$) we can identify three phases, linked by two phase transitions, in the $\mu \leq 0$ region. For $\mu \geq 0$, the model shows the same phases with particles replaced by holes.

- $Q = 0$**: Empty Band.** This region corresponds to an empty band, with $n_c = 0$. This is due to the dressed energies being positive at all momenta in this region, which means $Q = 0$, and then (2.50) implies

$$\mu \leq \mu_0 \equiv -2 - 2u \tag{2.52}$$

- $0 < Q < \pi$**: Intermediate Filling.** We have $0 < n_c < 1$: the integral equations in (2.50) can be solved only numerically in this region. Analytical results for $B = 0$ can be obtained in proximity of the transitions to the Empty Band: these show the density behaves as

$$n_c(\mu) \approxeq \frac{1}{\pi}\sqrt{\mu - \mu_0} \equiv h(u, \mu) \tag{2.53}$$

  Where $\mu_0(B)$ is defined in (2.52) (this transition is described by a nonrelativistic effective theory as shown in **Section 1.3.2**). We have shown this phase is described by a Luttinger Liquid, whose parameters are, for not–weak coupling, an unknown function of μ and U. The two excitation velocities $u_{(\rho,\sigma)}$ may be described as the equivalent of v_F (defined in (1.18)) for the charge and spin excitation spectra: the spin parameter K_σ flows to its fixed point $K_\sigma^* = 1$, and the remaining Luttinger parameter K_ρ can be linked to the isothermal compressibility (as shown in [32]).

$$u_\rho = \left(\frac{\partial\kappa(p)}{\partial p}\right)_{p=p(Q)} = \left(\frac{\kappa'(Q)}{p'(Q)}\right) \qquad u_\sigma = \left(\frac{\partial\epsilon_1(p_1)}{\partial p_1}\right)_{p_1=p_1(A)} = \left(\frac{\epsilon_1'(A)}{p_1'(A)}\right) \qquad K_\rho = \frac{\pi}{2}u_\rho n^2 \kappa_T \tag{2.54}$$

  This phase also experiences, as shown in **Section 1.3.2**, a transition to an half–filled band, in proximity of whom analytical expansions yield (in terms of the Bessel Function $J_1(\omega)$)

$$n_c(\mu) \approxeq 1 - C_1 \cdot \sqrt{\mu_-(u) - \mu} \equiv l(u, \mu) \tag{2.55}$$

$$C_1 \equiv \frac{1}{a_1 \cdot \sqrt{\alpha_1}} \qquad a_1 \equiv \frac{1}{2\rho(Q = \pi, k = \pi)} \qquad \alpha_1 \equiv 1 - 2\int_0^{+\infty} \frac{\omega \cdot J_1(\omega)}{1 + \exp(2u\omega)}\, d\omega \tag{2.56}$$

- $Q = \pi$**: Half Filled Band.** This phase has $n_c = 1$ and, as shown in **Section 1.3.2**, is a Mott Insulator. The condition $Q = \pi$ allows simplifications in (2.50): the phase boundary can be found from the condition $\kappa(\pm\pi) = 0$, and for $Q = \pi$ the numerical equations can be solved exactly by Fourier Transform, allowing to find the chemical potential $\mu_-(u)$ at which the system undergoes the phase transition to the half–filled band.

$$\mu_-(u) = 2 - 2u - 2\int_0^{+\infty} \frac{J_1(\omega)e^{-\omega u}}{\cosh(\omega u)}\,\frac{d\omega}{\omega} \tag{2.57}$$

$$\kappa_\pi(k) = -2\cos k - 2u - \mu - 2\int_{-\infty}^{+\infty} \frac{J_1(\omega)\cdot\cos(\omega\cdot\sin k)\, e^{-\omega u}}{\omega\cosh(\omega u)}\, d\omega \tag{2.58}$$

$$\rho_\pi(k) = \frac{1}{2\pi} + (\cos k)\int_{-\infty}^{+\infty} \frac{J_0(\omega)\cdot\cos(\omega\cdot\sin k)}{2\pi\cdot(1 + \exp(2u|\omega|))}\, d\omega \tag{2.59}$$

  In this phase $n_c = 1$ for any value of chemical potential $\mu > \mu_-(u)$: the chemical potential is then a noninvertible function of n_c.

2.3 Numerical Solution

In this section we outline the method we employed to find the $(T = 0, B = 0)$ ground state properties of the Hubbard Model, and analyze the computed solutions in order to verify their accuracy, using numerical and analytical conditions.

2.3.1 Algorithm Description

In this section we describe the algorithm and the methods used to find the $n(\mu)$ function for the Hubbard Model at $T = 0$ and $B = 0$. The calculation of this function requires the numerical solution of an integral equation; we outline the general setup needed to find the solution, as described in [25], and then the numerical concepts used to actually solve the problem, as discussed in [33][1].

We will need the equations in (2.50) for the dressed energy $\kappa_Q(k)$ (the dependence on Q will be explicited henceforth) and for the root density $\rho_Q(k)$ (only these quantities matter) along with the relation between $\rho_Q(k)$ and the numerical density n_c in (2.41).

$$\kappa_Q(k) = -2\cos k - \mu - 2u + \int_{-Q}^{+Q} (\cos k')\, R\,(\sin k' - \sin k)\, \kappa_Q(k')\, dk' \qquad R(x) \equiv \int_{-\infty}^{+\infty} \frac{e^{i\omega x}}{1 + e^{2u|\omega|}}\, \frac{d\omega}{2\pi} \tag{2.60}$$

$$\rho_Q(k) = \frac{1}{2\pi} + \int_{-Q}^{+Q} \cos k \cdot R\,(\sin k' - \sin k)\ \rho_Q(k')\, dk' \qquad n_c = \int_{-Q}^{+Q} \rho_Q(k)\, dk \tag{2.61}$$

Q takes values in $[0, \pi]$, and satisfies the equation $\kappa_Q(\pm Q) = 0$: this condition could be used to find it as a function of μ, but it would require knowledge of the $\kappa(k)$ function at fixed μ, which in turn needs Q in order to be acquired (solving (2.60)).

A basic solution method would be to fix μ, set a value for Q, solve (2.60), and then check if $\kappa_Q(\pm Q) = 0$: if this happens the solution is correct, while if doesn't the problem needs to be solved again with different Q (still at fixed μ). Another way can be shown taking advantage of the quantities

$$\xi_Q(k) \equiv 1 + \int_{-Q}^{+Q} \xi_Q(k')\, (\cos k') \cdot R\,(\sin k' - \sin k)\ dk' \tag{2.62}$$

$$\overline{\kappa}_Q(k) \equiv -2\cos k - 2u + \int_{-Q}^{+Q} \cos(k') \cdot R\,(\sin k' - \sin k)\, \overline{\kappa}_Q(k')\, dk' \tag{2.63}$$

These quantities obey the relation $\kappa_Q(k) = \overline{\kappa}_Q(k) - \mu\xi_Q(k)$, which gives (if applied for $k = Q$) a way to determine μ as a function of Q (both as an evaluation point and as a parameter in determining $\overline{\kappa}_Q$ and ξ_Q).

$$\mu = \frac{\overline{\kappa}_Q(Q) - \kappa_Q(Q)}{\xi_Q(Q)} = \frac{\overline{\kappa}_Q(Q)}{\xi_Q(Q)} \tag{2.64}$$

We can prove these two relations involving the auxiliary unknown ξ_Q:

$$\left(\frac{\partial \kappa(k)}{\partial k}\right)_{k=Q} = \xi_Q(Q) \cdot \frac{\partial \mu(Q)}{\partial Q} \qquad \chi_n(B=0) = \frac{\partial n_c(\mu)}{\partial \mu} = \frac{\xi_Q^2(Q)}{\pi u_\rho} \tag{2.65}$$

[1] Although the mathematical concepts and the ideas behind the algorithm have been taken from this source, our code is different from the algorithm shown in [33].

The Charge Excitation Velocity u_ρ and the Luttinger Parameter K_ρ can then be determined using the compressibility property (1.8), along with (2.51), (2.54) and (2.65):

$$u_\rho = \left(\frac{\kappa'(k)}{p'(k)}\right)_{k=Q} = \xi_Q(Q) \cdot \frac{\partial\mu(Q)}{\partial Q} \cdot \frac{1}{2\pi\rho(Q)} \qquad K_\rho = \frac{\pi}{2} u_\rho \cdot n^2 \cdot \frac{1}{n^2}\chi_n = \frac{\xi_Q^2(Q)}{2} \tag{2.66}$$

These relations allow to find u_ρ and K_ρ from the solution of the $B = 0$ problem, whose solution algorithm we can now outline.

- At fixed u, $Q \in [0, \pi]$ is chosen as free parameter, and (2.62) and (2.63) are numerically solved to find the functional form of $\overline{\kappa}_Q(k)$ and $\xi_Q(k)$.
- The previously found functions are evaluated in Q, and their knowledge allows to find the value of μ corresponding to the choice of Q using (2.64).
- If μ is within the desired range of values, the integral equation in (2.61) is solved in order to find the root density $\rho_Q(k)$, which is then integrated over $[-Q, Q]$ to find the fermionic density n_c: although formally a function of Q, this can be interpreted as a function of μ, since $\mu = \mu(Q)$.

Computational Methods. As outlined in the previous sections, the overall problem can be solved in steps: each of them consists in an integral problem for a function $f(x)$,

$$f(x) = g(x) + \int_{-L}^{L} K(x, y) f(y)\, dy \tag{2.67}$$

- In order to solve it, at first it must be discretized: all functions are sampled on a root vector $\{x_i\}$. Discretized integrals are calculated as

  $$\int f(x)\, dx \approxeq \sum_{i=1}^{N} f(x_i) \cdot w_i \tag{2.68}$$

  Where the *sampling weights* $\{w_i\}$ ensure all points are properly weighted in the sum. Weights and sampling positions depend on the chosen integration method: in our program we have chosen **Gauss–Legendre Integration**.

- The problem becomes then finding the $f(x_i)$ vector by solving the vector equation

  $$f(x_i) = g(x_i) + \sum_{j=1}^{N} (K(x_i, x_j) f(x_j) w_j) \tag{2.69}$$

  which can be rewritten as the equation system

  $$\left[\sum_{j=1}^{N} (K(x_i, x_j) w_j - \delta_{ij})\right] f(x_j) = -g(x_i) \tag{2.70}$$

  This system can be solved using standard linear algebra techniques: in our program we have chosen a solution method based on **LU Decomposition**. Pivoting has been kept in account for numerical stability.

2.3.2 Solution Testing

In this section we use the analytical conditions extracted in the previous sections to check the behaviour of the solutions of our problem, along with describing the numerical checks the solutions have undergone to verify their accuracy.

For a value of u, values of Q can be sampled in the interval $[0, \pi]$, and then the corresponding μ and $n(\mu)$ can be found. This allows to create datasets depending on two accuracy parameters (namely, the number of sampling points N_K for the "inner" integration in ω in (2.60), with a cutoff chosen at $\omega_{\max}$ defined so that $R(\omega > \omega_{\max}) \leq 10^{-16}$, and the number N_S of sampling points for the "outer" integrations in k in (2.60), (2.61)).

As the error over Gaussian Integration is not easy to estimate, the *reference* dataset created for a choice (N_S, N_K) is compared with a *control* one created with a higher precision (for instance, $\left(\frac{3}{2}N_S, \frac{3}{2}N_K\right)$) and the dataset is accepted only if all μ and $n_c(\mu)$ in the reference data match those in the control data within a certain precision (10^{-6} has been taken as testing precision: however, most datasets match their control data at higher precision).

In addition to this numerical test, all datasets must respect precise analytical conditions, derived in previous sections, which may help to check wether the used approximation level is good or insufficient.

1. The first condition to be respected is $n_c(u, Q = \pi) = 1$ for all u (as we derived when describing the Half–Filled Band in the Phase Diagram). The program is geared to yield $n_c(u, Q = \pi)$ in every dataset, and this control allows to easily neglect badly approximated ones.

2. The system undergoes a first phase transition for $\mu \to \mu_0 = (-2 - 2u)$, as it passes from the Empty Lattice to Intermediate Filling. The density function $n_c(\mu)$ must behave as $h(u, \mu)$ in (2.53).

   This behaviour can be checked on calculated data: it has been observed, however, that this behaviour is followed in a region whose amplitude shrinks for decreasing u, and therefore may not be a significant control for very low–u datasets.

3. Once μ_0 is cleared, n_c must increase monotonically with μ until the boundary to the Mott Insulator is reached: this second phase transition happens when the chemical potential assumes the value $\mu_-(u)$ shown in (2.57). In proximity of the phase boundary $n_c(\mu)$ must behave as $l(u, \mu)$ in (2.55).

   The program can calculate $\rho_\pi(k = Q)$ in (2.59), which can be used to determine the coefficients in $l(u, \mu)$ using calculation programs. This control allows to check consistency in the data close to $n_c = 1$ (at the half–filling phase boundary). This behaviour as well restricted to a region whose size shrinks for small u, and therefore may not be significant for these datasets.

4. Density is fixed to 1 for $\mu > \mu_-(u)$ (the system is in the Mott–Insulating Phase) and therefore no datasets must have non–half–filled entries in this region. At half–filling ($Q = \pi$), the dressed energy $\kappa_Q(k)$ and the root density $\rho_Q(k)$ must behave as $\kappa_\pi(k)$ and $\rho_\pi(k)$ in (2.58), (2.59). These functions may be sampled and then compared with the approximation to the same functions generated by the program as $\kappa_Q(k) = \overline{\kappa}_Q(k) - \mu\xi_Q(k)$ and $\rho_Q(k)$ at fixed $Q = \pi$.

Higher u allows faster and more accurate calculations both by accelerating the decrease of $R(x)$ in (2.60) (therefore allowing lower cutoffs and lower N_K without losing precision) and by allowing datasets with lower N_S to pass the numerical test (and the analytical ones as well). Lower u, instead, forces resorting to higher N_K and N_S, with resulting large increases in the calculation time.

Therefore, although solutions for small u at sufficient high sampling respect the analytical conditions (1), (2) and (3) (although the convergence region for the latter two shrinks for decreasing u)

and the numerical test in our datasets is respected within 10^{-11} (we calculated up to $u = 0.0833$), we focused our analysis on solutions for $u \geq 0.25$ (that is, $U/w \geq 1$).

In **Figure 2.1** are shown the $n_c(\mu)$ functions for several values of $u \geq 0.25$: all the pictured datapoints satisfy the numerical conditions as well as the analytical test (1). **Figure 2.2** show the datasets satisfy the analytical condition (2) and (3) (although the convergence region shrinks with decreasing u) and in **Figure 2.3** it is shown the analytical condition (4) is respected.

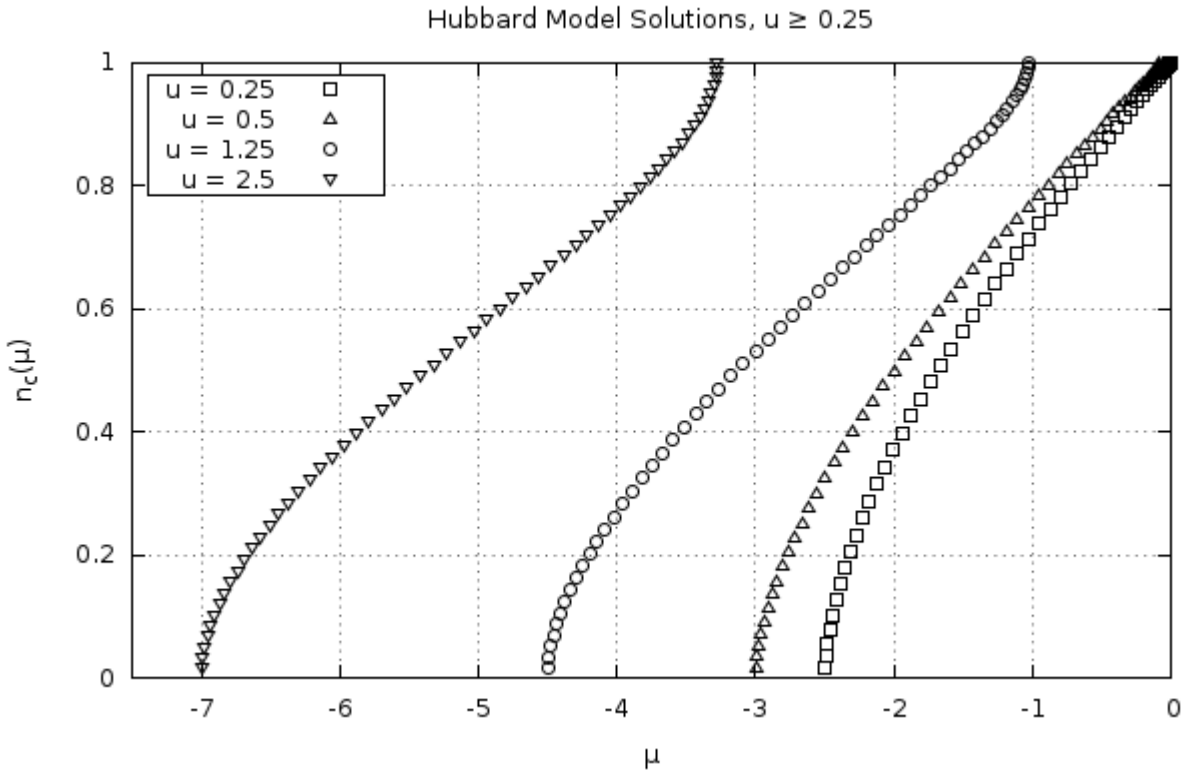

Figure 2.1: $n_c(\mu)$ *solutions for* $u \geq 0.25$ *and* $B = 0$.

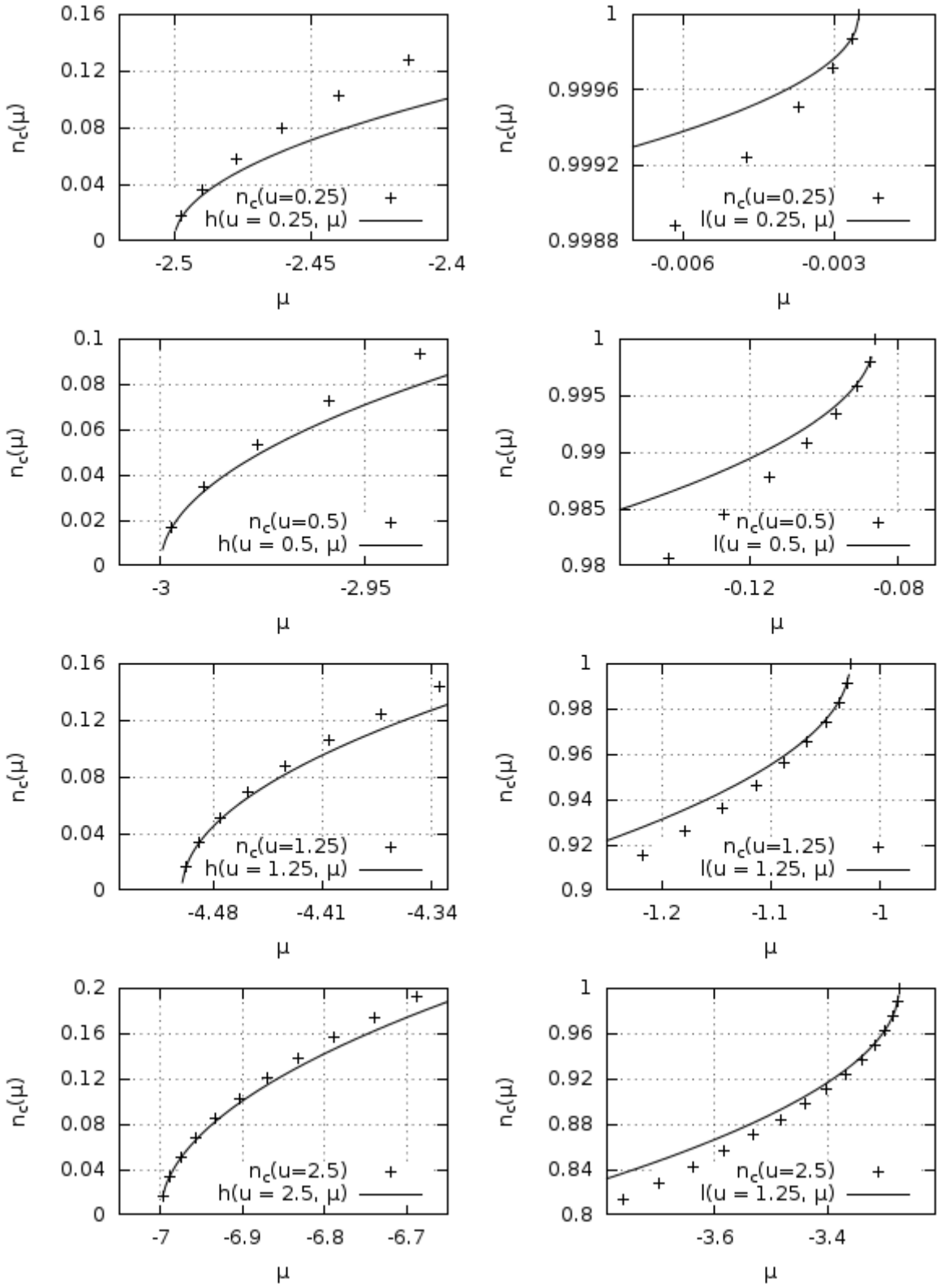

Figure 2.2: *Low–Density (left side) and High–Density (right side) behaviour of the Solutions for* $u = 0.25,\ 0.5,\ 1.25,\ 2.5$.

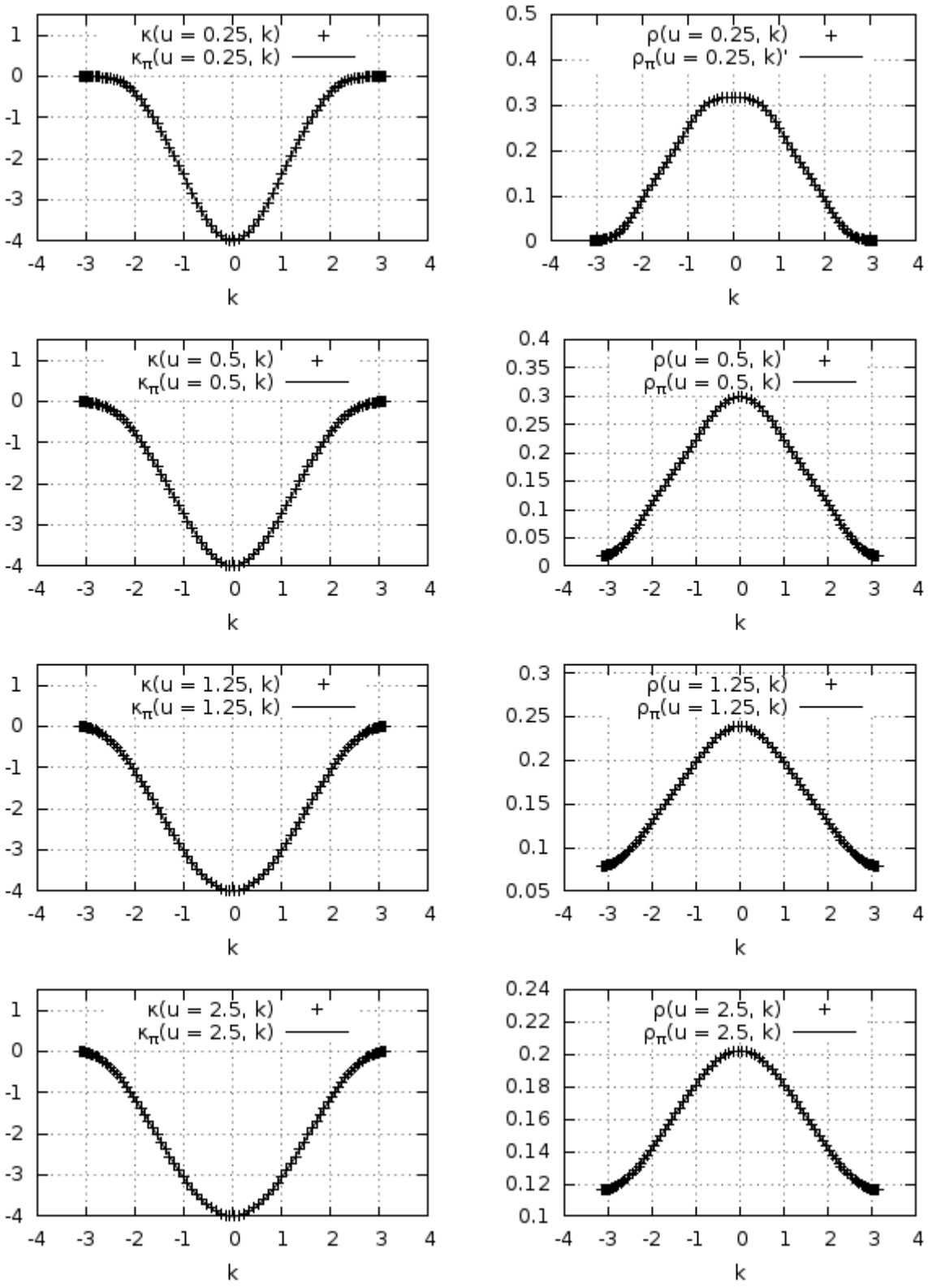

Figure 2.3: *The $\kappa(k)$ (left side) and $\rho(k)$ (right side) functions, as computed analitically (filled line) and from the numerical solutions (points) for $u \geq 0.25$ and $B = 0$.*

Chapter 3

Lattice Models in Trapping Potentials

3.1 Local Density Approximation

In this section, following the arguments in [21], we introduce the **Local Density Approximation** *(LDA) formalism, the simplest method to treat inhomogeneity effects in a system whose homogeneous behaviour is known. The main idea behind the method is using in every point the behaviour of the homogeneous model, in terms of an effective, position–dependent chemical potential.*

If a trapping interaction is applied to a homogeneous systems (more generally, if a position–dependent potential is present) introduces a spatial inhomogeneity, which causes changes with respect to the homogeneous behaviour: the **Local Density Approximation** (LDA) allows to approximate quantities like the density function in the presence of an external potential by introducing an effective, position–dependent μ. Henceforth, we will restrict to the analysis of lattice systems, and all couplings in the Hamiltonians will be normalized with respect to w (the kinetic coupling).

If the unconfined "Canonical" Hamiltonian of a lattice system is $\widehat{H}_0$, in the LDA its confined, "Grand Canonical" version $\widehat{K}$ can be rewritten as

$$\widehat{K} = \widehat{H}_0 - \sum_{i=1}^{L} \mu \widehat{N}_i + \sum_{i=1}^{L} V(x_i)\widehat{N}_i = \widehat{H}_0 - \sum_{i=1}^{L} \left(\mu - V(x_i)\right) \widehat{N}_i \equiv \widehat{H}_0 - \sum_{i=1}^{L} \mu_{\text{eff}}(x_i)\widehat{N}_i \tag{3.1}$$

The outcoming density as a function of the chemical potential also depends, implicitly, on the position, as $n(\mu(x))$. Usually the confining interaction of a trapped system is a power–law potential, defined in terms of the **Trap Size** l as $V(x) = (x/l)^p$: we will apply our formalism to the spinless version of the tight–binding model,

$$\widehat{K} = -w \sum_{i=1}^{L} \left(\widehat{c}_{i+1}^{\dagger} \widehat{c}_i + \widehat{c}_i^{\dagger} \widehat{c}_{i+1} \right) - \mu \sum_{i=1}^{L} \widehat{c}_i^{\dagger} \widehat{c}_i \tag{3.2}$$

In a confining potential, the LDA density can be found from (1.7) as

$$\langle n_x \rangle_{\mathrm{LDA}} = \rho_{\mathrm{LDA}} \left(\frac{x}{l} \right) \equiv \begin{cases} 1 & \frac{x}{l} \leq (\mu - 2)^{1/p} \\ \frac{1}{\pi} \arccos \left((1/2) \left(\left(\frac{x}{l} \right)^p - \mu \right) \right) & (\mu - 2)^{1/p} \leq \frac{x}{l} \leq (\mu + 2)^{1/p} \\ 0 & (\mu + 2)^{1/p} \leq \frac{x}{l} \end{cases} \tag{3.3}$$

l is the charachteristic scale on which trap density changes. (3.3) may be used to calculate the total number of particles as a function of the chemical potential: for even p,

$$N_{\mathrm{LDA}} = \sum_x \langle n_x \rangle_{\mathrm{LDA}} = \int_{-\infty}^{+\infty} \rho_{\mathrm{LDA}} \left(\mu(x) \right) \, dx + O(1) = 2l \int_0^{+\infty} \rho \left(\mu - y^p \right) \, dy + O(1) \equiv l \cdot C(\mu) + O(1) \tag{3.4}$$

The $O(1)$ error implies an $O(l^{-1})$ error on the quantity N/l: for this quantity, the $O(l^{-1})$ term contains both the error due to the passage from a discrete sum to the integral (which is $O(l^{-1})$) and the error of the LDA itself, which the analysis shown in [21] shows being $O(l^{-1})$ as well for the spinless tight–binding system (the LDA corrections are studied there for a confined Hardcore Bose–Hubbard System, equivalent to a confined, spinless, fermionic tight–binding system as shown in **Section 1.2**).

This approximation is used to effectively approximate the behaviour of confined systems of cold fermions described by the Hubbard Model ([19], [20]), confined cold bosons described by the Bose–Hubbard Model ([21]) and confined Fermi Gases ([24]). In the latter two systems it is shown the LDA results become more accurate with increasing trap size, with corrections dependent on negative powers of l, and therefore vanishing in the $l \to +\infty$ limit: we will later confirm that this behaviour is shown by a confined Hubbard System as well.

Despite its usefulness, and rather good accuracy for increasing trap size, the LDA approximation has some shortcomings: it allows to obtain with good accuracy only *local* quantities, since does not keep into account correlations between different points, and for the same reasons its accuracy decreases in proximity of critical points (where correlation effects become relevant).

3.2 Trap–Size Scaling

The accuracy of the LDA method decreases in proximity of critical points, since correlations between different points start to become relevant. In this case, even local quantities like the particle density develop sizable deviations from the LDA behaviour: these corrections can be analyzed in the **Trap–Size Scaling** *(TSS) method, which allows (using the RG formalism) to find the leading scaling behaviour in terms of the trap size; the general RG arguments shown in the first subsection are taken from [23].*

A model–specific analysis is required to find the scaling functions connected to this scaling behaviour: an example of this calculation is done for a confined, noninteracting tight–binding system to describe its behaviour in proximity of the transition to the empty lattice at $\mu = (-2)$, adapting the arguments in [21, 22] (the TSS formalism is applied there to a confined Hardcore Bose–Hubbard System, equivalent to a spinless, fermionic tight–binding system as shown in **Section 1.2***).*

General Formalism

The critical behaviour of a system is modified when a trapping potential is applied: within the trap, the original critical behaviour can be observed around the middle of the trap only if the correlation length ξ is much smaller than the trap size but large enough to show the universal scaling behaviour. If the latter condition is verified while the former is not (we will work in this hypothesis) the trap will change the features of the observed critical behaviour, though some of the original ones may remain.

Taking in consideration only local contributions, the LDA starts to fail in proximity of any phase transition, where correlations become relevant. This approximation can be improved taking in account scaling behaviours, which are modified by the presence of a confining potential: the **Trap–Size Scaling** (TSS) framework can be used to evaluate these modifications. In this method, we define a critical exponent θ linking the correlation length and the trap size as

$$\xi \sim l^{\theta} \tag{3.5}$$

We will suppose the system undergoes a $T = 0$ quantum phase transition. If we suppose the critical point is close enough, irrelevant scaling fields and their contributions can be neglected. If the model has a relevant scaling field g, whose scaling dimension is y_g, and $v \equiv l^{-1}$ has scaling dimension y_v, invariance under a scaling transform of parameter b is achieved only if the singular part of the free energy density follows, at the quantum critical point, the scaling law

$$F(g, T, v, x) = b^{-(d+z)} \cdot F\left(gb^{y_g}, Tb^{z}, vb^{y_v}, xb^{-1}\right) \tag{3.6}$$

x is the distance from the center of the trap. If the rescaling factor b is chosen so that $vb^{y_v} = 1$ (implying $b = l^{1/y_v}$) and the **Trap Exponent** is defined as $\theta \equiv 1/y_v$, we find the free energy density follows the TSS behaviour

$$F = l^{-\theta(d+z)} \cdot \mathcal{F}\left(gl^{\theta/\nu}, Tl^{\theta z}, xl^{-\theta}\right) \tag{3.7}$$

The trap exponent depends on the universality class of the model and may be calculated using RG methods. It modifies the behaviour of all quantities near the critical point: for instance, the gap energy Δ (and any low–energy scale at $T = 0$) and the correlation length at the trap center (as well as any length scale linked to the critical mode) are expected to behave as

$$\Delta = l^{-\theta z} \cdot D\left(\overline{g} l^{\theta/\nu}\right) \qquad \xi = l^{\theta} \cdot X\left(g l^{\theta/\nu}, T l^{\theta z}\right) \tag{3.8}$$

With $D(y) \sim y^{z\nu}$ for $y \to 0$ and $X(y,0) \sim y^{-\nu}$ for $y \to 0$, to match the free scaling behaviours $\Delta \sim g^{z\nu}$ and $\xi \sim g^{-\nu}$. For a general operator $O(x)$, of RG dimension y_o, its expectation value and equal–time correlation function are expected to behave as

$$\langle O(x) \rangle = l^{-\theta y_o} \cdot \mathcal{O}\left(g l^{\theta/\nu}, T l^{\theta z}, x l^{-\theta}\right) \qquad \langle O(x) O(0) \rangle_c = l^{-2\theta y_o} \cdot \mathcal{G}_O\left(g l^{\theta/\nu}, T l^{\theta z}, x l^{-\theta}\right) \tag{3.9}$$

In the limit $p \to \infty$ the trapped system becomes a homogeneous system inside a box of size $L = 2l$ with open boundary conditions. This system can be described by finite–size scaling, with L^{-1} becoming a relevant parameter of scaling dimension $(+1)$, and therefore we should find $\theta(p \to +\infty) = (y_{L^{-1}})^{-1} = (+1)$. In order to find θ for a power–law potential, $V(x) = (x/l)^p = v^p x^p$ (all energies are rescaled by the hopping coefficient) the confining interaction may be seen as a RG perturbation, and the trap exponent can be found knowing the structure of the effective theory.

Let us take, for instance, the spinless tight–binding model (3.2): its effective theory in proximity of the critical point $\mu = (-2)$ can be derived from (1.14), removing the spin sum, passing in the coordinate domain, and neglecting all higher–order gradients, as

$$\mathcal{L} = \Psi^*(x) \frac{\partial \Psi(x)}{\partial \tau} + \frac{1}{2m} \Psi^*(x) \nabla^2 \Psi(x) - \mu' \cdot \Psi^*(x) \Psi(x) \tag{3.10}$$

Here $\mu' \equiv (\mu + 2)$: we can define $y_\mu \equiv \dim(\mu')$ as shown previously. The external potential term would take the form $V = (v^p x^p \Psi^*(x) \Psi(x))$: this term has the same nature of the chemical potential one, with simply $(v^p x^p)$ replacing μ'. These terms share the same scaling dimension only if $p y_v - p = y_\mu$, and then

$$\theta = \frac{1}{y_v} = \frac{p}{p + y_\mu} \tag{3.11}$$

As expected, $\theta \to 1$ for $p \to \infty$: this formalism allows, for instance, to predict the $T = 0$ confined scaling behaviour at the $\mu = \pm 2$ transitions of the Noninteracting Tight–Binding Model (we had $y_\mu = 2$, according to (1.16), and therefore $\theta = p/(p-2)$).

TSS for the Spinless Tight–Binding Model

In the previous section we found the TSS trap exponent for the $\mu = (-2)$ critical point of the spinless tight–binding model (3.2): we can now obtain additional information (for instance, the structure of the scaling functions) about the TSS behaviour from the Hamiltonian itself, in absence of magnetic field and in proximity of the unconfined critical point $\mu = (-2)$ (in correspondence to the transition to the empty lattice). The Model Hamiltonian can be rewritten as

$$H = \sum_{i,j} \widehat{c}_i^\dagger h_{ij} \widehat{c}_i \qquad h_{ij} = \delta_{ij} - \delta_{i,(j-1)} - \delta_{i,(j+1)} + (V(x_i) - \overline{\mu})\, \delta_{ij} \tag{3.12}$$

Defining $\overline{\mu} \equiv (\mu - 1)$. The TSS behaviour can be derived diagonalizing the model, by passing in the momentum domain: new canonical fermionic coordinates can be defined as $\eta_k \equiv \sum_i \phi_{ki} \widehat{c}_i$, with the ϕ_{ki} satisfying the equations

$$h_{ij} \phi_{kj} = \omega_k \phi_{ki} \tag{3.13}$$

In these coordinates the Hamiltonian becomes $H = \sum_k \omega_k \eta_k^\dagger \eta_k$, describing a gapped system with gap amplitude $\Delta = \min_k |\omega_k|$. The matrix ϕ_{ki} defined in this fashion turns out to be orthogonal, and therefore it can be easily inverted obtaining

$$\widehat{c}_i = \sum_k \phi_{ki} \eta_k \tag{3.14}$$

In the TSS formalism, the interesting critical behaviour is found in the large–l limit: since the transition correlation length ξ will depend on l through the trap exponent, all lengths will be rescaled in terms of a positive power of l, and become effectively continuous in the limit $l \to +\infty$. This implies that the Hamiltonian h_{ij} in (3.13) can be approximated, replacing the discrete differences in terms of a derivative expansion in the continuum limit. This way, (3.13) becomes (in terms of the continuous function $\phi_k(x) \equiv \phi_{kx}$)

$$\left[-\overline{\mu} + \left(\frac{x}{l}\right)^p - \frac{1}{2}\frac{d^2}{dx^2} - \frac{1}{24}\frac{d^4}{dx^4} + \dots \right] \phi_k(x) = \omega_k \phi_k(x) \tag{3.15}$$

Close to the transition we might neglect the higher derivative terms, which depend on higher powers of the inverse correlation length ξ^{-1}: in this approximation, the model can be rewritten in terms of the rescaled quantities

$$X \equiv l^{-p/(p+2)} x \qquad \overline{\mu}_r \equiv l^{2p/(p+2)} \overline{\mu} \qquad \Omega_k \equiv l^{2p/(p+2)} \omega_k \qquad \varphi_k(X) \equiv l^{p/(2(p+2))} \phi_k\left(l^{p/(p+2)} X\right) \tag{3.16}$$

Under this rescaling, (3.15) becomes

$$\left(-\frac{1}{2}\frac{d^2}{dX^2} + X^p \right) \varphi_k(X) = (\Omega_k + \overline{\mu}_r)\, \varphi_k(X) \equiv \overline{\Omega}_k \varphi_k(X) \tag{3.17}$$

At the unconfined fixed point $\overline{\mu} = (-1)$ the length x may be written in terms of its invariant scaling function as $x = \xi \cdot X$, and comparing the coordinate scaling in (3.16) with the the trap exponent definition $\xi = l^\theta$ implies $\theta = p/(p+2)$ in this model (as derived using RG analysis in the previous section). The dominant correction (the neglected quartic derivative) is an $O(l^{-2\theta})$ term: this should be the accuracy of the TSS predictions.

The solutions of (3.17) for $\overline{\Omega}_k$ and $\varphi_k(X)$ depend on the value of p: for $p = 2$ we find

$$\overline{\Omega}_k = \Omega_k + \overline{\mu}_r = \sqrt{2}\left(k + \frac{1}{2}\right) \qquad \varphi_k(X) = \frac{2^{1/8}}{\pi^{1/4} 2^{k/2} (k!)^{1/2}} \cdot H_k\left(2^{1/4} X\right) \cdot \exp\left(-\frac{X^2}{\sqrt{2}}\right) \tag{3.18}$$

With $k \in \mathbb{N}$, $X = x l^{-1/2}$ and with the $H_k(z)$ being Hermite polynomials. We can now calculate the TSS behaviour of the particle density: in particular, exploiting (3.14) and the structure of the system ground state in the momentum domain (with all momentum states with negative energy contribution singly occupied), we find

$$\langle n(x) \rangle \equiv \left\langle \widehat{c}_x^\dagger \widehat{c}_x \right\rangle = \sum_{k_1, k_2} \phi^*_{k_1 x} \phi_{k_2 x} \left\langle \eta^\dagger_{k_1} \eta_{k_2} \right\rangle = \sum_{k:\Omega_k < 0} \phi_k^2(x) = l^{-\theta} \sum_{k:\Omega_k<0} \varphi_k^2(X) \equiv l^{-\theta} \mathcal{N}(\overline{\mu}_r, X) \tag{3.19}$$

The sum is taken only on occupied levels (those whose occupation is favoured by their energy $\Omega_k = \overline{\Omega}_k - \overline{\mu}_r$ being negative) and this is the only dependence on $\overline{\mu}_r$ in $\mathcal{N}$. A similar analysis can also be made for the density–density correlation function: its scaling behaviour is

$$G_n(x) \equiv \langle n(x)n(0)\rangle - \langle n(x)\rangle \langle n(0)\rangle = l^{-2\theta}\mathcal{G}_n\left(\overline{\mu}_r, X\right) \tag{3.20}$$

This scaling behaviour is confirmed if the definition of G_n in terms of the density operators is expanded. The scalar product (3.20) can be calculated using the Wick Theorem, which allows to rewrite it in terms of sums and products of two–operators scalar products, obtaining the scaling function

$$\begin{aligned}\mathcal{G}_n(\overline{\mu}_r, X) &= \left[\sum_{k:\Omega_k<0}\varphi_k(X)\varphi_k(0)\right]\cdot\left[\sum_{k:\Omega_k>0}\varphi_k(X)\varphi_k(0)\right] \\ &= \delta(X)\left[\sum_{k:\Omega_k<0}\varphi_k(X)\varphi_k(0)\right] - \left[\sum_{k:\Omega_k<0}\varphi_k(X)\varphi_k(0)\right]^2\end{aligned} \tag{3.21}$$

The last equation can be derived taking advantage of the completeness of the $\varphi_k(X)$ set, which reads $\sum_k \varphi_k(X)\varphi_k(0) = \delta(X)$. As previously, the dependence on $\overline{\mu}_r$ is restricted to determining, through Ω_k, the occupied, and therefore contributing, levels.

Fixed–N Formalism. While our previous results for the transition to the empty lattice were obtained at fixed the chemical potential, the TSS behaviour can also be studied at fixed particle number N: this number will be asymptotically linked to the chemical potential by a definite relation $N/l = C(\mu)$, like the LDA relation in (3.4) (expected to become exact, as already discussed, for $l \to +\infty$).

Since $N/l \to 0$ in the $l \to +\infty$ limit at fixed N, this regime corresponds to the $\overline{\mu} \to (-1)$ limit studied in the previous paragraph, and therefore shows the same scaling behaviour: the TSS behaviour of the thermodynamical quantities at fixed N can be obtained from the results in terms of μ, simply noting the number of occupied levels is, for spinless particles, exactly the number of particles, and no other dependencies from μ arose:

$$\langle n(x)\rangle = \sum_{i=1}^{N}\phi_i^2(x) = l^{-\theta}\sum_{i=1}^{N}\varphi_i^2(X) \equiv l^{-\theta}\mathcal{N}_N(X) \tag{3.22}$$

$$G_n(x) = l^{-2\theta}\left[\delta(X)\left(\sum_{i=1}^{N}\varphi_i(X)\varphi_i(0)\right) - \left(\sum_{i=1}^{N}\varphi_i(X)\varphi_i(0)\right)^2\right] \equiv l^{-2\theta}\mathcal{G}_N(X) \tag{3.23}$$

N does not change under the rescaling of l, and therefore (unlike the chemical potential) it appears only as a parameter, and not a variable, in the scaling functions.

Trapped Thermodynamic Limit. Another TSS limit can be found keeping the chemical potential fixed: in this case, $C(\mu) = N/l$ must be kept constant, and therefore the number of particles will have to increase to have simultaneously $l \to \infty$ and $N \to +\infty$ while N/l remains constant.

If N/l is linked, even asymptotically, to the chemical potential (as in the LDA relation (3.4)) this limit consists in working at fixed chemical potential. This limit will be called **Trapped Thermodynamic Limit**, and its charachteristic TSS behaviour will be studied, along with the one in the Dilute Limit, for the Hubbard Model.

Chapter 4

Results

4.1 Results for the Homogeneous Model

In this section we show some results we can gather from the Bethe Ansatz *solutions: namely, the Phase Diagram of the model for $T = 0$ and the Luttinger Parameters K_ρ, u_ρ of the conducting phase. These results allow to determine more precisely the behaviour of the model, and comparing them with the same results in other works also allows a further control of the solution accuracy.*

In this section we will use the numerical solutions of the Bethe *Ansatz* Equations to understand the charachteristics of the $T = 0$ Phase Diagram of the Hubbard Model. Henceforth, all chemical potentials determining the function $n_c(\mu) \equiv n_\uparrow(\mu) + n_\downarrow(\mu)$ (derived from (2.61) using the Hamiltonian (1.39)) will be adapted to be compatible with the solutions of (1.37) (compatibility is ensured increasing all chemical potentials by $2u$, since in the former Hamiltonian a term $-2u\widehat{N}$ has been added).

As U increases, the transition to the empty lattice remains at $\mu = \mu_0$, from (2.52), while the transition point $\mu = \mu_-(u)$ to the Mott Insulating phase changes following (2.57). Keeping in account the $(+2u)$ shifting, these chemical potentials assume the values

$$\mu_0(U) = (-2) \qquad\qquad \mu_-(U) = 2 - 2\int_0^\infty \frac{J_1(\omega)e^{-\omega U/4}}{\cosh(\omega U/4)}\,\frac{d\omega}{\omega} \tag{4.1}$$

The function $\mu_-(U)$, plotted in **Figure 4.1**, becomes 0 for $U \to 0$ (the transition happens at very small chemical potentials for small U, but it does not happen at $U = 0$, since the model becomes free and no Mott Insulating Phase can exist any longer) and becomes $(+2)$ for $U \to +\infty$.

Some $n_c(\mu)$ curves obtained from our solution algorithm are shown in **Figure 4.2**. We previously found $n_c(\mu)$ shows a square–root behaviour in proximity of the transitions to the Empty Lattice and to the half–filled Mott Insulator, as in (2.53) and (2.55):

$$n_c(\mu \cong \mu_0) \cong \frac{1}{\pi}\sqrt{\mu - \mu_0} \qquad\qquad n_c(\mu \cong \mu_-(U)) \cong 1 - C_1 \cdot \sqrt{\mu_-(U) - \mu} \tag{4.2}$$

As shown in the solution testing, the square–root region of these curves shrinks with increasing U. The Mott–Insulating Phase extends over a chemical potential region of width $\Delta\mu = 2\,|\mu_-(U) - U/2|$: the particle–hole symmetry ensures $n(\mu) = 2 - n(U - \mu)$ for $\mu > U/2$ (the symmetry point for the Hamiltonian (1.37)) and therefore the model shows another Conductor–Insulator transition at $\mu = (U - \mu_-(U))$ and a transition to a Band Insulator (an empty lattice of holes) at $\mu = (+2 + U)$.

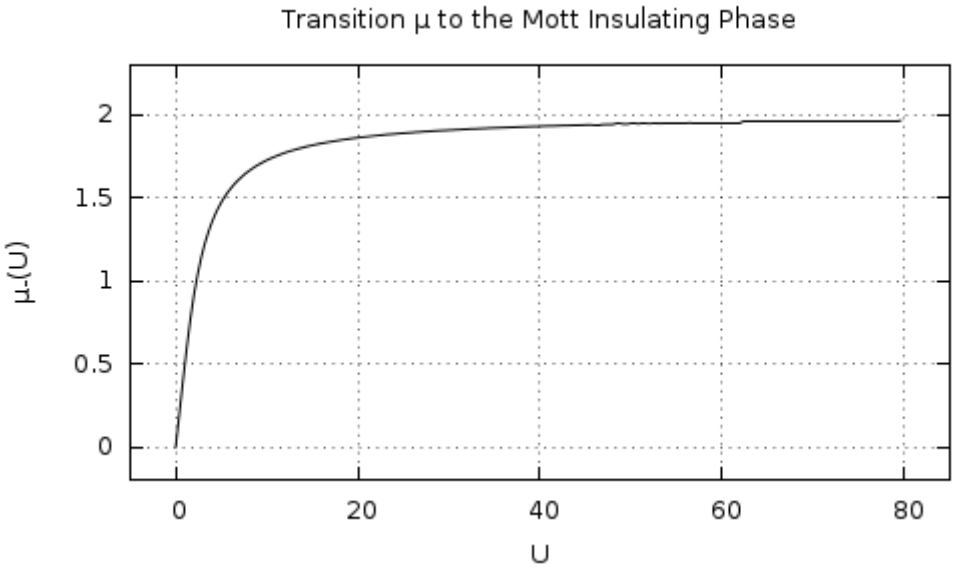

Figure 4.1: $\mu_{-}(U)$ *Function.*

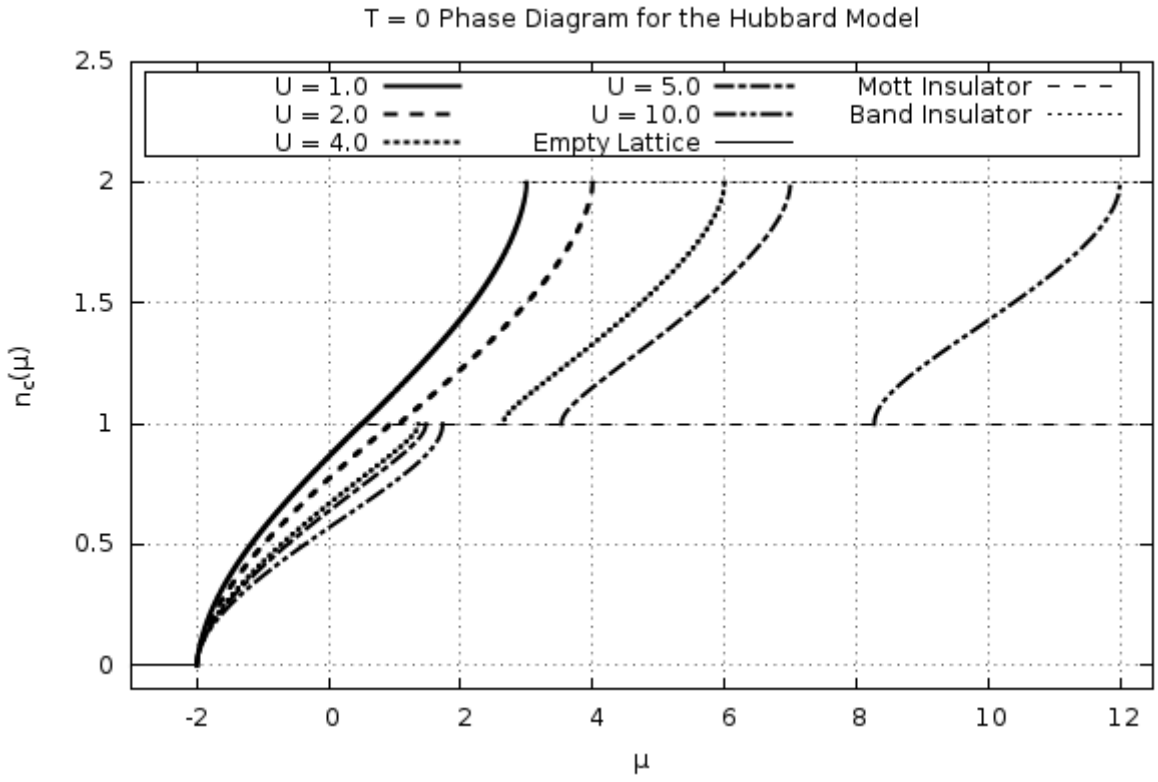

Figure 4.2: $T = 0$ *Phase Diagram.*

The conducting phases outlined in **Figure 4.2** can be charachterized by the correlation functions of their excitations, whose asymptotic behaviour is determined (as shown in (1.43) and (1.46)) by the Luttinger Parameter K_ρ (for $U > 0$ the other Luttinger Parameter, K_σ, flows to its fixed point, $K_\sigma^* = 1$). The data we collected also allows to compute the charge excitations velocity u_ρ.

We report in **Figure 4.3** the results for K_ρ and u_ρ as computed using our Bethe *Ansatz* solution data and (2.66), both as a function of the particle density n_c and of the chemical potential μ. The resulting functions $K_\rho(n_c)$ and $u_\rho(n_c)$ plotted here are in good agreement with those shown in [26].

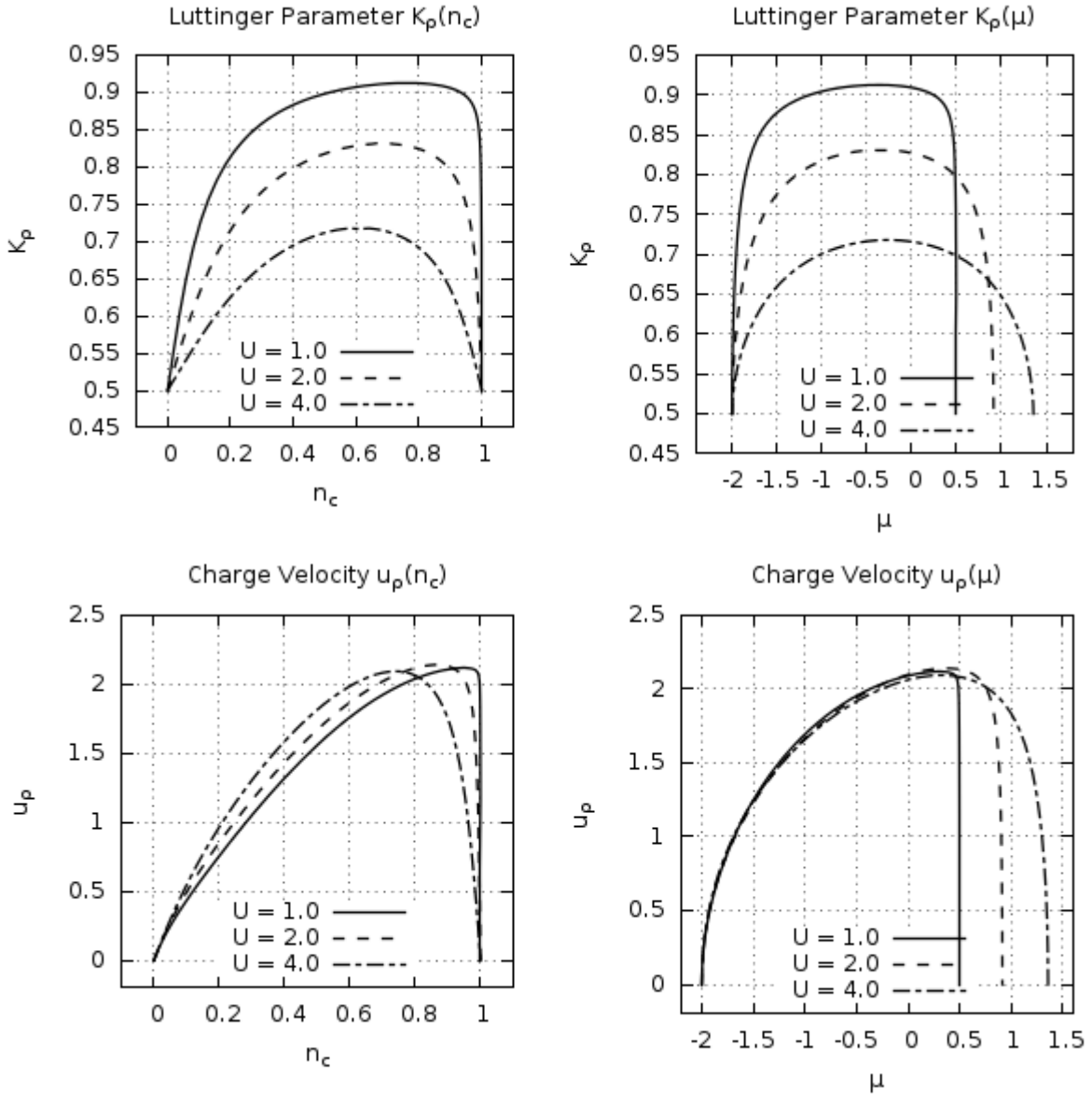

Figure 4.3: *Luttinger Parameters for the Repulsive Hubbard Model, in function of the numerical density (left column) and of the chemical potential (right column).*

4.2 Trap–Size Scaling in the Dilute Limit

The TSS formalism is applied to a Hubbard System in a harmonic confining potential, in order to determine the scaling behaviour of the density function and of the correlation functions in the **Dilute Limit** *(large trap size l at fixed particle number N). Simulation data shows the system has a TSS behaviour in the large–l limit at fixed rescaling interaction strength U_r. All simulation data has been generated by M. Campostrini.*

Let us consider a fermionic confined system, described by the Hubbard Model, whose confining potential has a power–law structure $V(x) = (x/l)^p$, with trap–size l and confining exponent $p = 2$: the effects induced by the presence of the trap can be kept in account using the TSS framework.

As previously underlined, in applying the TSS limit the lattice system is effectively described by the equivalent continuous theory (for instance, since the coordinates are rescaled as $X \equiv x/l^\theta$, and for increasing l the variable X becomes continuous). Quantities like the overall density (comprensive of both spin polarizations) or the density–density correlation function become effectively functions of a continuous coordinate, and are defined as

$$\rho(x) = \langle n(x) \rangle \equiv \left\langle \widehat{C}^\dagger_{x\uparrow} \widehat{C}_{x\uparrow} + \widehat{C}^\dagger_{x\downarrow} \widehat{C}_{x\downarrow} \right\rangle \qquad G_n(x) = \langle n(x) n(0) \rangle - \langle n(x) \rangle \langle n(0) \rangle \tag{4.3}$$

In this section we will analyze the behaviour in the **Dilute Limit** (that is, for large l at fixed number of particles N). In the dilute limit the system has small particle density, since the charachteristic size along which density changes is l (and the correspondent density is N/l) and its critical properties are therefore described by the effective action (1.40),

$$S_0 = \int_0^{+\infty} \int \left\{ \sum_\sigma \Psi^*_\sigma(k) \left[\frac{\partial}{\partial \tau} + \left(\frac{k^2}{2m} - \mu' \right) \right] \Psi_\sigma(k) + U \iint \Psi^*_\downarrow(q) \Psi_\uparrow(k) \Psi^*_\uparrow(p) \Psi_\downarrow(k - p + q) \, \frac{dp \, dq}{(2\pi)^2} \right\} \frac{dk}{2\pi} \, d\tau \tag{4.4}$$

As previously stated, this theory has as relevant parameters μ and U, whose RG dimensions are $\dim(\mu) = (+2)$, $\dim(U) = 1$: our general discussion of the TSS formalism allows to define the trap exponent

$$\theta = \frac{p}{p + y_\mu} = \frac{p}{p+2} = \frac{1}{2} \tag{4.5}$$

Exploiting (3.9), and $\dim(\langle n(x) \rangle) = 1$, we can compute the TSS behaviour of the particle density and of the density–density correlation: their TSS behaviour will be

$$\rho(x, U, N, l) = l^{-\theta} R_N(X, U_r) \qquad G_n(x, U, N, l) = l^{-2\theta} P_N(X, U_r) \qquad \begin{cases} X \equiv l^{-\theta} x \\ U_r \equiv l^\theta U \end{cases} \tag{4.6}$$

In terms of unknown scaling functions R_N, P_N (whose amplitudes will likely depend on N since it is a conserved quantity in this case). This TSS Hypothesis has been verified by comparing numerical simulation data to the predicted TSS behaviours: the numerical results have an error conservatively estimated as not larger than 10^{-6}.

As can be seen in **Figure 4.4** and in **Figure 4.5**, the model density (points) shows the scaling behaviour (4.6) at fixed U_r, since the data generated at different values of l align if multiplied for the predicted power of l and plotted in function of the rescaled coordinate X. We will henceforth

study the system in the hypothesis of large trap size (asymptotically, $l \to +\infty$) at fixed rescaled interaction strength U_r.

In order to calculate the scaling functions, we can, as done for the spinless tight–binding model, pass to a continuum description. The continuum theory equivalent to the Hubbard Model is the $(1/2)$–Spin Gaudin–Yang Model (1.33) with the inclusion of a confining potential (written here in the first–quantization version, since we are working at fixed N):

$$\widehat{H} = \sum_{i=1}^{N} \left(\left(\frac{x_i}{l} \right)^2 - \frac{1}{2} \frac{d^2}{dx_i^2} \right) + g \sum_{i<j} \delta \left(x_i - x_j \right) \tag{4.7}$$

In this passage, the interaction g of the Gaudin–Yang model is in general an unknown function of the Hubbard interaction strength U, and then of U_r: knowledge of the mapping between the two models would be required in order to obtain the scaling function for arbitrary U_r. This can be obtained, nevertheless, in two limiting cases.

One such limiting case is $U = U_r = 0$, in which the system is described by a confined, noninteracting, $(1/2)$–Spin Gaudin–Yang Model, whose Hamiltonian is identical to the sum of two of the spinless versions of (4.7) with $g = 0$, with $N/2$ particles each (the two spin components do not interact, and each counts as a system of $N/2$ particles). In the fixed–N formalism, the scaling functions of each component are those in (3.22), (3.23), and the resulting scaling behaviour (due to the lack of correlation between the two components) is

$$\rho(x, U_r \to 0, N, l) = l^{-\theta} \cdot 2\mathcal{N}_{(N/2)} \left(\frac{x}{l^\theta} \right) \qquad G_N(x, U_r \to 0, N, l) = l^{-2\theta} \cdot 2\mathcal{G}_{(N/2)} \left(\frac{x}{l^\theta} \right) \tag{4.8}$$

Another interesting limit is the $U_r \to +\infty$ case. The results for this case can be derived from the behaviour of the $(1/2)$–Spin Gaudin–Yang model (4.7) in the limit of infinite repulsion $g \to +\infty$ (while the mapping $g(U_r)$ is in general not known, we can assume the Hubbard Model in the limit of infinitely strong repulsion will map in the same limit of the $(1/2)$–Spin Gaudin–Yang model: this assumption is confirmed by our results).

The behaviour of the model in this limit has been studied in [34]: in particular, the density and density correlation functions of this model become those of a spinless, confined, noninteracting Gaudin–Yang Model of N particles. The result is found exploiting the possibility to reduce the effect of an infinitely–strong interaction to a hard–core boundary condition, which has the same structure of a Pauli condition: in particular, the system wavefunction vanishes when two fermions of the same spin polarization occupy the same site, effectively "strengthening" the Pauli Principle.

This identification also implies that, despite the wavefunctions of the two models remain different (in particular, the wavefunction of the hardcore, confined, $(1/2)$–Spin Gaudin–Yang model still has a spin part, while those of the spinless, confined, noninteracting Gaudin–Yang model do not) the density profile (and therefore the density correlations) share the same behaviour for both models. The resulting scaling behaviour, still in terms of (3.22), (3.23), is then

$$\rho(x, U_r \to +\infty, N, l) = l^{-\theta} \cdot \mathcal{N}_N \left(\frac{x}{l^\theta} \right) \qquad G_n(x, U_r \to +\infty, N, l) = l^{-2\theta} \cdot \mathcal{G}_N \left(\frac{x}{l^\theta} \right) \tag{4.9}$$

The density and the density correlation functions of an 1D harmonically confined Hubbard system show, as previously, a scaling dependence from the trap size l in the dilute limit: this time the scaling functions associated to the scaling behaviour are those of a spinless, confined, noninteracting fermionic system of N particles.

We expect that the rescaled particle densities and density correlation functions converge to the scaling behaviour (4.8) for $U_r \to 0$, and to the scaling behaviour (4.9) for $U_r \to +\infty$. The predicted scaling behaviours are plotted in **Figure 4.4** and **Figure 4.5** at fixed values of U_r, and convergence to the predicted TSS behaviours is good for both $\rho(x)$ and $G_n(x)$.

As an observation, we might note that the $U \to +\infty$ limit in a confined system described by the Hubbard Model, followed by the $l \to +\infty$ limit, is not equivalent to the limiting case $U_r \to +\infty$. While in the latter case we have the TSS behaviour illustrated above, in the former the fermions will gather in the sites at the center of the trap, with one fermion per site (this is the least–energy configuration, since it makes the divergent interaction contribution vanish and minimizes the confining potential contribution). This configuration remains the same for any trap size, and therefore does not have any kind of scaling behaviour.

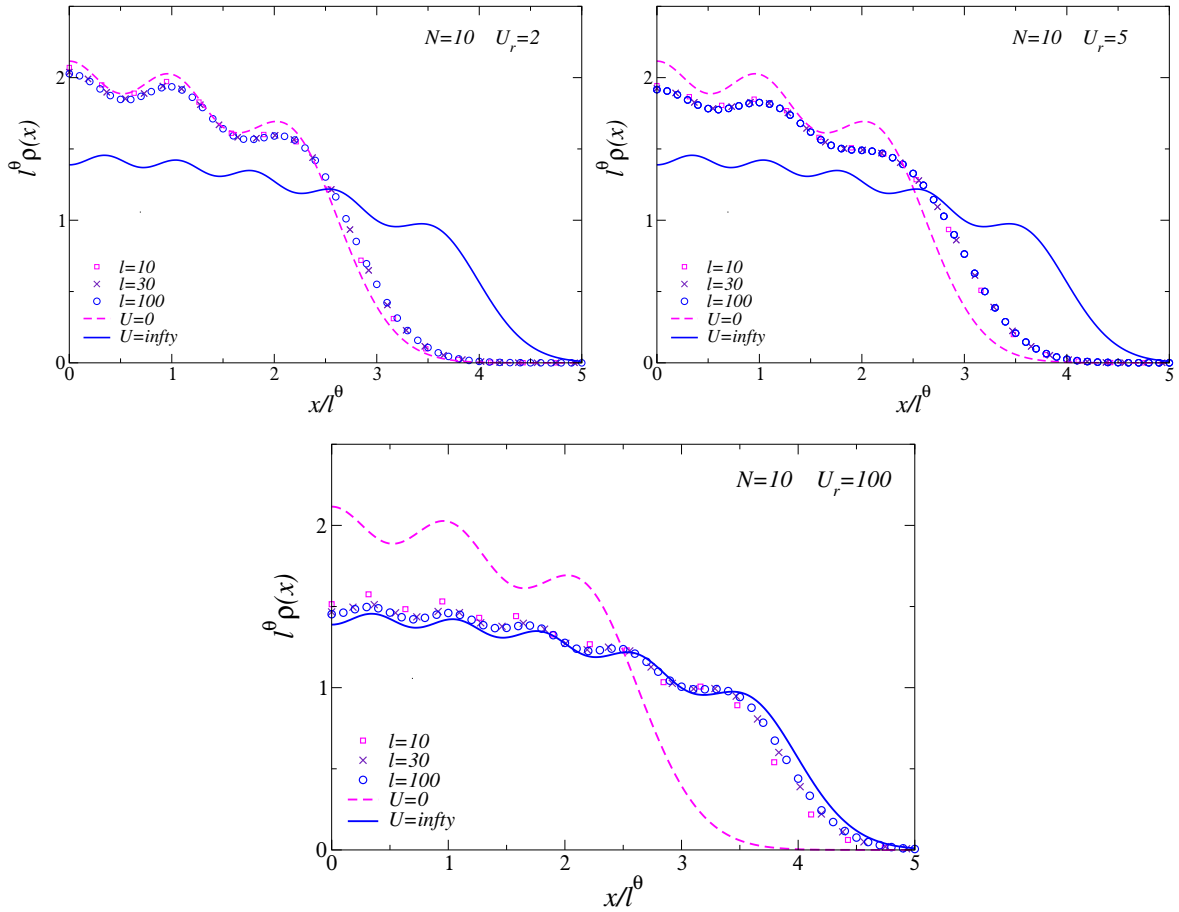

Figure 4.4: *TSS behaviour of the particle density at fixed* $N = 10$ *and* $U_r = 2,\ 5,\ 100$.

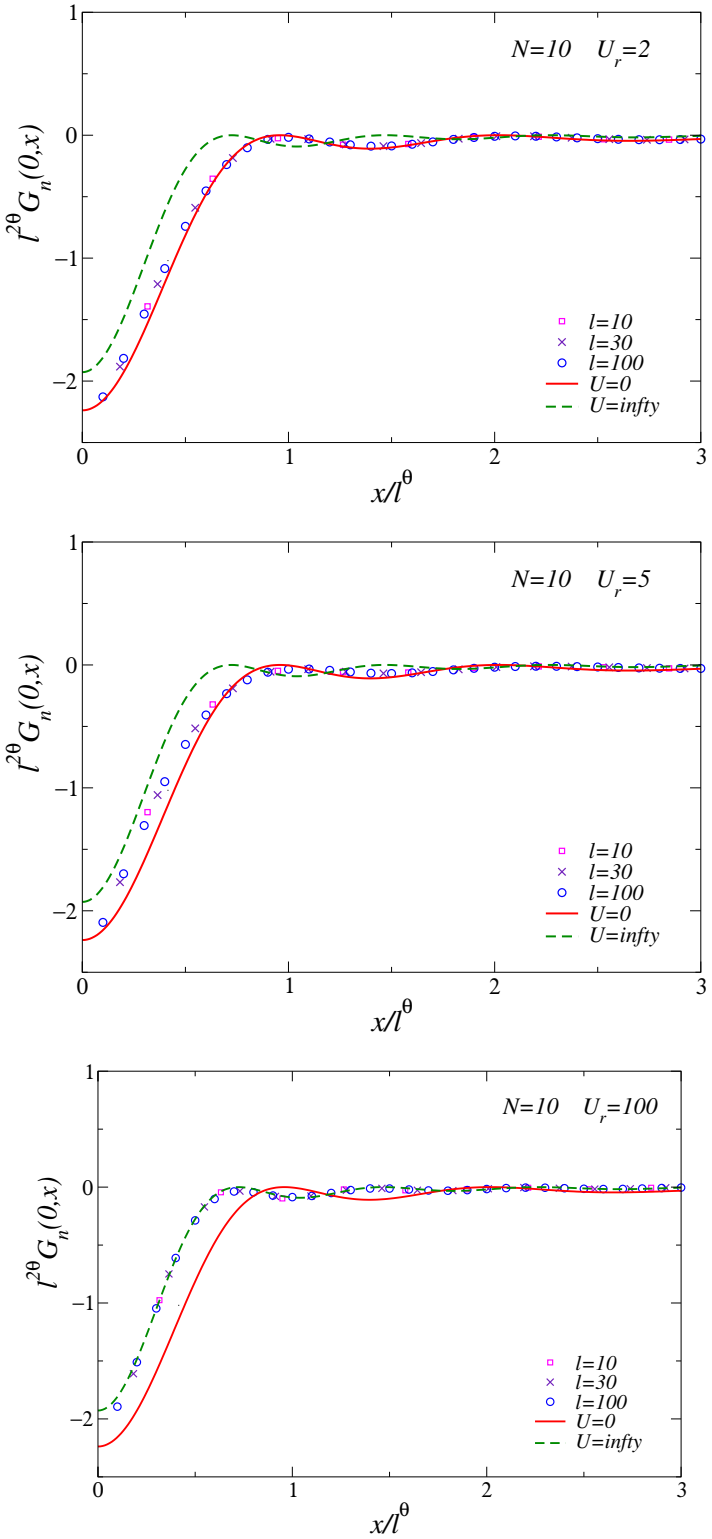

Figure 4.5: *TSS behaviour of the the density correlation function at fixed* $N = 10$ *and* $U_r = 2,\ 5,\ 100$.

4.3 Trap–Size Scaling in the Trapped Thermodynamic Limit

A Hubbard system in a harmonic confining potential is analyzed in the Trapped Thermodynamic Limit ($l \to +\infty$ at fixed N/l). The solutions of the homogeneous Hubbard model are used to describe the behaviour of the confined Hubbard system using the LDA method; subsequently, simulation data is used to calculate the deviations from the LDA behaviour, and the behaviour of these corrections is studied. All simulation data has been generated by M. Campostrini.

4.3.1 LDA Results

The Trapped Thermodynamic Limit (large l while keeping N/l fixed) is another limit in which the confined system shows trap–size dependence. In this case, the particle number N is not a fixed parameter, while the density N/l is: in the LDA approximation, the last condition is equivalent to fixing μ, since the two quantities are linked by a relation $N/l = C(\mu)$ like (3.4) for the spinless tight–binding model.

This relation is expected to hold at least asymptotically, since the LDA should improve for $l \to +\infty$ (as proven in the next section). All observations and comparisons, therefore, will be done between systems at fixed N/l (that is, at fixed μ: this is the equivalence criterion for variable particle number).

As previously, we will choose a Harmonic Potential, and the knowledge of the confining potential allows to establish an "effective chemical potential" $\mu_{\text{eff}}(x)$, linked to the total particle number N (counting both spin polarities) by the equivalent of (3.4),

$$N = \sum_x \langle n_x \rangle_{LDA} \to \int_{-\infty}^{+\infty} n_c\left(\mu_{\text{eff}}(x)\right)\, dx + o(l) = 2\int_0^{+\infty} n_c\left(\mu - \left(\frac{x}{l}\right)^2\right)\, dx + o(l)$$
$$= 2l\int_0^{\sqrt{\mu-\mu_0}} n_c\left(\mu - y^2\right)\, dy + o(l) \equiv l \cdot C(\mu) + o(l) \tag{4.10}$$

The corrections to the LDA estimate for the function $C(\mu)$ are therefore $(N/l - C(\mu)) = o(1)$: these keep into account both the error coming from the passage from the sum over sites to the continuous integral (of order $O(l^{-1})$) and the intrinsic error of the LDA itself, which is conservatively estimated as $o(1)$ (the results shown in the next section will give the order of this correction, and show that it is $o(1)$ everywhere in the confined system).

$n_c(\mu)$ becomes 0 for $\mu \leq \mu_0$, and this generates the upper integration limit $\sqrt{\mu - \mu_0}$. (4.10) allows to link the center chemical potential μ to the parameter N/l by inverting $C(\mu)$ at a given U; the resulting function $\mu(N/l)$ is shown in **Figure 4.6** (the non–analiticities are due to the Conductor–Insulator Transitions).

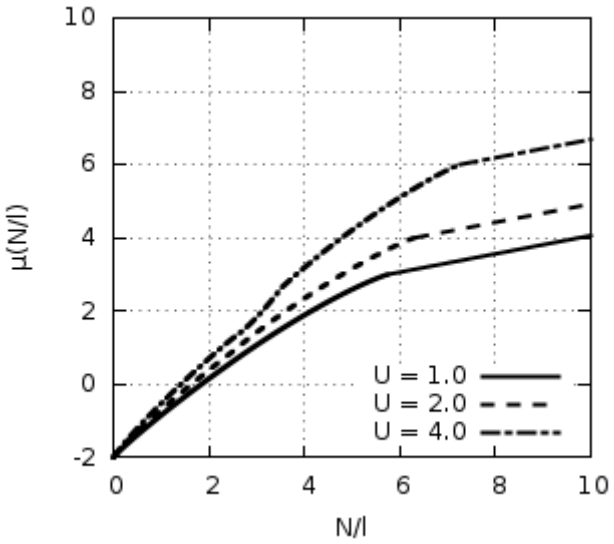

Figure 4.6: $\mu(N/l)$ *function for* $U = 1, 2, 4$. *The non–analiticities are due to the Conductor–Insulator transitions.*

Once μ is known for a given N/l and U, the function $\rho^{\mathrm{LDA}}(x) = n_c\left(\mu_{\mathrm{eff}}(x)\right)$ can be computed, obtaining the plots in **Figure 4.7**.

We can see from **Figure 4.7** that the LDA predicts the coexistence of Insulating (the fixed–density sections of the system, both at $\rho = 1$ and $\rho = 2$) and Conducting Phases (with variable density) in the confined system for high enough N/l. This phenomenon has already been found using the LDA approach for Hubbard systems ([19]) and has been confirmed by numerical simulations ([10]).

In the LDA approximation, the "transition coordinates" can be computed exactly imposing $\mu_{\mathrm{eff}}(x) = \mu - (x/l)^2$ assumes the values (-2) (for the vacuum–conductor transitions), $\mu_{-}(U)$ (for the Mott–Insulator–Conductor transition at $\rho^{\mathrm{LDA}}(x) < 1$) and similarly for the other transitions, using the phase boundaries given in **Section 4.1**. As shown in the plots, different interaction strengths allow different extensions of the Insulating *plateaux* (the Mott–Insulating one is present at $U = 1$ as well, albeit very narrow and hardly visible).

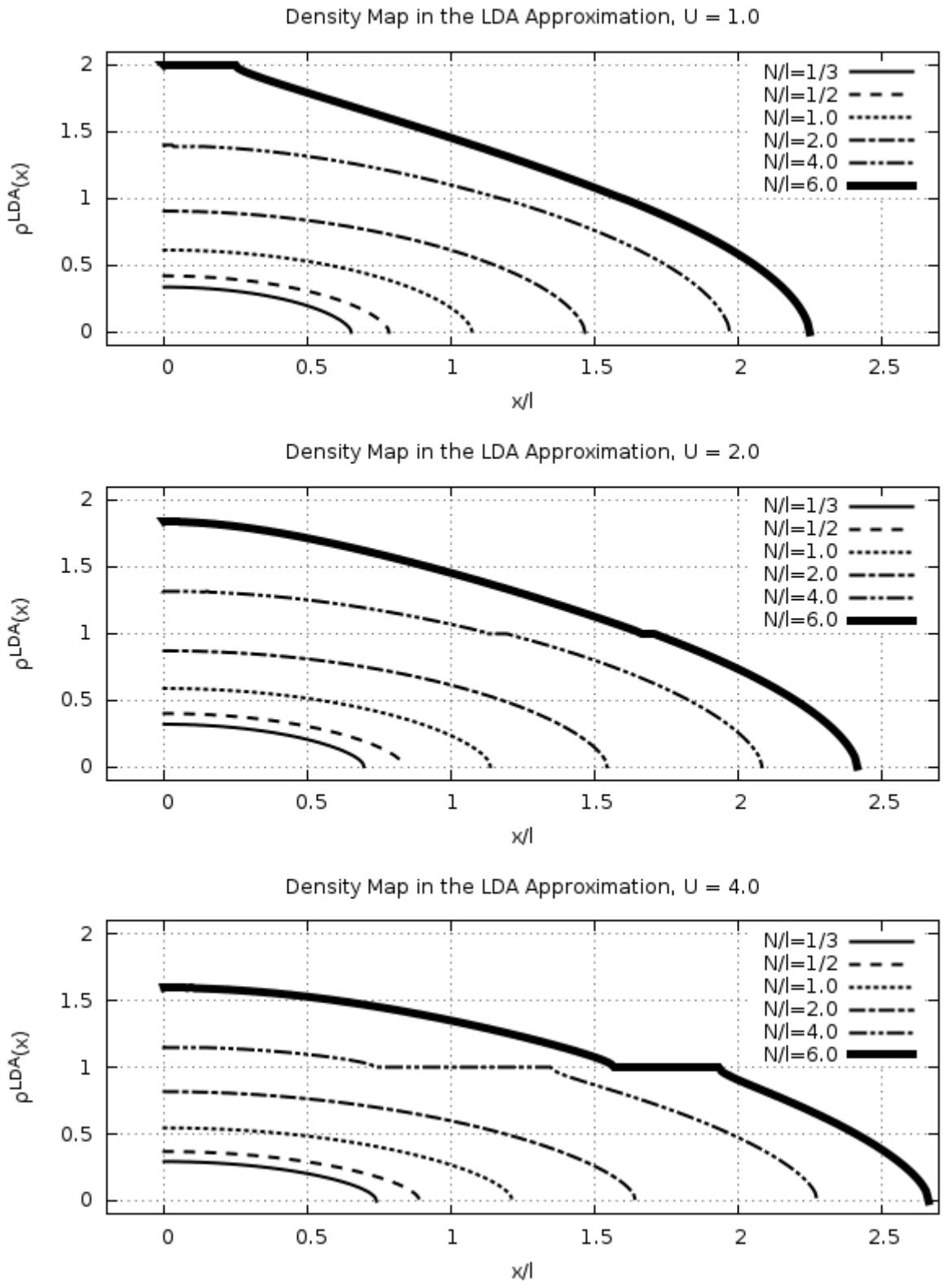

Figure 4.7: $\rho^{\mathrm{LDA}}(x)$ *maps for* $U = 1, 2, 4$.

The corrections to the LDA results can be obtained using numerical simulations to determine the system behaviour: the simulations have been run, at fixed U, for several values of the fermionic number N and the trap size l, and the error on the numerical results can still be considered, as previously, not larger than 10^{-6}. Since we expect the LDA to approximate well the simulation data, simulated datasets at fixed U with the same N/l should be very similar (in the LDA, they would be identical). This is confirmed by plots like the one in **Figure 4.8**, where density datasets $\rho(x)$ (obtained by numerical simulations) ρ at $U = 1,\, 2$ and $N/l = 1,\, 1/2$ are shown to differ for small deviations, which decrease for high particle number.

We can observe that, for higher l at fixed N/l, the transition to $\rho = 0$ happens at a smaller x/l: the transition point moves slightly for increasing U at higher x/l, and moves significantly more towards lower x/l for decreasing N/l. This behaviour is very similar to the one shown in **Figure 4.7**, and is another hint of a good accuracy of the LDA results in approximating the real density behaviour.

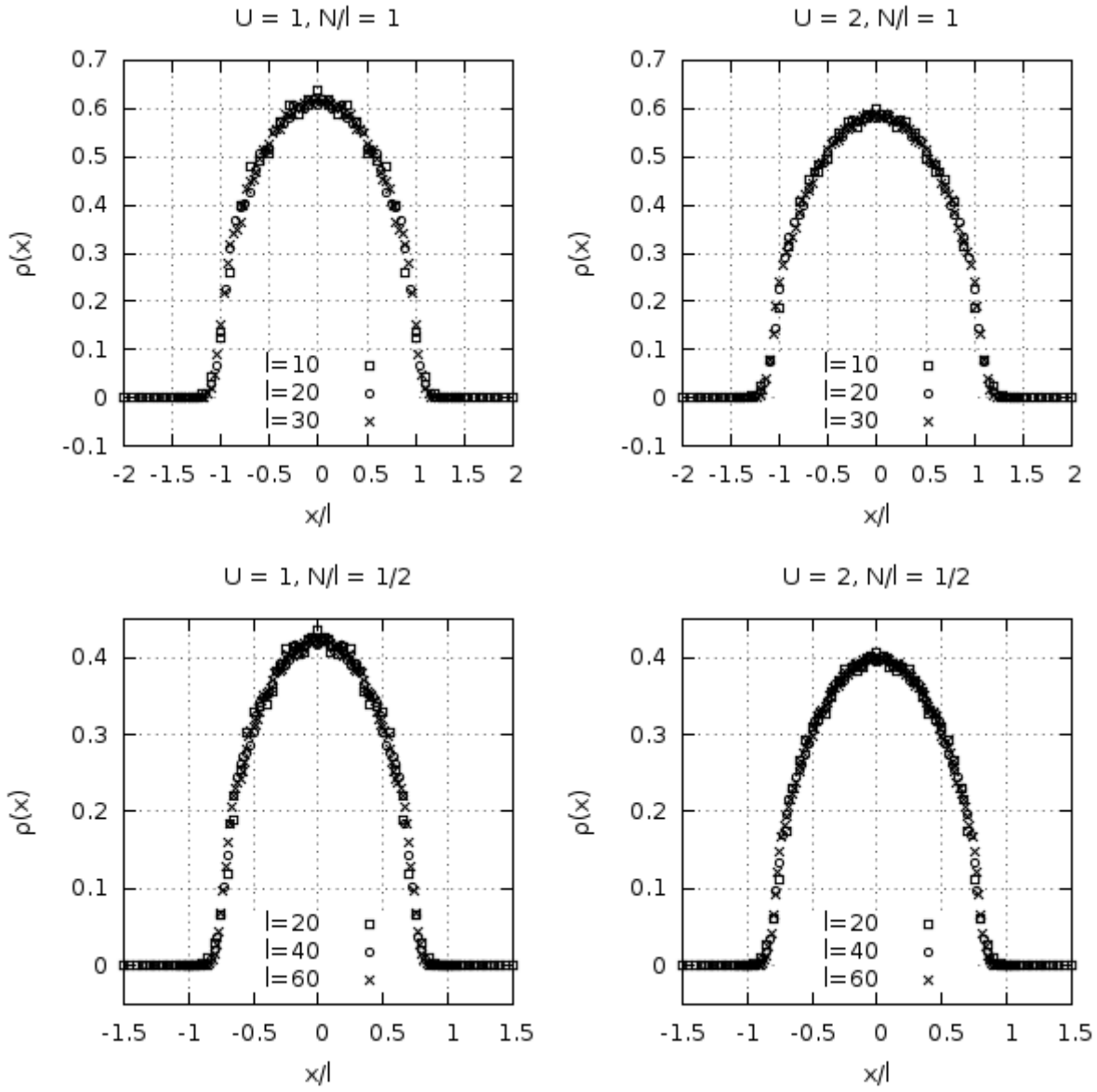

Figure 4.8: $\rho(x)$ *for* $U = 1,\, 2$ *and* $N/l = 1,\, 1/2$.

In **Figure 4.9** the LDA results are compared directly with the system density: this is well approximated by the LDA results, with the difference between them being an oscillating function, more visible for decreasing l (as expected, since for $l \to +\infty$ the LDA should improve). As shown in the plots, the transition point pointed out by the numerical data is always at a larger x/l than the LDA one, and converges to it for increasing l.

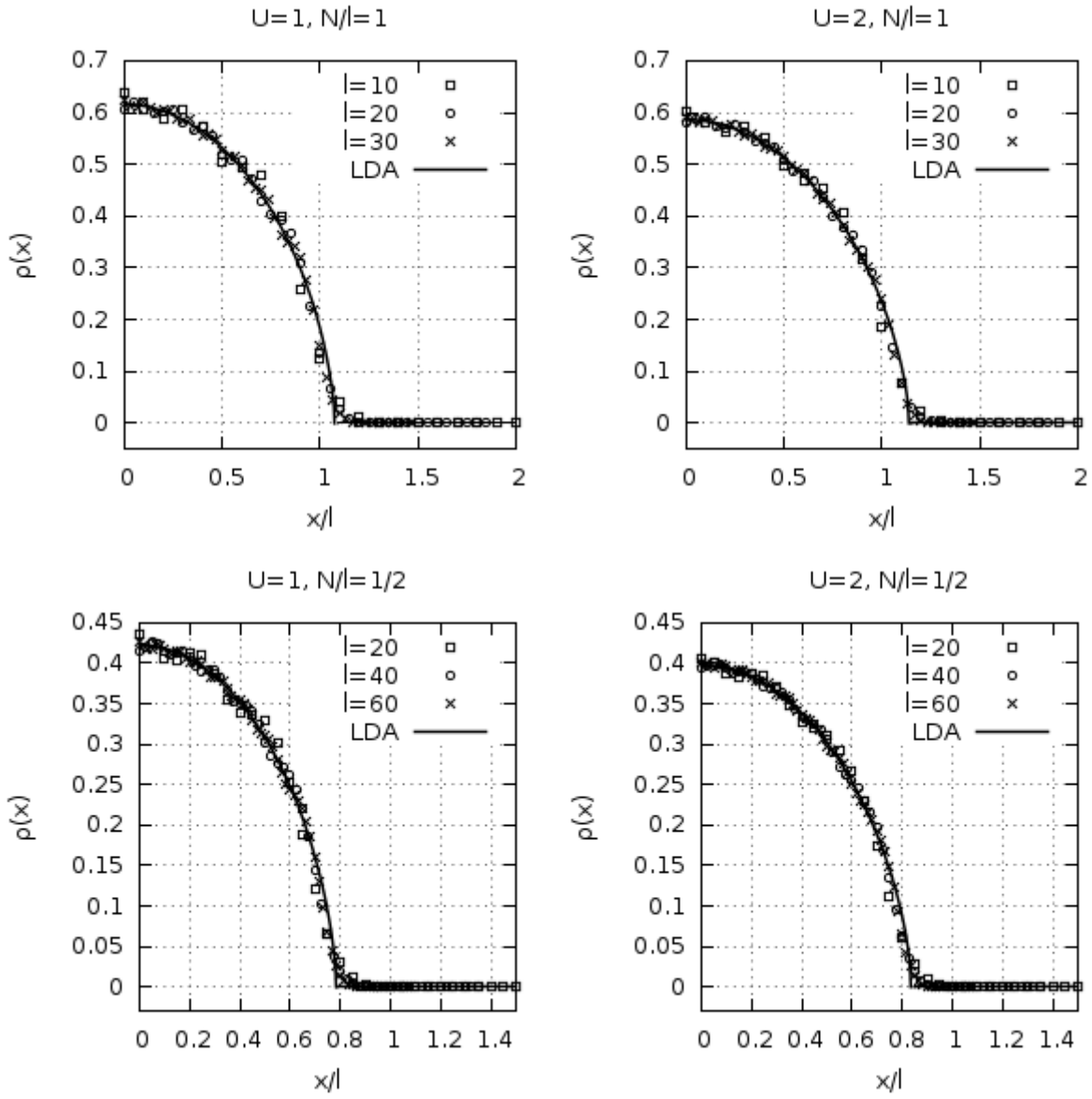

Figure 4.9: $\rho(x)$ *and* $\rho^{\mathrm{LDA}}(x)$ *Data for* $U = 1,\ 2$ *and* $N/l = 1,\ 1/2$.

As the deviations from the LDA results are small, the latter can be used to approximate well the behaviour of the system. In the next section the structure of the corrections and their dependence on the trap size l will be analyzed.

4.3.2 TSS Corrections

The deviations shown by simulation data from the LDA results can be analyzed in order to find their dependence on the trap size l: here we will concentrate on studying the leading behaviour in this parameter. As we will show, corrections to the LDA results follow two different behaviours in terms of l: one in proximity of the trap center, following (4.11), and another in proximity of the Mott Transition point to the empty lattice, following (4.13).

Trap Size Dependence around the Trap Center. The corrections to the LDA results in the conducting phase of the Hubbard Model might share the structure of the same corrections for the conducting phase of the Bose–Hubbard Model in the Hardcore Limit (which, we recall, was equivalent to a noninteracting, spinless, tight–binding fermionic gas).

These phases are similar: both are described by a bosonic relativistic theory ((1.41) for the former and the spinless version of (1.18) for the latter), and the interaction term in the former model is RG–irrelevant in the conducting phase, therefore suggesting equivalence in the critical behaviour (at least for the dominant scaling exponents: spin and interactions will likely be felt in subleading corrections and in scaling amplitudes).

The corrections to the Hardcore Bose–Hubbard Model in the conducting phase have been thoroughly studied in [21]: the corresponding dominant trap–size dependence for the Hubbard Model would be

$$\Delta\rho \equiv \left(\rho^{\mathrm{LDA}}\left(\frac{x}{l}\right) - \rho\left(\frac{x}{l}\right)\right) \qquad \Delta\rho = O\left(l^{-1}\right) \tag{4.11}$$

As shown in **Section 1.3.2**, in the conducting phase U is a marginal parameter, and therefore does not rescale in the Trapped Thermodynamic Limit. The function $L_c \equiv (l \cdot \Delta\rho)$ is plotted in **Figure 4.10** for $U = 1.0$ and in **Figure 4.11** for $U = 2.0$. The analysis of this plot shows L_c is an oscillating function, whose overall number of peaks is $(N + 3)$, where N is the number of particles: this suggests the oscillation frequency might depend on the number of particles (as for the Hardcore Bose–Hubbard Model, where an oscillating term, dependent on the Fermi Momentum, appeared in the corrections).

The amplitude of these oscillations decreases, around the trap center, for increasing l at fixed N/l (the different number of particles implies a different number of peaks, but the comparison can be done by observing the "oscillation envelope" is, near the trap center, approximately the same function for all values of l at fixed N/l, and decreases slowly for increasing l). Furthermore, the amplitude of the corrections also appears to decrease by increasing U at fixed N/l and l.

While the leading behaviour of the density is $O(l^{-1})$, the rescaled density differences L_c have an oscillating behaviour around $L_c = 0$, and appear to have vanishing average if this is taken around the trap center, suggesting that the actual correction to the LDA behaviour in this region is of an higher order than $O(l^{-1})$.

This argument, however, holds only for the region around the trap center, since the peaks at the boundary of the fermionic cloud do not oscillate, and (as we will show) their corrections are more relevant than $O(l^{-1})$, being at a lower order. While our data is sufficient to state these results, more data and a more advanced analysis will be required for a thorough analysis.

TSS at the Fermionic Cloud Boundary. The dependence shown in (4.11) breaks down in proximity of the boundaries of the fermionic cloud, where sizable differences between systems at different l start to arise in the peak heights, suggesting l^{-1} is replaced, as leading behaviour, by a smaller power of the parameter $1/l$. This change in trap–size dependence is caused by the appearance of critical modes related to the transition to the vacuum phase.

This phenomenon can be treated by adapting the TSS formalism at the dilute transition, shown

in the previous section. ρ becomes 0 only asymptotically: however, due to the small deviations of the simulation data $\rho(x)$ with respect to the LDA results (which instead show a sharp transition) the transition coordinate in the lattice may be approximately localized in the LDA transition point x_t defined by the condition $\mu_{\text{eff}}(x_t) = \left(\mu - (x_t/l)^2\right) = (-2)$. The function $\mu_{\text{eff}}(x)$ might be expanded around this position.

$$x_t = l \cdot \sqrt{\mu + 2} \qquad \mu_{\text{eff}}(x \cong x_t) = \left[\mu - \left(\frac{x}{l}\right)^2\right]_{x \cong x_t} = (-2) - 2\sqrt{\mu+2}\left(\frac{x - x_t}{l}\right) + \dots \tag{4.12}$$

The dilute–transition TSS formalism may be applied to describe the anomalous behaviour at $x \cong x_t$, but with a (locally) linear confining potential, i. e. $p = 1$. The TSS *ansatz* may be applied at first to the model density $\rho(x)$, and we must take the scaling exponents of the low–density effective theory (4.4): the Trap Exponent ζ and the expected scaling become (as implied by (3.9) and (3.18), knowing $\dim(U) = \dim(n) = 1$ and $\dim(G_n) = \dim(\mu) = 2$ in this theory)

$$\rho(x \cong x_t) = l^{-\zeta} \cdot L_t\left(\frac{x - x_t}{l^\zeta}, l^\zeta U\right) \qquad \zeta = \frac{p}{p + y_\mu} = \frac{1}{3} \tag{4.13}$$

While in the previous section U was a marginal parameter, invariant under rescaling, in the low–density effective theory U is relevant, and the rescaled interaction strength $U_s \equiv l^\zeta U$ will appear in the scaling functions. $Y \equiv l^{-\zeta}(x - x_t)$ is taken as rescaled coordinate since, due to the definition of trap exponent in (3.5), the dominant modes in proximity of the transition will have a correlation length scale $\xi \sim l^\zeta$. We note that x_t varies even at fixed N/l since it depends linearly on l.

This scaling behaviour (for both density and coordinate rescaling) is confirmed by the plots in **Figure 4.12**, where the numerical density datasets converge if rescaled following (4.13) and in terms of the rescaled coordinate Y. We must note that in these plots we compare datasets at constant N/l and U, which in general would not guarantee the satisfaction of the scaling behaviour (4.13) (this appears when data at the same U_s are compared). Since the available data did not allow comparison between data at constant U_s, comparisons at constant U were done.

The error in doing this should be small, since the chosen values of l would induce only small changes in the U_s needed for comparison: instead of comparing data at the same U they should be at $\left(U, \sqrt[3]{2}U, \sqrt[3]{3}U\right)$, and therefore the difference between the needed interactions and the used ones is very small. As can be seen comparing the $U = 1.0$ and the $U = 2.0$ data, a slight change in the interaction strength would produce only a small change in the obtained data, and therefore the plotted data should show the scaling behaviour (4.13) anyway.

This argument explains the good convergence in proximity of the transition point $Y = 0$, which gradually breaks down (along with the validity of (4.13)) away from the transition point. While our results cannot be taken as rigorous results to prove the scaling behaviour, they are a good qualitative proof of it, since the datasets wouldn't be very different considering constant U_s instead of constant U.

In **Figure 4.13** the scaling behaviour (4.13) is tested on the $\Delta\rho$ function, the difference between the density and the LDA results. Again, data has been compared at constant U, and therefore the scaling behaviour cannot be rigorously proven: however, as can be seen from the plot, the small differences in the required U_s for the optimal plot allows to see the expected scaling behaviour is followed well (again, while our results cannot be a rigorous proof of (4.13), they are a good qualitative proof of it, for the same reasons outlined earlier).

The small magnitude of the deviations in peak heights and positions for varying l (likely caused by the choice of constant U rather than constant U_s) imply good accuracy of (respectively) the scaling behaviour of the quantity $\Delta\rho(x \cong x_t)$ and of the coordinate $(x - x_t)$. As both the numerical data and the density differences follow this scaling behaviour, the LDA density ρ^{LDA} will show the scaling behaviour (4.13) on its own as well. As previously, the scaling behaviour (4.13) begins to fail far enough from the transition point.

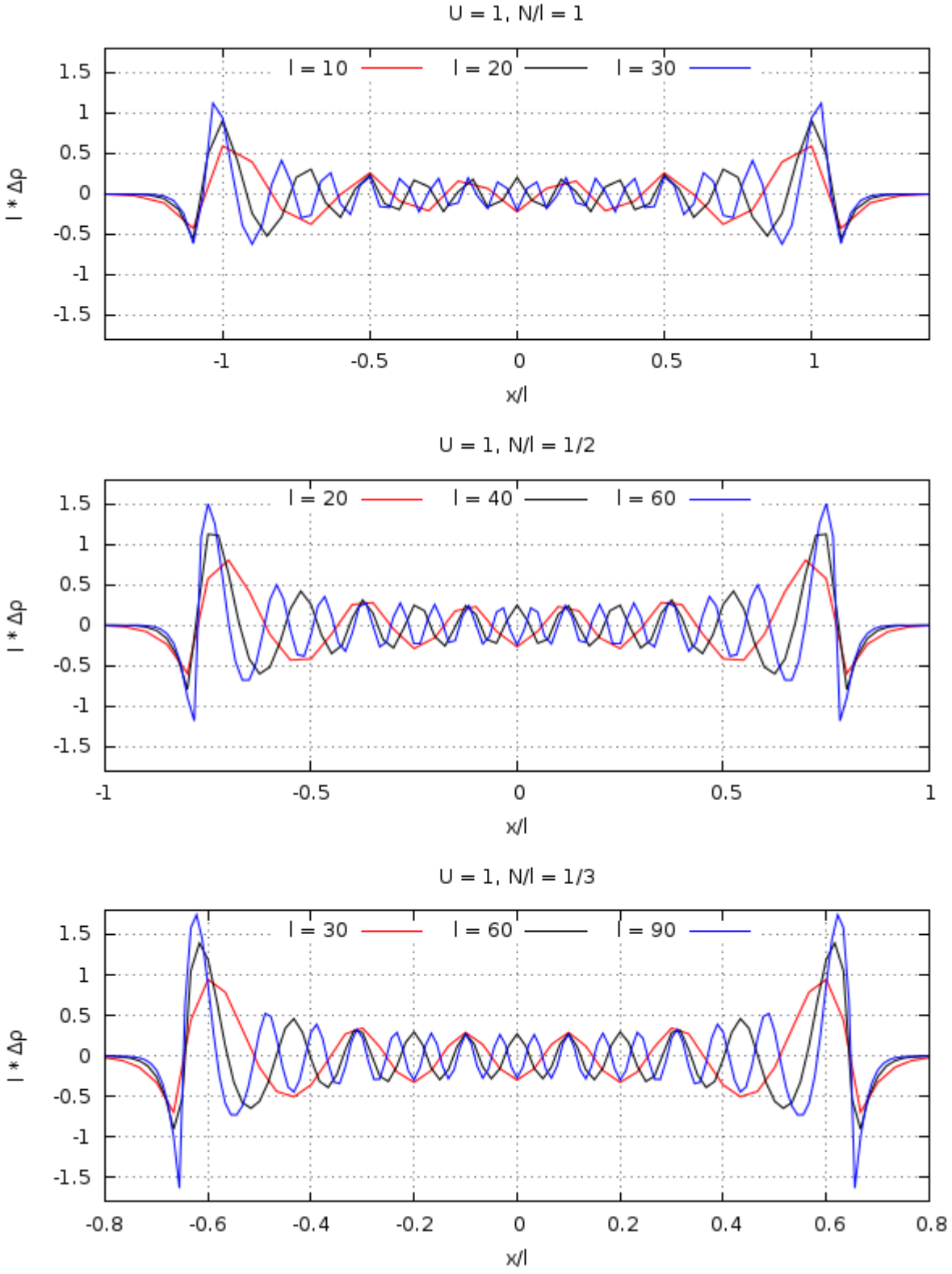

Figure 4.10: *Rescaled Deviations from the LDA around the Trap Center,* $U = 1.0$.

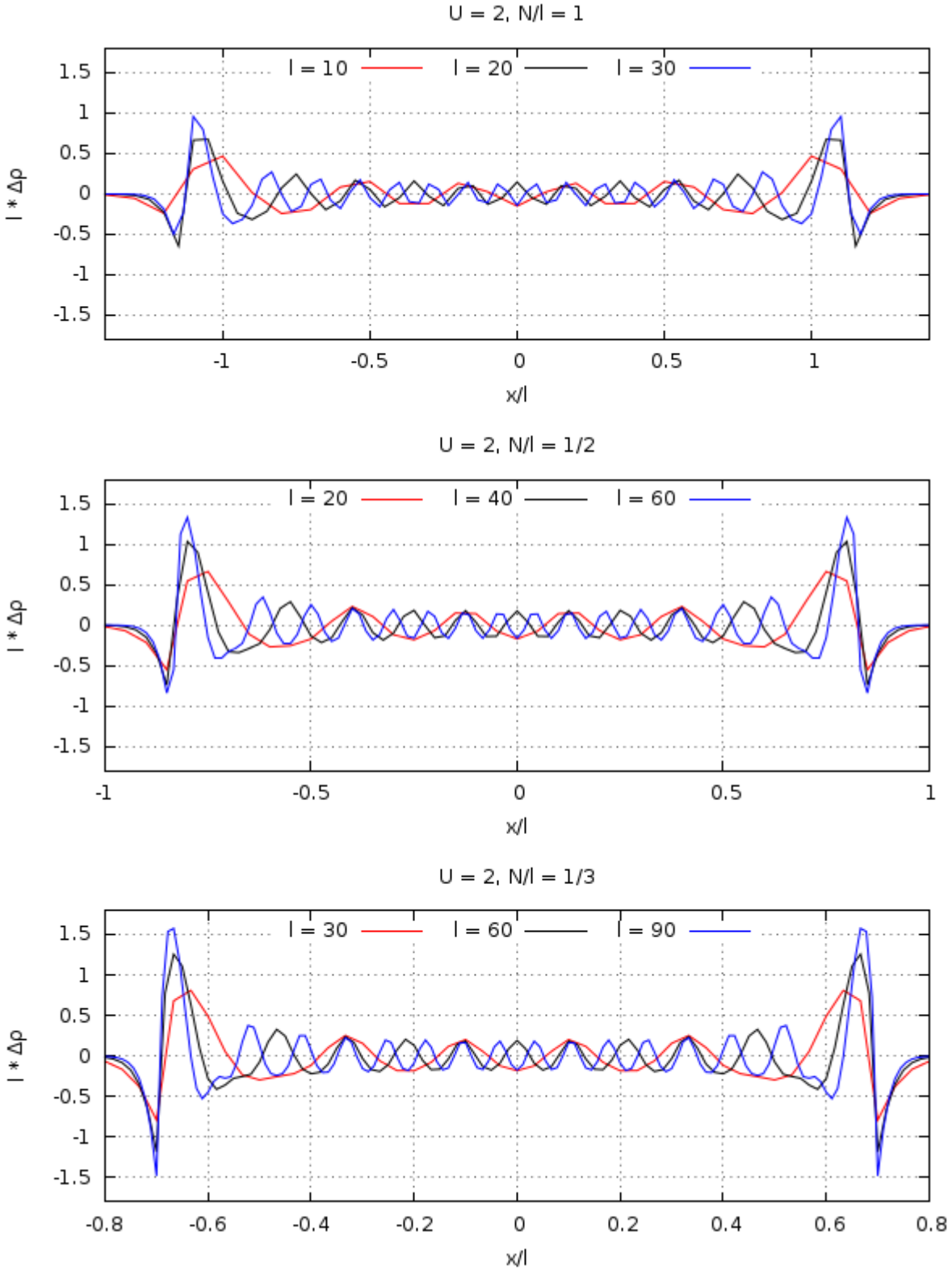

Figure 4.11: *Rescaled Deviations from the LDA around the Trap Center,* $U = 2.0$.

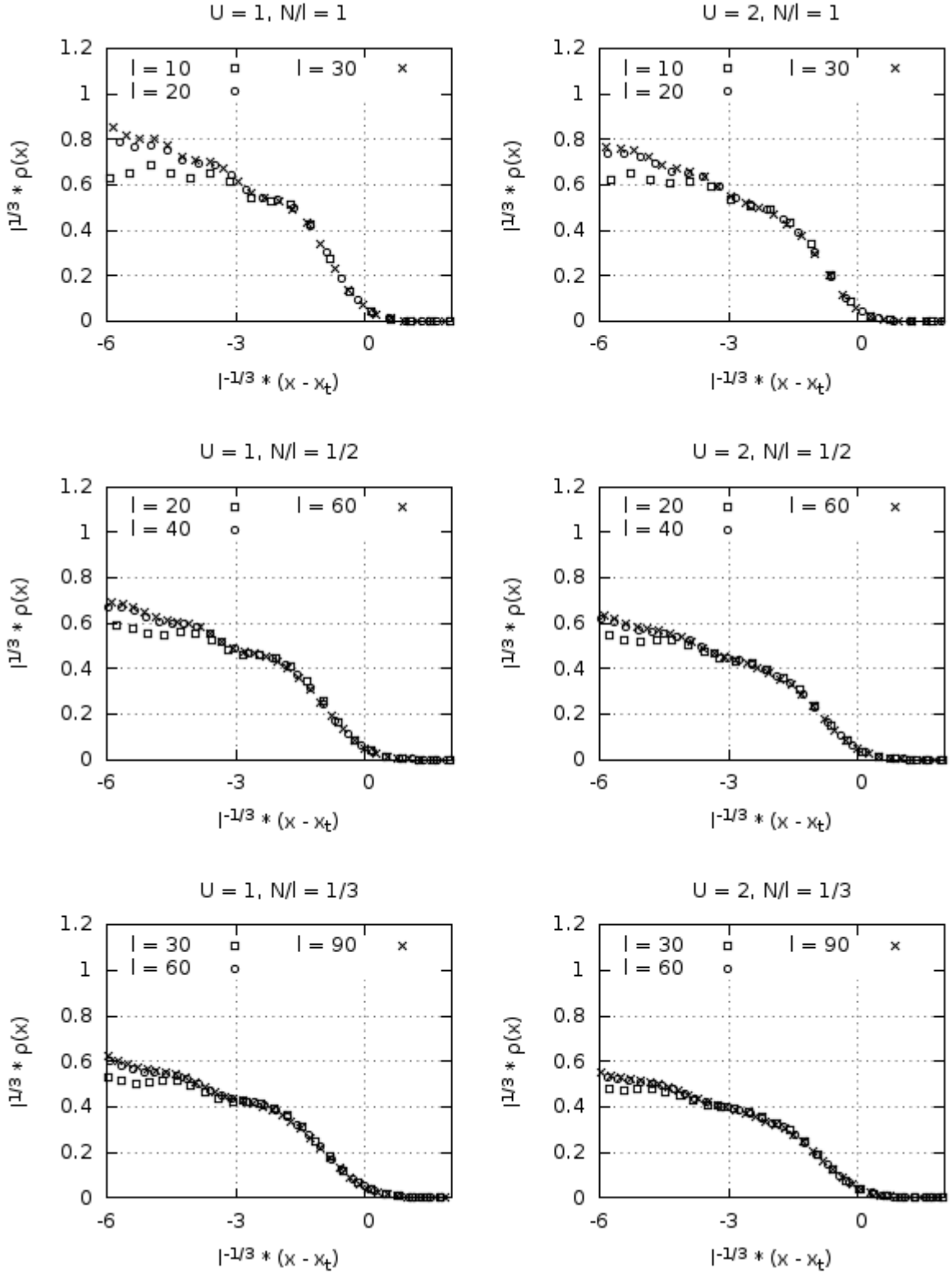

Figure 4.12: *Rescaled Density at the Fermionic Cloud Boundary.*

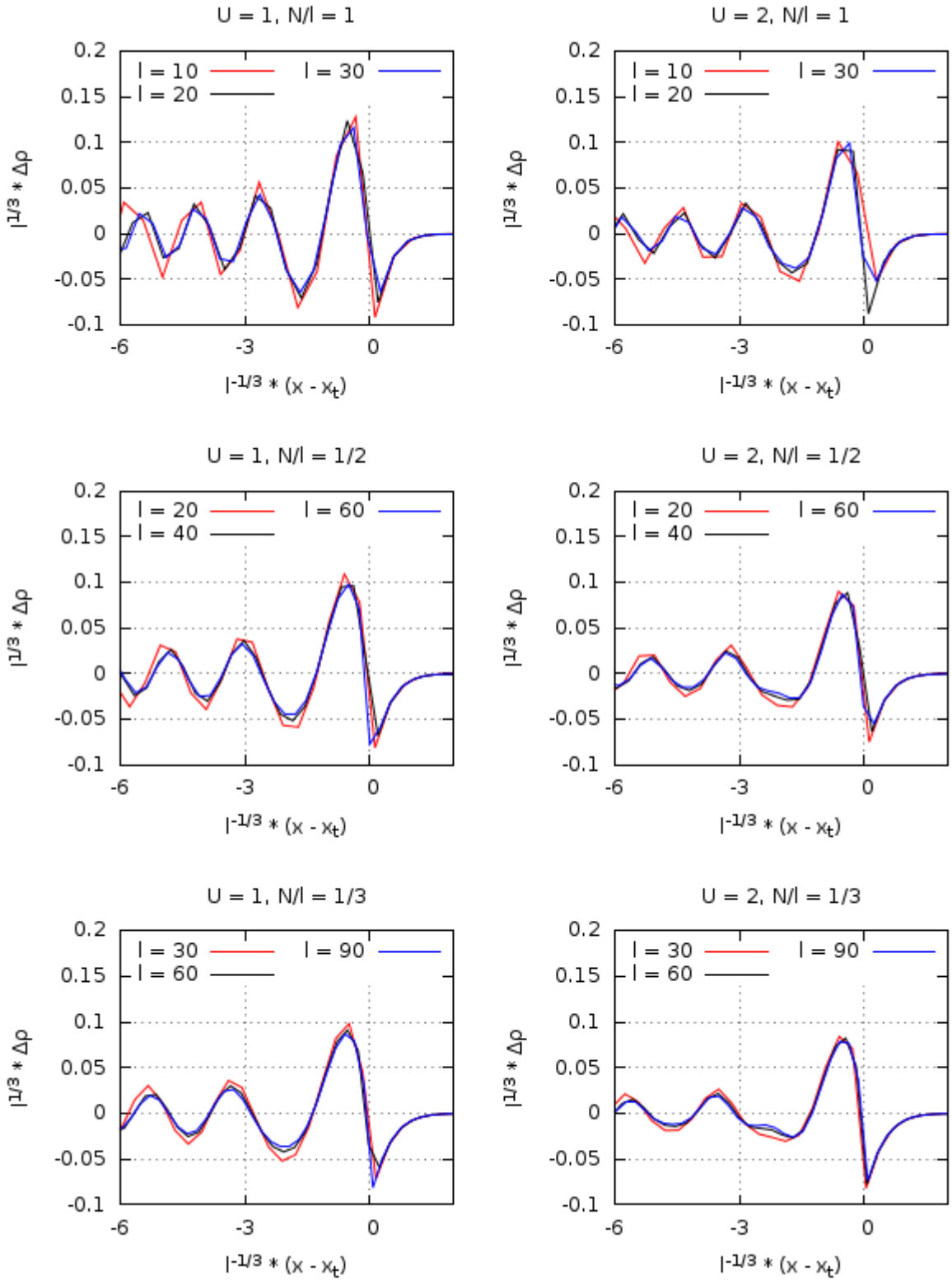

Figure 4.13: *Rescaled Deviations from the LDA at the Fermionic Cloud Boundary.*

Conclusions

In the present work, we study the behaviour of a one–dimensional, unpolarized fermionic system with repulsive interactions, described by the Hubbard Model, in the presence of a harmonic confining potential: this description can be applied to study systems of cold fermionic atoms in optical lattices, to keep into account the effects of the trapping potential in the experimental setup. Our analysis can be generalized to the case of any power–law potential $V(x) = (x/l)^p$.

In particular, we study the corrections to the behaviour predicted by the LDA method, commonly employed to describe these inhomogeneous systems: this method consists in approximating the behaviour of a confined system using the μ–dependent behaviour of the homogeneous system in terms of a position–dependent chemical potential $\mu_{\rm eff}(x)$. We analyze the structure of these corrections and their dependence on the trap size l in the large–l limit, by means of the TSS framework.

At first, the behaviour of the homogeneous Hubbard Model, instrumental to compute the LDA results, is determined applying the Bethe *Ansatz* method, which leads to integral equations, solved numerically to find the density of the homogeneous model, as a function of the chemical potential. We then use this result to determine, in the LDA, the spatial density $\rho(x)$ of a confined system.

In a confined system, density is highest in the center of the trap and decreases for increasing distance from it. The LDA predicts the coexistence, for high enough density, of insulating and conducting phases in the confined system. We use the LDA results to compute the boundaries of the fermionic cloud inside the trapped system.

In order to study the validity of the LDA and to determine the nature of the corrections to this approximation, we compare its predictions with numerical simulation data for a trapped Hubbard system, at fixed N/l and increasing trap size l. In the large–l limit at constant chemical potential (that is, at fixed N/l, since the two quantities are linked at least asymptotically in the LDA approximation) the corrections show two different behaviours, in different regions of the confined system.

- ◇ Around the trap center, the corrections $\Delta\rho = \left(\rho^{\rm LDA}(x/l) - \rho(x/l)\right)$ to the LDA behaviour are $O(l^{-1})$. The rescaled density differences $(l \cdot \Delta\rho)$ have an oscillating behaviour around $(l\Delta\rho) = 0$, suggesting that the corrections to the LDA behaviour might be of higher order than $O(l^{-1})$, if the average is computed around the trap center. The oscillation amplitudes of the corrections also decrease for increasing fermionic interaction strength U.
- ◇ The behaviour of the fermionic density differs away from the trap center, close to the boundary of the fermionic cloud, showing larger corrections to the LDA results. This new scaling behaviour can be interpreted as due to the appearance of modes correlated to the transition to the $\rho = 0$ phase. This behaviour is described within the TSS framework associated with an effective linear confining potential around the fermionic cloud boundary. The resulting scaling law is

$$\rho = l^{-1/3} L_t \left(\frac{x - x_t}{l^{1/3}}, l^{1/3} U \right) \tag{4.14}$$

  where x_t is the coordinate calculated as the transition point to $\rho = 0$ in the LDA. This behaviour is substantially confirmed by the analysis of the data up to $l = 90$.

More data and a more detailed analysis will be required for a thorough study of the structure of the corrections to the LDA, leaving it to a further work.

We also study the large–l regime at fixed particle number N. In this case the density and the density–density correlation function show a TSS behaviour with trap exponent $\theta = 1/2$. We show that a nontrivial TSS behaviour is obtained by keeping $U_r = Ul^\theta$ fixed in the limit of large trap size. The $U_r = 0$ and $U_r \to +\infty$ TSS behaviours correspond to those of, respectively, a $(1/2)$–Spin noninteracting Fermi gas of N particles and a spinless noninteracting Fermi gas of N particles.

Bibliography

[1] FELDNER H., MENG Z. Y., HONECKER A., CABRA D., WESSEL S., ASSAAD F. F., *Magnetism of Finite Graphene Samples: Mean–Field Theory compared with Exact Diagonalization and Quantum Monte Carlo Simulation*, Phys. Rev. B **81**, 115416 (2010).

[2] GIULIANI A., MASTROPIETRO V., *The 2D Hubbard model on the honeycomb lattice*, Comm. Math. Phys. **293**, 301 – 346 (2010).

[3] MA T., HU F., HUANG Z., LIN H., *Controllability of ferromagnetism in graphene*, Appl. Phys. Lett. **97**, 112504 (2010).

[4] YAZYEV O. V., *Emergence of magnetism in graphene materials and nanostructures*, Rep. Prog. Phys. **73**, 056501 (2010).

[5] IMADA M., FUJIMORI A., TOKURA Y., *Metal–insulator transitions*, Rev. Mod. Phys. **70**, 1039–1263 (1998).

[6] KOHNO M., *Mott Transition in the Two–Dimensional Hubbard Model*, Phys. Rev. Lett. **108**, 076401 (2012).

[7] YANAGISAWA T., MIYAZAKI M., YAMAJI K., *Correlated–Electron Systems and High–Temperature Superconductivity*, Journal of Modern Physics **4**, No. 6A, 33 – 64 (2013).

[8] DAGOTTO E., *Correlated electrons in high–temperature superconductors*, Rev. Mod. Phys. **66**, 763 (1994).

[9] SÖFFING S. A., BORTZ M., EGGERT S., *Density profile of interacting Fermions in a one–dimensional optical trap*, Phys. Rev. A **84**, 021602(R) (2011).

[10] RIGOL M., MURAMATSU A., *Numerical simulations of strongly correlated fermions confined in 1D optical lattices*, Opt. Commun. **243**, 33 (2004).

[11] XIANLONG G., POLINI M, TOSI M. P., TANATAR B., *Effect of Disorder on the Interacting Fermi Gases in a One–Dimensional Optical Lattice*, Int. J. Mod. Phys. B **22**, 4500 (2008).

[12] GOLDMAN N., *Mott–Insulator Transition for Ultracold Fermions in Two–Dimensional Optical Lattices*, Phys. Rev. A **77**, 053406 (2008).

[13] GUAN X., BACHELOR M. T., LEE C., *Fermi gases in one dimension: From Bethe Ansatz to experiments*, ArXiv: 1301.6446v2 (2013).

[14] BLOCH I., DALIBARD J., ZWERGER W., *Many–Body Physics with Ultracold Gases*, Rev. Mod. Phys. **80**, 885 (2008).

[15] LEWENSTEIN M., SANPERA A., AHUFINGER V., DAMSKI B., SEN(DE) A., SEN U., *Ultracold atomic gases in optical lattices: mimicking condensed matter physics and beyond*, Adv. Phys. **56**, 243 (2007).

[16] JÖRDENS R., STROHMAIER N., GÜNTER K., MORITZ H., ESSLINGER T., *A Mott insulator of fermionic atoms in an optical lattice*, Nature **455**, 204 (2008).

[17] SCHNEIDER U., HACKERMÜLLER L., WILL S., BEST T., BLOCH I., COSTI T. A., HELMES R. W., RASCH D., ROSCH A., *Metallic and Insulating Phases of Repulsively Interacting Fermions in a 3D Optical Lattice*, Science **322**, No. 5907, 1520 (2008)

[18] GREINER M., BLOCH I., MANDEL O., HÄNSCH T. W., ESSLINGER T., *Quantum phase transition from a superfluid to a Mott insulator in a gas of ultracold atoms*, Nature, **415**, 39 (2002).

[19] SNYDER A., TANABE I., DE SILVA T., *Compressibility and entropy of cold fermions in one dimensional optical lattices*, Phys. Rev. A **83**, 063632 (2011).

[20] CUI X., WANG Y., *Phase diagram of imbalanced fermions in optical lattices*, Phys. Rev. B **79**, 180509(R) (2009).

[21] CAMPOSTRINI M., VICARI E., *Quantum critical behavior and trap–size scaling of trapped bosons in a one–dimensional optical lattice*, Phys. Rev. A **81**, 063614 (2010).

[22] CAMPOSTRINI M., VICARI E., *Equilibrium and off–equilibrium trap–size scaling in one–dimensional ultracold bosonic gases*, Phys. Rev. A **82**, 063636 (2010).

[23] CAMPOSTRINI M., VICARI E., *Trap–size scaling in confined–particle systems at quantum transitions*, Phys. Rev. A **81**, 023606 (2010).

[24] VICARI E., *Entanglement and Particle Correlations of Fermi Gases in Harmonic Traps*, Phys. Rev. A **85**, 062104 (2012).

[25] ESSLER F. H. L., FRAHM H., GÖHMANN F., KLÜMPER A., KOREPIN V. E., *The One–Dimensional Hubbard Model* (Cambridge University Press, 2005).

[26] GIAMARCHI T., *Quantum Physics in One Dimension*, Clarendon Press (2003).

[27] NEGELE J. W., ORLAND H., *Quantum Many–Particle Systems*, Westview Press (2008).

[28] SACHDEV S., *Quantum Phase Transitions*, Cambridge University Press (2011).

[29] JAKSCH D., BRUDER C., CIRAC J. I., GARDINER C. W., ZOLLER P., *Cold Bosonic Atoms in Optical Lattices*, Phys. Rev. Lett. Vol. **81**, No. 15, 3108 (1998).

[30] KÖHL M., STÖFERLE T., MORITZ H., SCHORI C., ESSLINGER T., *1D Bose Gases in an Optical Lattice*, Applied Physics B: Lasers and Optics **79**, 1009 (2004).

[31] SPIELMAN I. B., PHILLIPS W. D., PORTO J. V., *The Mott insulator transition in a two dimensional atomic Bose gas*, Phys. Rev. Lett. **98**, 080404 (2007).

[32] SCHULZ H. J., *The Metal–Insulator Transition in One Dimension*, arXiv:cond-mat/9412036v1.

[33] PRESS W. H., TEUKOLSKY S. A., VETTERLING W. T., FLANNERY B. P., *Numerical Recipes – The Art of Scientific Computing*, Cambridge University Press (2007).

[34] GUAN L., CHEN S., WANG Y., MA Z., *Exact Solution for Infinitely Strongly Interacting Fermi Gases in Tight Waveguides*, Phys. Rev. Lett. **102**, 160402 (2009)